NASA CR 134700

Department of Aerospace Engineering

University of Cincinnati

EROSION IN RADIAL INFLOW TURBINES - VOLUME III:

TRAJECTORIES OF EROSIVE PARTICLES IN RADIAL INFLOW TURBINES

By

W. B. Clevenger

and

W. Tabakoff

August 1974

Supported by:

NATIONAL AERONAUTICS AND SPACE ADMINISTRATION

Lewis Research Center

Contract NGR 36-004-055

NASA CR 134700

EROSION IN RADIAL INFLOW TURBINES - VOLUME III:

TRAJECTORIES OF EROSIVE PARTICLES IN RADIAL INFLOW TURBINES

BY

W. B. Clevenger

and

W. Tabakoff

August 1974

Supported by

NATIONAL AERONAUTICS AND SPACE ADMINISTRATION

Lewis Research Center

Contract NGR 36-004-055

1. Report No.	2. Government Accession No.	3. Recipient's Catalog No.
NASA CR 134700		

4. Title and Subtitle	5. Report Date
EROSION IN RADIAL INFLOW TURBINES - VOLUME III: TRAJECTORIES OF EROSIVE PARTICLES IN RADIAL INFLOW TURBINES	August 1974
	6. Performing Organization Code

7. Author(s)	8. Performing Organization Report No.
W.B. Clevenger, Jr. and W. Tabakoff	
	10. Work Unit No.

9. Performing Organization Name and Address	11. Contract or Grant No.
Department of Aerospace Engineering University of Cincinnati Cincinnati, Ohio 45221	NGR 36-004-055
	13. Type of Report and Period Covered
12. Sponsoring Agency Name and Address	Contractor Report
National Aeronautics and Space Administration Washington, D.C. 20546	14. Sponsoring Agency Code

15. Supplementary Notes

Final Report. Project Manager, Jeffrey E. Haas, Fluid Systems Components Division, NASA, Lewis Research Center, Cleveland, Ohio 44135

16. Abstract

A study of the theoretical trajectories that erosive particles follow in the gas flow fields of a typical radial inflow turbine is presented. Included in the study is a discussion of the theoretical trajectories that the particles follow in the scroll, in the nozzles, in the vortex between the nozzles and the rotor, and in the rotor passages. The results are presented in terms of the characteristic length, a similarity parameter which relates the particles that follow the same trajectory in equivalent flow fields.

17. Key Words (Suggested by Author(s))	18. Distribution Statement
Radial Turbine Erosion Similarity Particulated Flow	Unclassified - unlimited

19. Security Classif. (of this report)	20. Security Classif. (of this page)	21. No. of Pages	22. Price*
Unclassified	Unclassified		$3.00

*For sale by the National Technical Information Service, Springfield, Virginia 22151

CONTENTS

SUMMARY

A study of the theoretical trajectories that erosive particles follow in the gas flow fields of a typical radial inflow turbine is presented. Included in the study is a discussion of the theoretical trajectories that the particles follow in the scroll, in the nozzles, in the vortex between the nozzles and the rotor, and in the rotor passages. The results are presented in terms of the characteristic length, a similarity parameter which relates the particles that follow the same trajectory in equivalent flow fields.

The study revealed that particles with characteristic lengths greater than about 30 cm would tend to strike the outer edges of the scroll with moderate angle, low velocity impacts. The characteristic length would correspond to silicon dioxide particles of approximately 80 microns in a turbine which has an inlet stagnation density equal to twice the density of standard sea level air.

In the nozzles, the study indicated that particles with characteristic lengths greater than about 15 cm tended to strike the pressure surface of the blade, and particles with characteristic lengths greater than about 30 cm would travel to the suction surface of the blade before they exited the nozzle passages. The study also revealed that particles with characteristic lengths as small as 0.5 cm will repeatedly strike the trailing edge of the suction surface of the nozzles blades with relatively high velocity, and at moderate impact angles. This characteristic length of 0.5 cm corresponds to a silicon dioxide particle of approximately 2 microns in a turbine which has an inlet stagnation density equal to twice the density of standard sea level air.

In the vortex, the results revealed that particles with characteristic lengths between about 0.5 and 30 cm would tend to move in the vortex region without penetrating to the rotor. Particles with characteristic lengths smaller than 0.5 would

probably penetrate the rotor without striking the blade surfaces, and particles with characteristic lengths greater than 30 cm seem to penetrate into the tip region of the rotor, only to be struck by the rotor tip. Particles with a characteristic length of 0.5 cm correspond to a silicon dioxide particle with a diameter of approximately 1.5 microns in a turbine which has an inlet stagnation density equal to twice the density of standard sea level air.

The motion of particles in the rotor revealed that the particles with characteristic lengths greater than about 15 cm would be overtaken by the rotor, which would strike the particle and accelerate in it to quite high tangential velocities. This would cause the centrifugal forces to be great enough to push the particle outward against the gas flow until the particle struck the nozzle blade trailing edges. These particles would strike the rotor tip with a high velocity and with an almost perpendicular impact angle. Particles with characteristic lengths smaller than about 6 cm would tend to pass through the rotor, if they could be made to penetrate the vortex region.

These theoretical trajectories were also analyzed to consider the particle velocity lag, the ratio of the particle velocity to the gas velocity, and the deviation angle, the difference between the direction of the particle velocity and the gas velocity. This information allowed an anlysis of the acceleration characteristics in the vortex region, which revealed that particles with characteristic lengths between 3 and 300 cm all tend to accelerate outward away from the turbine axis.

Two design concepts were considered to provide mechanisms that might help to reduce the amount of erosion that occurs in the radial turbine. The theoretical effectiveness of these mechanisms in removing the particles that accumulate near the rotor tip was studied.

The first concept is to combine an axial type nozzle with a radial turbine. Between the nozzles and the rotor there would then exist a 90° bend that would turn the whirling flow into the

rotor. Such a configuration might allow installation of an opening in the bend wall that would capture particles that bounced in this region. The study of the trajectories in such a flow field revealed that particles with characteristic lengths greater than 60 cm could be effectively removed in this way. This characteristic length corresponds to a silicon dioxide particle of approximately 160 microns in a turbine which has an inlet stagnation density equal to twice the density of standard sea level air.

The second concept is to design a rotor blade that has a forward sweep, which would tend to deflect particles into the rotor. This boost might allow more particles to penetrate the rotor and reduce the amount of erosion caused by the accumulated particles in the vortex region. This study revealed that most of the larger particles, with characteristic length greater than 10 cm, would probably be deflected inward by such a rotor blade, and might possibly penetrate far enough to pass through the rotor.

Experimental results are presented that illustrate the phenomena of particle motion in the nozzle and vortex region of a radial turbine. These results demonstrate qualitatively the nature of motion of particles in such a region, and illustrate the accumulation of particles in the vortex region.

INTRODUCTION

The purpose of this study is to investigate the erosion phenomena in radial inflow turbines and to study ways of eliminating this erosion. The overall study includes an investigation of erosive particle trajectory similarity, investigation of the balance between radial aerodynamic drag and centrifugal forces acting on the particles, investigation of the theoretical trajectories that particles follow as they pass through a radial inflow turbine, and a review of the phenomena of erosion of blade materials by the action of particles.

The results of these investigations will be published in a series of five volumes which will cover the indicated topics, with the fifth volume presenting the numerical programs that were developed. This report considers the third topic.

In recent times, the problem of particle erosion has become important due to the significant decreases in the rated operating lifetimes and performance of gas turbine engines which are used in dusty environments. The most significant affects of erosion have been observed on active military helicopters, where operations at low altitudes and remote landing fields have greatly increased the number of particles that enter the engines. Although these helicopters have main engines which utilize axial flow turbines, some also have auxiliary engines used as power sources for special devices which utilize radial turbines, as shown schematically in Figure 1.

Radial inflow turbines have also been used on small portable power plants which are also likely to be used in areas where dust ingestion will occur. Finally, radial inflow turbines are seriously being considered for future use in transportation vehicles such as trucks, buses, and automobiles. These engines will at times have incomplete filtering of incoming air, leading to the ingestion of erosive size particles that could seriously

threaten the future performance of the engine.

These radial turbine engines have, however, a more serious erosion problem than axial flow turbines. In radial turbines, the larger particles experience a radially outward centrifugal force that is greater than the radially inward component of the aerodynamic drag force. In the axial flow turbine the centrifugal force acts perpendicular to the aerodynamic drag force. Thus, in radial turbines most particles are prevented from passing through the rotor and strike the trailing edges of the stators and the leading edges of the rotor many times. In axial flow turbines, the particles generally move outward to the tip region, but all particles have a tendency to pass through the turbine.

The results presented in this report express the sizes of particles in terms of the characteristic length. This term is a similarity parameter which relates the particles that follow the same trajectory in equivalent flow fields. Volume I[1] of this series of reports explains the derivation and applicability of the characteristic length.

Volume II[2] explains the derivation of two special values of the characteristic length that are related to the flow pattern and geometry of a radial inflow turbine. These special values represent limiting characteristic lengths that are related to sizes of particles which will move radially inward or radially outward within the vortex region of the turbine. The first, called the orbit characteristic length, represents the lower limit of particle sizes that will not pass through the rotor, but instead will accumulate in the vortex region. The second, called the limit characteristic length, represents the lower limit of particle sizes that will experience an acceleration in the radial direction in the vortex.

This study will concentrate on the patterns of theoretical trajectories as the particles pass through a typical radial inflow turbine. Included in the investigation will be the scroll, the nozzles, the vortex between the nozzles and the rotor, and the rotor passages. In each of these passages, the movement of

the particles will be considered and the nature of the impacts on the surfaces of the contours and blades determined. This information will be useful in evaluating the ability of new turbine designs to reduce the severity of erosion.

These theoretical trajectories will also be analyzed to consider the particle velocity lag, the ratio of the particle velocity to the gas velocity, and deviation angle, the difference between the direction of the particle velocity and the gas velocity. This information will be useful in evaluating the limit characteristic length which is dependent upon the velocity lag, and was derived based upon the assumption of zero deviation angle.

There are two design concepts which show promise as mechanisms that might reduce the seriousness of the erosion problem in the radial turbine. Both of these concepts will be considered in terms of their effectiveness in removing the erosive size particles from the rotor tip region.

The first concept is to combine an axial type nozzle with a radial turbine rotor. Such a design requires that a 90° annular bend turn the whirling flow into the rotor passages. This deflection of the flow would allow the installation of slots on the outer wall of the turning vortex, and a properly designed slot would capture the particles that accumulated in this region.

The second concept is to design the rotor blade with a forward sweep so that particles that entered and accumulated near the rotor tip would perhaps be deflected inward. If the inward deflection were of a large enough magnitude, the particles would leave the rotor exit and be removed from the vortex-rotor tip region.

Experimental results are presented that illustrate the phenomena of particle motion in the nozzle and vortex region of a radial inflow turbine. These results demonstrate qualitatively the nature of the motion of particles in such a region and illustrate the accumulation of particles in the vortex region.

There are many reports that have dealt with the motion of particles in a gas flow field. Several authors have concentrated

on the effect of particle motion in flow fields that are treated as two phase flows. Reference (3) considers the effect of such particles on the performance of a one-dimensional nozzle, while Reference (4) considers the same effect on an axisymmetric nozzle. These authors treat the flow in terms of a two-phase flow with the gas and solid particles satisfying continuity, momentum, and energy considerations.

Reference (5) takes this same approach in considering the effects of the particles in the flow field of a two-dimensional axial flow nozzle passage.

The information from such an approach is useful, but the problem becomes quite complicated with the addition of variable particle sizes and densities, and the realization that each species of particle must satisfy continuity, momentum, and energy equations. In addition, this type of solution does not provide information about trajectories, which is required if conclusions about the locations and magnitudes of erosion are to be considered.

Most other authors consider the trajectories of particles in detail and assume that the particles have no influence on the gas flow. References 6 and 7 present results for cascades and annular flow geometries respectively. The analytical parts of these reports result from the integration of the equations of motion of a particle superimposed on the flow field. This same method will be used in the development of the analytical work that will be presented here.

References 8 and 9 report the results of test programs where controlled sand ingestion into an actual radial inflow turbine was performed. These reports provide evidence concerning the primary places that erosion will occur and the seriousness of such erosion.

Several additional references which discuss special topics were cited and will be discussed at the locations where they are first indicated within the text.

MODELS

Two slightly different turbines have been used in the results presented in this report. For the analytical work and the numerical solutions for the particle trajectories, a typical model turbine configuration was selected, and the flow fields throughout the turbine determined. For the experimental results, a slightly different model turbine was used. This part of the report will describe these models in detail.

Analytical Model Turbine

The general characteristics of a typical radial inflow turbine were selected as the basis for development of a model turbine for the analytical work presented in this report.

Figure 2 shows the details of the turbine configuration. The configuration included the scroll, a free vortex that connects the scroll to the nozzle blades, the nozzle blade passages, a free vortex after the nozzle blades, and the rotor. These regions are assumed independent of each other and the exit conditions for one region are used as the inlet conditions for the next region. The interface between these regions are indicated in Figure 2, while Table I gives the details of the dimensions at these locations.

The general characteristics of the turbine were that it have an equivalent flow rate of 0.220 kg/sec, with a total to total efficiency of 88%. The equivalent rotating speed was 30,800 rpm. Figure 3 indicates the velocity diagrams that describe the direction and magnitude of the flow at the inlet and exit stations of the nozzles and rotor.

The gas flow in the scroll is assumed to be incompressible, and the scroll sectional area is assumed to change in direct proportion to the decrease in mass flow that occurs as the gas enters the nozzle-vortex region. Based on this, the velocity

of the gas across the scroll sections is constant and uniform. Although this solution is quite simple compared to the complicated nature of the three-dimensional problem, it does provide an approximately realistic gas flow field into which the particles can be introduced.

The full three-dimensional solution of the scroll flow field would add axial components to the radial and tangential components of the gas flow. The added axial component would accelerate the particles in the axial direction and probably influence in a minor way the trajectories in the vortex and nozzle regions. However, because the magnitudes of the velocities are more than an order of magnitude greater than in the vortex regions, and these velocities are predominantly in the tangential and radial directions, the effect of the axial components of the particle velocity that results from three dimensional flow in the scroll will probably be small.

Figure 4 illustrates the contoured and free vortex region that exists between stations 2 and 3. The flow in these regions along the center line are assumed to satisfy requirements of constant angular momentum and continuity. These flows, as well as the flow in all remaining regions of the turbine, are compressible. Volume II of this set of reports contains detailed derivations of the equations that describe the gas flow in the inward moving free vortex. Because the motion of particles in the scroll was assumed to occur in the plane of the section center, all particles entered the contoured vortex region at the center where there are no axial velocity components. Therefore, the particles did not strike the side walls of this region and the effects of such impacts were not studied.

Figure 5 illustrates the nozzle blade configuration that was selected for this analytical model turbine. There were 29 equally spaced blades. The solution of the gas flow in the nozzle was based on the assumption of an irrotational two-dimensional flow field. A velocity gradient technique was used

to determine the flow through the passage. Although such techniques are of nominal accuracy because they require determination of the blade radius of curvature, the results are sufficiently accurate to study the patterns of trajectories that occur in this region. The solution streamlines are also indicated in Figure 5.

There exists after the nozzles, a second free vortex that occurs until the gas enters the rotor. This vortex also satisfies the requirements of two-dimensional free vortex motion as described in Volume II[2] of this series of reports.

The quasi-orthogonal method given in Reference (10) was used to determine the gas flow in the rotor passage. There were 12 rotor blades in the model used in this study, with no splitter blades. The rotor tip diameter was 7.52 cm. Figures 6a, 6b, and 6c show three views of the solution streamlines that occurred when this method was used. These figures illustrate the difference in the solution streamlines that occurs when the same rotor is used with a hot gas or an equivalent cold gas solution. The hot gas solution assumed an inlet stagnation temperature of 1478°K with an inlet stagnation pressure of 8.55 atm. The equivalent cold gas solution has inlet stagnation conditions that are identical to standard sea level air. The differences result because of the differences in the ratio of specific heats in the two cases. This ratio has an influence on the variation of gas density across the passage.

In this investigation, only the equivalent solution was used to study the particle trajectories. However, as explained in Reference (1), the presentation of results in terms of the characteristic length allows one to apply the results to any equivalent gas flow because different size particles that follow the same trajectories in equivalent hot or cold gas flows will have the same characteristic length.

Experimental Model Turbine

At the start of this project, it was felt that there should be an attempt to accummulate some experimental data in the form of high speed motion pictures of particle trajectories in the radial inflow turbine. This led to the development and subsequent construction of a model turbine that would allow the collection of such data.

Figure 7 shows the details of the experimental turbine configuration, and Table 2 gives details of the dimensions. In this particular turbine, the arrangement of the scroll was chosen to give a flat surface on one side of the passage so that a plastic cover could be attached to the front of the turbine. As shown in the figure, this plastic cover made up all of one side of the turbine and allowed the taking of high speed motion pictures that illustrate the phenomena.

Figure 8 shows the inlet velocity diagram at the rotor inlet for the case of maximum rpm. Because of the nature of the data to be taken, a flat plate rotor with 16 blades was used. This flat plate rotor was limited to a maximum rotating speed of 2000 rpm, and this limited the equivalent weight flow with the rotor installed to 0.060 kg/sec. Only particle trajectory characteristics at the vortex and rotor inlet were considered, and no attempt was made to study the performance of this turbine or to determine possible performance levels.

In addition, a set of 18 flat plate nozzles were used instead of a contoured nozzle blade as used in the analytical turbine model. Figure 9 shows the characteristics of this nozzle blade. The gas had an exit angle of approximately 70° at the nozzle exit.

ANALYTIC PROCEDURE

The analysis of particle trajectories in a fluid flow field not only require the solution of the flow field but also require the equations of motion of a particle. This part of the report will present the derivation of these equations of motion as well as presenting a brief review of the results that have been presented in Volumes I[1] and II[2] of the complete report on erosion in radial inflow turbines.

Equations of Motion of Particles in a Rotating Reference Frame

The equations of motion of a particle in a rotating reference frame must be derived and understood if the trajectories of particles in turbine rotors is to be determined numerically. In addition, these equations are the basis upon which similarity parameters and related terms are derived.

The equations of motion of a particle in a cylindrical coordinate system offers a basis for determining the parameters that will be most influential in determining the properties of particles that will have similar trajectories. The most general case will be that of the dynamic equations of three-dimensional particle motion in a rotating reference frame. Figure 10 illustrates the coordinate system used throughout this report.

The position of the particle with time is given by

$$\bar{r} = r\,\bar{e}_r + z\,\bar{e}_z \qquad (1)$$

Because we have not yet restricted the problem to one of rotation about the z-axis, $\bar{e}_z$ is a unit vector which has a direction that changes with time. Also, because the origin of the rotating reference frame will be taken as the same point as the origin of the inertial reference frame, the position vector is the same in both rotating and inertial reference frames.

Taking the derivatives of the position vector, Equation (1), with respect to time in the absolute reference frame gives

$$\frac{d\bar{r}}{dt} = \frac{\delta r}{\delta t}\,\bar{e}_r + r\,\frac{\delta \bar{e}_r}{\delta t} + \frac{\delta z}{\delta t}\,\bar{e}_z + r\,\frac{d\bar{e}_r}{dt} + z\,\frac{d\bar{e}_z}{dt}$$

$$= \frac{\delta r}{\delta t}\,\bar{e}_r + r\,\frac{\delta \theta}{\delta t}\,\bar{e}_\theta + \frac{\delta z}{\delta t}\,\bar{e}_z + r\,\frac{d\bar{e}_r}{dt} + z\,\frac{d\bar{e}_z}{dt} \qquad (2)$$

The first three terms of Equation (2) represent the velocity vector with respect to the rotating reference frame. If the velocity is zero in the rotating reference frame, then the first three terms are zero and the last two terms must therefore describe the rate of rotation of the rotating coordinate system. Thus, for this case where the velocity of a particle with respect to the rotor is zero, the particle velocity in the absolute reference frame is

$$\frac{d\bar{r}}{dt} = \bar{\Omega} \times \bar{r} \qquad (3)$$

where $\bar{\Omega}$ is a vector which points in the axial direction and which has magnitude equal to the rotating speed.

In general then, Equation (2) can be written

$$\frac{d\bar{r}}{dt} = \frac{\delta \bar{r}}{\delta t} + \bar{\Omega} \times \bar{r} \qquad (4)$$

where $\delta\bar{r}/\delta t$ represents the particle velocity with respect to the rotor.

It is useful to note at this point that if $\bar{r}$ had been a vector, $\bar{q}$, located at some other point than the origin. And if

$$\bar{q} = q_r\,\bar{e}_r + q_\theta\,\bar{e}_\theta + q_z\,\bar{e}_z \qquad (5)$$

then

$$\frac{d\bar{q}}{dt} = \frac{d}{dt}(q_r \bar{e}_r) + \frac{d}{dt}(q_\theta \bar{e}_\theta) + \frac{d}{dt}(q_z \bar{e}_z)$$

$$= \frac{\delta q_r}{\delta t}\bar{e}_r + \frac{\delta q_\theta}{\delta t}\bar{e}_\theta + \frac{\delta q_z}{\delta t}\bar{e}_z + q_r \frac{\delta\theta}{\delta t}\bar{e}_\theta$$

$$- q_\theta \frac{\delta\theta}{\delta t}\bar{e}_r + q_r \frac{d\bar{e}_r}{dt} + q_\theta \frac{d\bar{e}_\theta}{dt} + q_z \frac{d\bar{e}_z}{dt} \qquad (6)$$

where Equation (6) represents the rate of change of the vector $\bar{q}$ with respect to time in the inertial reference frame. As in the case with $\bar{r}$, if $\bar{q}$ is not allowed to move with respect to the rotating reference frame, then

$$\frac{\delta q_r}{\delta t} = 0, \quad \frac{\delta q_\theta}{\delta t} = 0, \quad \frac{\delta q_z}{\delta t} = 0, \quad \frac{\delta \bar{e}_r}{\delta t} = 0, \quad \frac{\delta \bar{e}_\theta}{\delta t} = 0 \qquad (7)$$

The last two equations result from the fact that the rate of change of $\bar{e}_\theta$ and $\bar{e}_r$ with respect to the rotating reference frame are also zero in this special case where $\bar{q}$ is fixed in the rotating reference frame. Therefore, for $\bar{q}$ fixed in the rotating referemce frame

$$\frac{d\bar{q}}{dt} = q_r \frac{d\bar{e}_r}{dt} + q_\theta \frac{d\bar{e}_\theta}{dt} + q_z \frac{d\bar{e}_z}{dt} \qquad (8)$$

But if $\bar{q}$ is fixed in the rotating reference frame, the rate of change of $\bar{q}$ with respect to time in the inertial reference frame is just the rate that $\bar{q}$ changes direction. This rate is given by $\bar{\Omega} \times \bar{q}$.

Thus, for any vector $\bar{q}$,

$$\frac{d\bar{q}}{dt} = \frac{\delta \bar{q}}{\delta t} + \bar{\Omega} \times \bar{q} \qquad (9)$$

where $d\bar{q}/dt$ is the time rate of change of $\bar{q}$ with respect to the inertial reference frame, $\delta\bar{q}/\delta t$ is the time rate of change of $\bar{q}$ with respect to the rotating reference frame, and $\bar{\Omega} \times \bar{q}$ represents the rigid body rotation of $\bar{q}$ about the axis of rotation.

Using the concept expressed in Equation (9), the acceleration vector can be determined by differentiating the velocity vector,

$$\frac{d^2\bar{r}}{dt^2} = \frac{d}{dt}\left(\frac{\delta\bar{r}}{\delta t}\right) + \frac{d}{dt}\left(\bar{\Omega} \times \bar{r}\right)$$

$$= \frac{\delta^2\bar{r}}{\delta t^2} + \bar{\Omega} \times \frac{\delta\bar{r}}{\delta t} + \frac{d\bar{\Omega}}{dt} \times \bar{r} + \bar{\Omega} \times \frac{d\bar{r}}{dt} \qquad (10)$$

$$= \frac{\delta^2\bar{r}}{\delta t^2} + 2\,\bar{\Omega} \times \frac{\delta\bar{r}}{\delta t} + \frac{d\bar{\Omega}}{dt} \times \bar{r} + \bar{\Omega} \times \left(\bar{\Omega} \times \bar{r}\right)$$

For the case of steady rotation about the z-axis with a rotating speed, ω, and using $\bar{r} = r\,\bar{e}_r + z\,\bar{e}_z$, this acceleration vector becomes,

$$\bar{a} = \frac{d^2\bar{r}}{dt^2} = \left[\frac{\delta^2 r}{\delta t^2} - r\left(\frac{\delta\theta}{\delta t}\right)^2 - 2\,r\,\omega\frac{\delta\theta}{\delta t} - r\,\omega^2\right]\bar{e}_r$$

$$+ \left[r\,\frac{\delta^2\theta}{\delta t^2} + 2\,\frac{\delta r}{\delta r}\,\frac{\delta\theta}{\delta t} + 2\,\omega\,\frac{\delta r}{\delta t}\right]\bar{e}_\theta$$

$$+ \frac{\delta^2 z}{\delta t^2}\,\bar{e}_z \qquad (11)$$

where $\delta/\delta t$ represents the time rate of change of r, θ, or z with respect to the rotating reference frame.

Newton's Second Law, $\bar{F} = m\bar{a}$, is used to relate the acceleration vector experienced by the particle and the resultant force that acts on the particle.

The forces that act on a particle include aerodynamic forces, gravitational forces, and electrostatic forces if the particle carries a charge. Electrostatic forces on charged particles can in some cases be quite significant in affecting the trajectories of the particles. However, to be significant, additional devices would have to be added to a turbine engine to generate an electric field within parts of the flow passage, and to charge the particles in some way. Because such devices are beyond the scope of this project, electrostatic forces will be neglected.

In order to consider gravitational forces, the orientation of the turbine with respect to the vertical and horizontal plane must be defined. Figure 11 shows the arrangement of these axes. The vertical axis of the turbine is the axis from which θ is measured. The angles ϕ and σ are shown in the positive direction, and based on this figure, the weight force vector is

$$\bar{W} = - mg \cos (\theta + \sigma) \bar{e}_r + mg \sin (\theta + \sigma) - mg \sin \phi \bar{e}_z \qquad (12)$$

In order to estimate when the influence of gravity will be important, consider that the distance traveled by a particle falling free in a vacuum will be

$$s = \frac{1}{2} g t^2 \qquad (13)$$

If we require that the allowable error in trajectories is 0.01 cm between the case with gravity included and the case neglecting gravity, then solving the equation above indicates that

$$t \leq 0.0032 \text{ seconds}$$

Therefore, if in our numerical solutions, the time should exceed 0.0032 seconds, then gravitational forces should not be neglected.

It was found that particles travelling in the scroll did tend to remain in this region for times greater than 0.0032 seconds, and therefore, it was necessary to include the affect of gravity.

For nonspherical particles, the aerodynamic forces will include drag, lift, and moment forces. Because most particles will spin rather than remain at some definable angle of attack, moment and lift forces are neglected and only drag forces are considered. This drag force acts in the direction of the air velocity with respect to the particle velocity, and is given by

$$\bar{D} = \frac{1}{2} \rho \ \bar{V}^2 \ A \ C_D \ [\frac{V_r}{|\bar{V}|} \bar{e}_r + \frac{V_\theta}{|\bar{V}|} \bar{e}_\theta + \frac{V_z}{|\bar{V}|} \bar{e}_z] \tag{14}$$

where $$\bar{V} = V_r \bar{e}_r + V_\theta \bar{e}_\theta + V_z \bar{e}_z \tag{15}$$

is the relative velocity of the gas with respect of the particle. The components of this relative velocity vector are

$$V_r = w_r - \frac{\delta r}{\delta t}$$

$$V_\theta = w_u - r\frac{\delta \theta}{\delta t} \tag{16}$$

$$V_z = w_z - \frac{\delta z}{\delta t}$$

where w_r, w_u, w_z are respectively the radial, tangential and axial components of the gas in the rotating reference frame in the most general case, and $\delta r/\delta t$, $r\ \delta\theta/\delta t$, and $\delta z/\delta t$ are respectively the radial, tangential and axial velocity components of the particle. It should be noted that when ω in Equation (11) is zero, corresponding to no rotation of the reference frame the relative velocities w_r, w_u, and w_z become absolute velocities.

Collecting the components of the acceleration drag, and gravity forces through Newton's Law yields

$$\frac{\delta^2 r}{\delta t^2} - r\left(\frac{\delta\theta}{\delta t}\right)^2 - 2\,r\,\omega\,\frac{\delta\theta}{\delta t} - r\,\omega^2 = \frac{1}{2}\,\frac{\rho V^2 A C_D}{m}\,\frac{V_r}{|\bar{V}|} - g\cos(\theta+\sigma) \qquad (17a)$$

$$r\,\frac{\delta^2\theta}{\delta t^2} + 2\,\frac{\delta r}{\delta t}\,\frac{\delta\theta}{\delta t} + 2\,\omega\,\frac{\delta r}{\delta t} = \frac{1}{2}\,\frac{\rho V^2 A C_D}{m}\,\frac{V_\theta}{|\bar{V}|} + g\sin(\theta+\sigma) \qquad (17b)$$

$$\frac{\delta^2 z}{\delta t^2} = \frac{1}{2}\,\frac{\rho V^2 A C_D}{m}\,\frac{V_z}{|\bar{V}|} - g\sin\phi \qquad (17c)$$

In some cases, these equations apply in the regions of the turbine where the flow field is viewed with respect to an inertial system. Such a situation occurs in the nozzle and vortex regions of the radial turbine, and in these regions, a less general set of equations of motion can be used. Setting $\omega = 0$ in equation 17 gives

$$\frac{d^2 r}{dt^2} - r\left(\frac{d\theta}{dt}\right)^2 = \frac{1}{2}\,\frac{\rho V^2 A C_D}{m}\,\frac{V_r}{|\bar{V}|} - g\cos(\theta+\sigma) \qquad (18a)$$

$$r\,\frac{d\theta}{dt^2} + \frac{dr}{dt}\,\frac{d\theta}{dt} = \frac{1}{2}\,\frac{\rho V^2 A C_D}{m}\,\frac{V_\theta}{|\bar{V}|} + g\sin(\theta+\sigma) \qquad (18b)$$

$$\frac{d^2 z}{dt^2} = \frac{1}{2}\,\frac{\rho V^2 A C_D}{m}\,\frac{V_z}{|\bar{V}|} - g\sin(\phi) \qquad (18c)$$

where again it is important to note that the velocities V_r, V_θ, and V_z are the components of the gas velocity with respect to the particle.

The drag coefficient of a spherical particle is well established experimentally over a large range of Reynold's numbers. Because of the significance of C_D in Equation (17), a discription of C_D in algebraic form is necessary for the numerical solution of the particle trajectory. The value of C_D was determined by using the following relations.

$$C_D = 4.5 + \frac{24}{Re} \qquad Re < 1.0 \qquad (19a)$$

$$C_D = 28.5 - 24.0\ (\text{Log Re}) + 9.0682\ (\text{Log Re})^2 - 1.7713\ (\text{Log Re})^3 + 0.1718\ (\text{Log Re})^4 - 0.0065\ (\text{Log Re})^5$$

$$1.0 < Re < 3000 \qquad (19b)$$

$$C_D = 0.4 \qquad 3000 < Re < 2.5 \times 10^{-5} \qquad (19c)$$

Where the Reynold's number is expressed as $Re = \rho_g V D_p/\mu_g$ with the velocity V representing the absolute value of the difference between the gas velocity and the particle velocity. These formulas were based on the drag coefficient versus Reynold's number data such as contained in many text books, and are plotted in Figure 12 to demonstrate how they fit various data points.

The purpose of this part of the progress report has been to derive the equations of motion of a particle in a rotating reference frame. These equations are integrated numerically to yield the position and velocity of particles in the radial turbine. Specific information on the integration methods and computer program will be contained in Volume V of this series of reports.

Similarity and the Force Balance Acting on Particles

References 1 and 2 present ideas that will be used in this work. Therefore, a brief outline of the results presented in those reports will help to emphasize and illustrate some of the results presented in this report.

Reference 1 describes the derivation and applicability of a similarity parameter that allows particles which follow a certain trajectory in a real gas turbine to be related to a particle that will follow the same trajectory in an equivalent cold gas turbine. The similarity parameter is a characteristic length and is given by the following equation

$$\delta = \frac{10}{3} \frac{\rho_p D_p}{\rho_g} \tag{20}$$

This similarity parameter results from the matching of the inertial and drag forces acting on a particle. The results presented in Reference 1 demonstrate that this parameter can be used in flow fields similar to those that occur in a radial turbine.

The characteristic length is a useful parameter because it allows the grouping of several variables that influence the trajectory of a particle into a single term. This allows a much wider range of applicability of trajectory data and allows the use of data from equivalent cold flow turbines and cascade tunnels.

In the subsequent work presented in this report, the variables are grouped together and comparisons are made with variations of particle size in terms of the characteristic length.

Usually, the critical gas density is used as the gas density upon which δ is based. This is in agreement with the ideas of similarity and equivalent flow fields and allows a constant value of δ throughout all flow fields. In the case of the rotor, the inlet critical density is used.

Reference 2 describes the derivation and applicability of several special values of characteristic length that have significance in terms of whether a particle will move radially inward

toward the axis or radially outward. These terms are derived by balancing the radial component of the aerodynamic drag force and the centrifugal force.

The first is designated as the orbit characteristic length δ_o and is given by

$$\delta_o = \frac{r_{tip}}{\tan^2 \beta g} \tag{21}$$

In this expression, r_{tip} is the tip radius and βg is the direction from the inward radial line of the gas velocity vector. Using this, the criteria for a particle that is to penetrate the vortex and rotor flow fields is

$$\delta < \delta_o \tag{22}$$

For the analytical model turbine used here, $\delta_o = 0.5$ cm, and for the experimental turbine used in the high speed motion picture studies, $\delta_o = 1.15$ cm. These values correspond to silicon dioxide particles of approximately 1.4 and 3.2 microns respectively in an equivalent turbine which has an inlet stagnation density equal to twice the density of standard sea level air. As an example, such a density would occur in a turbine with inlet stagnation conditions of 1111 ^{o}K and 7.7 atm.

A second special value of characteristic length is also presented in Reference 2. This value, called the limit characteristic length, represents the limiting size of particle that will first experience an acceleration in the radial direction. Such an acceleration must occur if the particle is to reverse its radial motion and become trapped in the vortex-rotor tip region of the turbine. The limit characteristic length is given by

$$\delta_L = \frac{(1-\zeta)^2}{\zeta^2} \frac{r_{tip} \cos \beta g}{\sin^2 \beta g} \tag{23}$$

In this equation, ζ is the velocity lag, defined as the ratio of the particle velocity to the gas velocity. The criteria for particles that are not to experience a radially outward acceleration throughout their motion through the free vortex and rotor regions is

$$\delta < \delta_L \tag{24}$$

The problem with evaluation of the limit characteristic length such as given in equation (23), is that typical values of the velocity lag, ζ, are not known for radial turbines. With the determination of this term, a measure of the limit characteristic length will have been completed. In addition, the derivation of the limit characteristic length requires the assumption that the deviation angle must be zero. The analytical results that are presented in the following will consider these terms at several locations in the turbine.

ANALYSIS OF TRAJECTORY PATTERNS

Four distinct regions of the flow through a radial inflow turbine were selected for study of the patterns that particles follow as they pass through the turbine. These regions included the scroll, the nozzles, the free vortex region between the nozzles and rotor, and the rotor region. The study, which includes all of these regions, considers a set of particles that are traced all the way through the system. The sizes of these particles is such that they all fail to penetrate the rotor and therefore, would be of the type that would cause erosion.

Table 3 indicates the characteristics of the particles that were traced through the turbine. The code designation indicated on this Table is a set of three numbers that are used to identify the particles in the various flow regions. The first number in the code refers to the particle's characteristic length. A range of particles sizes corresponding to characteristic lengths from 3 to 300 cm was selected for the study. This corresponds to silicon dioxide particles with diameters from about 8 to 800 microns, in an equivalent turbine that has an inlet stagnation density equal to twice the density of standard sea level air.

The second number in the code refers to the percent velocity lag at the scroll inlet. It should be noted that the velocity lag used in the code refers to the velocity that the particle has at the scroll inlet only. As the gas tends to accelerate or decelerate the particle, the particle is not restricted to the velocity it has at the inlet to the scroll but is free to accelerate and decelerate.

The third number of the code refers to the position at the scroll inlet. The number represents the percent of the radial span measured from the smallest radial dimension of the scroll inlet section. As in the previous case, this refers only to the initial point from which the trajectory of the particle is traced.

In the figures that follow, this code is included with the trajectory to specifically designate the particle.

Scroll

Before the gas enters the nozzle and vortex regions of the radial inflow turbine, it usually enters a scroll which is designed to distribute the air uniformly into the nozzles. Usually the velocities in the scroll are relatively small compared to the velocities that occur in the vortex regions of the turbine. However, to gain a better understanding of the nature of the particle trajectories throughout the turbine, it was decided to consider the trajectories in the scroll flow field.

Figure 13a indicates the patterns that occur as particles with characteristic lengths equal to 15 cm pass through the scroll. These trajectories reveal that particles of this size generally do not strike the scroll surfaces, but instead tend to move with the flow into the nozzle regions. Similar results were observed when the trajectories of particles with characteristic lengths of 3 and 6 cm were plotted. The only difference between the trajectories for these small particles and the particles with characteristic length equal to 15 cm was the angular position where the particle left the scroll. The smaller particles tended to leave the scroll at a smaller angular position than the larger particles that started at the same position.

The trajectory patterns that occur for particles with characteristic lengths equal to 30 cm is illustrated in Figure 13b. This size particle tends to move outward from the axis and eventually strikes the scroll outer surface. After striking the scroll, all particles of this size tended to bounce many times, almost tangentially, as they moved along the scroll contour. Eventually, these particles struck the portion of the contour that is suppressed to prevent interference with the scroll inlet. Once the particles bounced off this suppressed contour, they

entered the nozzles at approximately the same location. Some of the trajectories are truncated at the point of the first bounce to avoid a confusing figure. These trajectories showed the same characteristics as the trajectory which is traced all the way around the scroll.

Figure 13c illustrates the trajectories of even larger particles with characteristic lengths of 60 cm. This figure indicates that as the particle size increases, the distance between bounces appears to increase with a corresponding decrease in the number of bounces. Near the end of the scroll contour, these particles start to follow the contour and eventually strike the suppressed contour as in the previous case. When this occurs, the particles bounce into the nozzle region of the turbine at approximately the same location. Two trajectories are truncated at the location where the first bounce occurs. These trajectories showed the same general trend as the trajectory that was traced all the way around the scroll contour.

A similar trace of the trajectories was done for particles with characteristic lengths of 150 cm. These traces showed the same general trends as indicated in Figure 13c, with the exception that the larger particle tended to travel longer distances between bounces with a corresponding decrease in the number of bounces.

Finally, Figure 13d illustrates the trajectories of very large particles with characteristic lengths of 300 cm. These trajectories reveal that particles of this size bounce few times and tend to travel quite large distances between their bounces. Because the distances between the trajectory and the scroll contour are quite large at places, these particles did not strike the suppressed scroll contour at the location where the suppressed contour joined the scroll contour. Two of the trajectories are truncated at the location where they crossed the lower trajectory. These trajectories showed the same general trends as the trajectory that was traced all the way around the scroll.

These trajectories have revealed that particles with characteristic lengths of 30 cm or greater will tend to move radially outward and strike the outer regions of the scroll contour. In addition, the portion of the scroll that is usually suppressed to avoid interference with the inlet portion of the scroll will be subject to a great deal of erosion because most particles with characteristic lengths of 30 cm or greater bounced on this relatively small portion of the scroll contour.

Table 4 gives the tabulated results of the velocity lag and deviation angle of three sizes of particles as they leave the scroll. This table indicates that the larger particles tend to have slower velocities as they leave the scroll, while the smaller particles have accelerated to the gas velocity. It is interesting to note that, except for the larger particles, the initial velocity of the particles does not appear to have an influence on the velocity lag as the particle leaves the scroll. It can also be seen from this table that the larger particles that bounce off the scroll contour appear to have a more random direction than those particles that did not bounce off the scroll surface. These bounces seem to have more influence on the nature of the particle motion than the initial values of the velocity or the initial values of the position.

Nozzles

For the patterns of particle trajectories in the nozzles, the continuation of the trajectories of the particles from the scroll were used. This was done because these trajectories indicated a good set of typical patterns and at the same time allowed the study of velocity lag and deviation angle at the exit from the stators. Figures 14 show the trajectories for specific sized particles, even though these particles may have gone through different nozzle passages. Because there are 29 nozzle blades, there are 29 nozzle passages. Therefore, the passage corresponding to a specific trajectory is indicated on the figure.

Figure 14a illustrates the trajectories of the smallest size particle considered in this particular study. The figure reveals that particles with characteristic lengths of 3 cm generally pass through the stator blades without striking the blade surfaces. Particles with characteristic lengths smaller than this would also be expected to demonstrate the same general motion.

Particles with characteristic lengths of 6 cm will follow trajectories similar to those illustrated in Figure 14b. This size particle generally tends to move through the nozzles passages without striking the blade surfaces, but its motion is less influenced by the gas flow and the response to changes in the gas motion is slower. Therefore, some of these particles will bounce occasionally off the pressure surface of the nozzle blades. These bounces occur at impact angles that are quite small.

Similar trajectories were plotted for particles with characteristic lengths of 15 cm and 30 cm. These trajectory traces showed the same general trends as Figure 14a with the exception that a few of the particles initially struck the suction surface. These particles then bounced over to the pressure surface side of the passage and then out of the nozzle passage exit. The impacts on both the suction and pressure surfaces of the blade occured with impact angles of moderate size.

Figure 14c shows the trajectories of particles with characteristic lengths of 60 cm. These larger particles are less influenced by the gas than the smaller particles, and the figure shows the tendency of the particle to travel from the pressure surface of the blade and impact on the suction surface of the blade. The impacts on both of these surfaces tend to be at even steeper angles, and the figures reveal that most of the particles then entering the turbine can be expected to strike the blade surface. It should be noted that all of these particles entered the same nozzle flow passage. This results from the fact that these particles all follow the scroll contour until they encountered the suppressed scroll. This caused all of these particles

to bounce with approximately the same angle into the nozzle region. This same result is observed in the trajectories for particles with characteristic length equal to 30, 60 and 150 cm, and implies that all the particles of this size range that enter the turbine can be expected to do erosion damage to a few of the nozzle blades near the scroll exit.

The trajectories that were studied for the case where the characteristic length of the particle was 150 cm indicated the same general type of trajectories as the ones shown in Figure 14c.

Finally, Figure 14d illustrates the trajectories found for very large, massive particles as they enter the nozzle passages. Because the trajectories of these particles are dominated by inertial forces, they tend to bounce many times before passing through the stator passages. The bounces that do occur, happen with impact angles that are quite steep and with velocities that are relatively low.

Table 5 lists the velocity lag and deviation angle at the exit from the nozzles. As expected, the velocity lag decreases rapidly as the particle size increases. Within the data for velocity lag, it can be observed that there is no trend that can be related to the initial velocity of the particle at the scroll inlet. In addition, the deviation angle still shows a fairly wide distribution for the larger particles. This wide distribution is caused by the apparent random nature of the bounces.

After these particles leave the nozzle passages, they enter the free vortex between the nozzles and the rotor. Some of the particles did not penetrate to the rotor, but instead reentered the nozzle passages near the nozzle trailing edges. Other particles entered the rotor at relatively low velocities, only to be struck by it and accelerated to high velocities. These particles then travelled radially outward.

The results presented in subsequent sections of this report will reveal that particles with characteristic lengths of 3 cm

did not tend to penetrate the vortex. The motion of these particles as they reentered the nozzle passage is shown in Figure 15a. This illustrates that these particles are influenced sufficiently by the gas flow to turn away from the trailing edges of the nozzle blades if there is adequate distance available. Those particles that do strike the nozzle surface do so with moderate angle and high velocity.

Similar plots for particles with characteristic lengths of 6 and 15 cm, which also did not tend to enter the rotor, indicated that particles of these sizes would strike the nozzle trailing edge surface with many high velocity, moderate angle impacts.

Figure 15b indicates the trajectories of particles with characteristic lengths of 30 cm. The results presented in the subsequent sections of this report will reveal that this size particle tends to pass through the vortex, into the rotor, and then to be struck by the rotor and accelerated radially outward against the incoming gas. These particles were assumed to leave the rotor with a velocity equal to the wheel speed of the rotor. The figure indicates that particles of this size strike the trailing edges of the nozzle blades with high velocity and at a moderate angle.

Similar traces of the trajectories of particles with characteristic lengths of 60, 150, and 300 cm, indicated the same results, that is, particles of these sizes tended to enter the rotor and accelerated to quite high velocities. These particles then travelled radially outward to impact on the trailing edges of the nozzle blades with high velocity and a moderate impact angle.

It should be noted that all the particles included in this study, except for an occasional very small particle, tended to strike the trailing edges of the nozzle at a moderate angle and with a high velocity.

Vortex

The results that are presented in this section for the trajectories the particles follow as they enter the vortex, use the same particles that have been traced through the scroll and nozzle regions of the turbine. This was done because the vortex is an easily defined flow field and because the trajectories yielded a good set of patterns. In the figures, all the trajectory traces were begun at the same point, even though the angular position is quite different in each case. This causes no change in the type of movement that occurs because the flow field is axisymetric.

Figure 16a illustrates the trajectories that occurred for the particles that have a characteristic length of 6 cm. These particles tended to move through the vortex without entering the rotor. The pattern that occurs in this figure results from the slightly different exit directions of the particles as they leave the nozzle passage.

Similar results, not shown herein, are indicated for particles with characteristic lengths of 3 cm. For this smaller particle, the particle exit velocity magnitude and direction all tended to be approximately the same, and as a result, these smaller particles did not show a spread in trajectories.

A pattern of trajectories that is very similar to the one indicated in Figure 16a also occurred for particles with characteristic lengths of 15 cm. The exception that did occur is that one of these larger particles did enter the rotor. This apparently occurred because the particle bounced off the suction surface of the nozzle blade and had a steeper inlet angle as it entered the vortex.

The trajectories that occur for particles with characteristic lengths of 30 cm are indicated in Figure 16b. More of these particles tended to penetrate all the way through the vortex and to enter the rotor. These particles tended to bounce more on the pressure and suction surfaces of the nozzle blades, and therefore,

these particles tended to have a greater distribution of inlet angles than the smaller particles. The figure reveals that because these larger particles do not accelerate sufficiently in the nozzle passages, they do not have a tangential velocity great enough to cause the centrifugal force to change the radial motion of the particle.

Particles that had characteristic lengths of 60 and 150 cm generally showed the same patterns of trajectories as the particles that are indicated in Figure 16b. Because these particles also tended to bounce off both the pressure and suction surfaces of the nozzle blades, the patterns of the trajectories in the vortex appear to have a distribution, with some of the particles entering the rotor, and some of the particles passing through the vortex and back into the nozzle blades.

Finally, Figure 16c indicates that the trajectories occur for the very large particles with characteristic lengths of 300 cm. All of these particles entered the rotor with very little change in the direction of the particle motion as the particle crosses the vortex.

Figures 16 indicate that most of the smaller particles tend not to penetrate to the rotor, but instead pass out of the vortex to restrike the nozzle trailing edges. However, as the particle size increases, more particles tend to penetrate into the rotor passages. This result was not anticipated before it occurred and is caused by the steeper inlet directions of the larger particles because of their impacts on the nozzle blades as these particles pass through the nozzle passages.

Table 6 gives the results of velocity lag and deviation angle as the particles leave the vortex. The table includes both those particles that entered the rotor and those particles that did not penetrate to the rotor. Of interest is the fact that the magnitude of the velocity lag has not changed appreciably from the values that resulted at the exit from the nozzles. However, the

deviation angle still shows quite a wide spread in magnitude because of the random nature of the bounces that occurred in the nozzle passages.

Rotor

Before the solutions to the trajectories in the scroll and nozzles had been obtained, the patterns of trajectories in the rotor were studied. This study included a wide range of particle sizes, with the most significant and illustrious examples corresponding to particles with characteristic lengths of 3, 6, and 15 cm. The study assumed inlet velocities at the rotor tip of one half the gas velocity, and velocity directions that were in the same direction as the gas. Table 7 compares the values of velocity lag and deviation angle between those assumed in this study and those that resulted from observation of particles through the scroll, nozzles, and vortex. As indicated, for the case with δ = 15 cm, the value assumed is quite close to that which occurs in the study. For the other cases, it should be noted that the results presented here are probably conservative because the particle would tend to have a slightly greater velocity.

The meridional view of the rotor with the solution streamlines resulting from the quasi-orthogonal method are shown in Figure 17. This grid of quasi-orthogonals and streamlines was used in the solution of the particle trajectories.

Figure 18 shows the initial position that each size particle was given and illustrates the five initial locations that were used in order to get a distribution of trajectories. This figure illustrates the starting points of the trajectories that are plotted in the meridional plane or axial view, respectively.

Figures 19a and b show the trajectories of particles that had δ = 15 cm. The figures illustrate the fact that these particles do not pass through the rotor. In addition, for particles that enter near the suction surface of the rotor blade, the particles

are struck by the rotor blade before they can be pushed out of the rotor by centrifugal forces. All the particles with characteristic length greater than 15 cm showed the same tendency, with the number of particles that are struck by the blade increasing as the characteristic length increases.

The trajectories that result when the characteristic length is 6 cm are shown in Figures 20a and b. The meridional view of these trajectories illustrates the fact that these particles move near the shroud and then tend to scrape along the shroud as they pass through the rotor. Two of the trajectories in this figure were truncated after the first bounce, but all showed the same general tendency to scrape along the shroud. The end view, shown in Figure 20b, indicates that these particles are driven inward by the drag forces. In this figure, the movement of the particle in the positive θ direction is caused by the particle's inertia as it penetrates deeper into the rotor. As the radius decreases, the tangential component of the gas in the absolute reference frame decreases more rapidly than the particle tangential velocity. This delay in the particle velocity causes the positive θ motion when the trajectory is viewed with respect to the rotor, and in some cases, leads to particles that will strike the pressure surface of the blade.

As the particle size decreases, the particles tend more and more to follow the streamlines of the flow. This action tends to prevent many of the particles from striking the blade surfaces. Figures 21a and b illustrate this phenomena for δ = 3 cm. Both meridional and end view figures show that the particles tend to follow the general pattern of the streamlines, and thus to cause less erosion damage. Studies done for the smaller characteristic lengths showed the same tendencies.

Figure 22 shows the trajectories of particles that are near the threshhold size. Indicated on this figure is the value of δ_{TIP} for each of the particles considered. Those particles that correspond to $\delta_{TIP} > 7.01$ cm were eventually pushed out the rotor

tip by the centrifugal force, and those particles that corresponded to $\delta_{TIP} < 6.40$ cm eventually passed through the rotor. The particle with $\delta_{TIP} = 6.71$ cm orbited the axis at a radius of 7.12 cm for at least three orbits, and represented the threshhold particle size. The discrepancy between this threshhold size of particle and the $\delta_o = 0.5$ cm size particle is probably caused by the overreaction of particle motion at the inlet to the rotor. Indeed, particles of the $\delta = 6$ cm size did not penetrate into the rotor. Therefore, the applicability of δ_o has not been negated by this study.

Particle Velocity Lag and Deviation

The primary purpose of the study of the particle trajectories through the scroll, nozzle, and vortex regions was to gain an understanding of the variation in velocity lag, ζ, and the difference between the particle velocity direction and the gas velocity direction.

Figure 23 shows the velocity lag that occurred at the scroll exit, at the stator exit, and as the particle left the vortex. It should be noted that the motion out of the vortex includes particles that enter the rotor and also those particles that return to re-enter the nozzle passage.

With the information presented in Figure 23, the velocity lag can be expressed as a function of the particle characteristic length. This can then be used to determine the limit characteristic length δ_L for this particular turbine. The results are plotted on a curve of δ_L versus δ, as shown in Figure 24. This figure indicates that all particles of the size range considered in this study would tend to accelerate radially outward, because the value of δ would always be greater than δ_L. In addition, the data seems to indicate that all particles will always have a

tendency to accelerate radially outward. This result implies that the other special value of characteristic length, the orbit characteristic length, is a more realistic measure of the size of particles that will always penetrate the rotor.

Finally, Figure 25 shows the variation in deviation angle versus characteristic length. This figure indicates a greater distribution of deviation angle as the particle size increases, which is caused by the more random nature of the bounces that the larger particles experience. In addition, the larger particles seem to have a greater negative deviation angle, which causes them to penetrate the vortex regions and enter the rotor with less difficulty.

ANALYSIS OF POSSIBLE DESIGN MODIFICATIONS

This section of the report considers several special ideas that might have value in terms of preventing the accumulation of particles near the radial turbine rotor tip.

Particle Trajectories in a Turning Vortex

One idea for the elimination of erosive particles from the region between the rotor and the nozzles of a radial, inflow turbine, is to combine a set of annular nozzles, such as exists in an axial flow turbine, with a radial inflow turbine rotor. Figure 26 shows a schematic of such a configuration. The air from the burners would pass through the axial type nozzles, causing it to whirl as it enters the 90° bend. The whirling air would then drive the radial inflow turbine rotor. Such a design can be used to make a smaller diameter engine and would eliminate the scroll type inlet that exists on most radial inflow turbines.

Such a configuration might offer advantage of increased turbine operating duration because the erosive particles could

possibly be removed from the region between the nozzles and the rotor by installing a trap that would capture the particles as they were thrown out of the rotor.

The purpose of this study was to investigate the theoretical trajectories of particles in the turning vortex. Such a study will show the size of the particles that will penetrate the inward flowing vortex, and the area on the shroud of the turning vortex where the trap could most efficiently be placed in order to capture the particles.

It is necessary to determine the fluid solution in order to know the gas velocity components at each point in the flow field, because these components have a significant influence on the motion of the particles. A compressible fluid solution was obtained. Basically, the solution assumes that there is no variation in $\lambda = V_u r$ along the streamlines, although the value of λ at different streamlines may be different, and that there is a linear variation in the radius of curvature of the streamlines between hub and shroud. The ability to vary λ from hub to shroud allows one to use the fact that for constant exit angle blades, the tangential component of velocity varies as $V_u = \text{constant}/r^n$ where $n = \sin^2 \alpha$ (11). Figure 27a indicates the streamlines for the solution that resulted and Figure 27b gives the inlet and exit mean velocity diagram.

The trajectories that would result from particles having 50% of the gas velocity at the inlet were studied, for δ's in the range $1.5 < \delta < 300$ cm, and for particles that entered at 20%, 40%, 60% and 80% of the hub to shroud distance.

The study includes a set of cases where the particle travels against the gas flow in the turning vortex, as would occur when the particle is thrown out of the rotor. The rotor inlet radius is 7.52 cm, and the region between the exit from the turning vortex, at a radius of 8.38 cm and the inlet to the rotor was assumed to be a free vortex.

Figures 28a through 28h show the meridional view of the inward turning vortex and the trajectories of particles that enter the flow filled with a velocity equal to 50% of the gas velocity. These figures correspond to particles with δ's from 300 cm to 1.5 cm, and cover the general range of interest in this study. Figure 28a shows the trajectories that resulted with δ = 300 cm. Of interest in this figure is the fact that the particles never penetrate the vortex, but are thrown outward by centrifugal forces. Trajectories were also studied for δ = 1500 cm and δ = 3000 cm, but these cases were not significantly different from the case with δ = 300 cm. Perhaps the most important information to be learned from this part of the study, is that for particles having δ equal to or greater than 300 cm, as in Figure 28a, the particles would not enter the rotor, but would remain trapped between the axial stator blades and the rotor. These particles would cause large amounts of erosion on the trailing edges of the stators and in very dusty environments would accumulate until blockage occured causing a corresponding decrease in the engine performance. The addition of a particle trap on the shroud surface of the vortex in the form of a slot sealed to prevent gas leakage would decrease the resulting erosion to the stator blades and prevent the accumulation of particles that collect in this region.

Figure 28b shows the trajectories of particles with δ = 150 cm. The particles shown tend to bounce many times before they eventually achieve enough kinetic energy to overcome the centrifugal force. Eventually, all of these particles are driven by the gas flow into the free vortex between r = 8.38 cm and r = 7.52 cm. The motion of these four particles in the turning vortex is considered later in this report.

Figures 28c through 28f show the same types of trajectories for various particles in the range $6 < \delta < 60$ cm. In all of these cases, the particles strike the shroud surface, which would indicate that a properly located trap would capture some of the particles.

Finally, Figures 28g and 28h show that as smaller and smaller values of δ are used, the particles tend more and more to follow the streamlines and thus to not be subject to capture by this method.

Figures 29a and 29b indicate the continuation of the trajectories of the particles that are shown in Figures 28b and 28c respectively. As indicated, the particles which had δ = 150 cm tended to eventually go all the way through the vortex, but these trajectories, which are shown in Figure 29a, did not penetrate the free vortex that existed near the inlet to the rotor. On the other hand, for the case where δ = 60 cm, the trajectories, which are shown in Figure 29b tended to penetrate the vortex region and enter the rotor. This result means that the particles with δ greater than 150 cm will tend to accumulate in the vortex region of the turbine and thus to lead eventually to blockage of the gas flow.

Figure 30 shows the trajectories of particles that enter against the inward flowing vortex in a way that would simulate their motion out of the rotor. The turbine presently under consideration for erosion treatment has an equivalent rotating speed of 30,000 rpm. The trajectories indicated in the figure would result from particles that leave the rotor tangent to the rotor tip and with a tangential velocity the same as the wheel speed.

In the study indicated, the particle δ's ranged from 1.5 to 3000 cm. Even though the previous study of particles entering the turning vortex indicated that particles with $\delta > 300$ cm would not tend to enter the rotor, there are conceivable circumstances where such particles would make it through the turning vortex. Therefore, these larger sizes were included.

The figure shows that for values of δ greater than 60 cm, the particle trajectory deviated only slightly from a straight line. For values of δ equal to 30 and 15 cm, the trajectory starts to bend and the particle tends to be more tangent to the exit radius as it leaves the free vortex. For δ = 6 cm the particle spirals about the axis but finally leaves the vortex. For δ's less than

3 cm, the particle was driven back into the rotor within a few degrees of where it entered the vortex.

Based on this result, a series of trajectories were generated to consider the movement of particles in the turning vortex as they left the rotor inlet. In this study, the trajectories of particles with $\delta > 6$ cm were investigated and their inlet velocities were approximated by assuming the particle left the rotor tangent to the rotor tip and with a velocity equal to 100% of the wheel speed. This study represents the continuation of the trajectories of the particles that are indicated in Figure 30.

Figures 31a through 31c show the trajectories of such particles for the three cases where δ = 300, 150, and 60 cm. For δ = 300 cm the particles would bounce all the way through the vortex. Previous results with this same size particle indicated that these particles, if they were to enter the turning vortex, would not strike the rotor but would always tend to be thrown outward.

For δ = 150 cm, as indicated in Figure 31b, the particles of this size were eventually driven back into the turning vortex and would not overcome the gas flow.

Figure 31c shows the case where δ = 60 cm. In this case, the particles were driven back into the free vortex region after being thrown out of the rotor. This size particle would probably be trapped permanently near the inlet to the rotor, and could not be successfully captured by the turning vortex trap. Based on this result, the effectiveness of a turning vortex trap in capturing particles that become caught between the rotor and stators of a radial inflow turbine is limited to particles with a characteristic length equal to or greater than 60 cm. This would correspond to a silicon dioxide sand particle in this particular turbine with a diameter of about 100 microns. However, a significant amount of erosion would still be caused by particles with diameters in the 5 to 100 micron range and such particles could not be successfully eliminated from the region between the nozzles and rotor of this particular turbine.

Figure 32 shows the collection of information on the location where the particles bounced off the shroud. The most effective particle collector would be a slot centered at about 35 degrees, with the effectiveness increasing as the width of the slot increased. In practical cases, the increasing width of the slot would probably correspond to increasing losses to the flow and some distortion of the streamline. Such a situation would represent a trade off between the losses involved and the amount of erosion prevention that would occur.

In order to have some measure of the effectiveness of the slot, a hypothetical slot centered at 35° and of varying widths was placed on the shroud and the number of particles that bounced within the boundaries of this slot were counted. This number was divided by the total number of particles considered in this study to obtain an approximate measure of the effectiveness of such a trap in capturing particles. Figure 33 indicates the result of this study, and from this figure it can be seen that a slot width of about 20° centered at 35° would capture about 50% of the particles that entered the turning vortex for the first time. Those particles that were not captured at first would, depending on their size, pass into the rotor, or perhaps strike the nozzles and then bounce back into the turning vortex again with a 50% chance of being captured.

Effect of Forward Swept Rotor Blades

Another concept that has been proposed as a design method that might help prevent erosion damage to radial turbines is to contour the rotor leading edge in a way that would deflect toward the axis particles that struck the rotor tip. The following results are a study of the effects of rotor leading edge contouring in order to deflect the particles toward the center of the rotor.

In the computational model, the aerodynamic forces on the particles were neglected, and only the deflection phenomena that was caused by interaction with the rotor at various points in the

particle trajectory were considered. Because the aerodynamic forces always act in the inward direction, the results that are presented here are probably conservative. However, by neglecting these aerodynamic forces, it was not necessary to solve the gas flow field in this complicated and unconventional blade passage.

This particular study was done quite early in the research project and the results that are presented correspond to a rotor with a tip of 8.66 cm with a rotating speed of 40,000 rpm. Table 8 gives the blade contour that was used. Although the dimensions of this rotor and the rotating speed are slightly different from the terms that have been used in all other parts of this report, the nature of the results would not change in a geometrically similar turbine . In this particular study, normal and tangential restitution coefficients were taken as 0.9 and 1.0, respectively.

Figure 34 shows the types of trajectories that occur for an analysis of this type. These particles enter the rotor with an inlet angle of 70°. At the same instant that the particle enters the rotor, the rotor overtakes the particle and deflects it in the manner indicated in the figure. Also indicated on the figure is the penetration, which is defined as the ratio of the smallest radius that the particle achieves after impact on the rotor to the rotor tip radius. These curves indicate that the particle will penetrate farther into the rotor if its inlet velocity tends to be smaller. However, as the particle velocity increases, the effect of the forward swept blades is less. The figures also indicate that under certain conditions, such as in the unlikely case where the particle velocity is equal to the rotor tip velocity, the forward swept blade might not help to remove the particles from the rotor tip region.

Figure 35 illustrates the case where the particle inlet angle is 70° and the rotor does not overtake the particle until the particle has travelled to its smallest radius within the rotor region. As in the previous case, this figure illustrates that the slower moving particles could be expected to benefit most from the forward

swept rotor blade. Similarly, Figure 36 illustrates the case where the particle with the same inlet angle penetrates all the way across the trajectory before the rotor overtakes it. These trajectories show the same trends that the two previous figures showed.

The average value of the penetration from these curves versus the particle inlet velocity with the inlet angle as a parameter is plotted on Figure 37. This figure indicates that for the slower moving particles, the rotor tip has the effect of causing the particles to penetrate to about 80% of the tip radius for any inlet angle. In addition, as the velocity of the particle increases, those particles that tend to enter the rotor at larger angles tend to not penetrate as much.

EXPERIMENTAL RESULTS

To help with the understanding of this phenomena, an experimental radial inflow turbine configuration was designed to allow the use of high speed motion pictures of the trajectories of particles in the radial turbine. These films illustrate the phenomena of particles accumulating in the vortex region of the radial inflow turbine. Because of the relatively low performance levels of the experimental turbine, the films generally illustrate qualitatively the phenomena that occurs as particles enter the vortex and rotor tip region.

One of the first things that was noted in this study was that all the particles appear to move all the way around the scroll before they enter the last couple of passages of the nozzles. However, this is in agreement with the analytical results because particles that are large enough to be recorded on the film and distinguished when the film is developed are necessarily rather large particles.

A second observation that agrees with the analytical results is the motion of the particles in the free vortex region of the

turbine. These particles were observed to accumulate in this region of the flow and to strike the trailing edges of the nozzle blades with a large number of moderate angle impacts. Because the experimental turbine used here is a relatively low performance device, the velocities that occur in the vortex region were much smaller than the usual velocities in such regions.

Another observation that can be made from the movies is that the particles tended to accumulate in the vortex region of the flow, and after a relatively short period of time, there was a sufficient number density of particles to apparently block the flow. If such an event were to occur in a real turbine in operation in a very dusty environment, such a blockage would cause an almost instantaneous drop in the performance of such a turbine.

Several films were taken with the flat plate rotor installed. These films show, in addition to the previous observations, the apparent almost perpendicular impacts that occur on the rotor tips. This is in agreement with the results that were predicted by the analytic study of the particle trajectories in the rotor. Because the particles used in these films had rather high characteristic lengths, they would be expected to impact on the rotor in this way.

A study of the rotor dynamics were made from one of these films. Initially, the rotor speed was 2000 rpm. The rather large number flow rate of particles was started, and the particles started to accumulate in the vortex region. During this time, the rotating speed of the rotor decreased almost linearly, and when the particle flow rate was stopped, the rpm continued to decrease, reaching a minimum of about 750 rpm. This drop in rpm occurred within approximately 3 seconds, indicating the almost instantaneous decrease in performance that could be expected. The ratio of particle mass flowrate to total mass flowrate in this particular experiment was 0.63, which is a very high ratio and would be experienced in only the most extreme conditions in the field.

Another film was used to accumulate data on the trajectories of particles through the nozzle regions of the turbine. The test

configurations did not use a rotor in this particular experiment and the velocity at the nozzle exit was 0.320 times the critical velocity and had an angle of about 70°. The data accumulated included plots of several trajectories as the particles entered the turbine configuration, the measurements of the velocity lag at the end of the scroll, and at the interface between the vortex and the nozzles.

Figures 38a through 38c illustrate the trajectories that occur in this region of the experimental turbine. These particles were 2000 micron particles having a specific gravity of about 1.1. Based on the inlet condition to the tunnel, the characteristic length is about 290 cm, which is within the range of the particle sizes that were considered in the analytical work. In some of these figures, every other frame is used to locate the particle so that the trajectory might be more easily observed. The time between points is indicated to clarify the distance, measurements that can be made from trajectory plots such as these.

Figure 38a illustrates some trajectories that are typical of those that occurred during the movie. The increasing distance between the points as the particle moves through the nozzles and into the vortex illustrates the acceleration in the tangential direction that occurs. These trajectories also show a difference from the types of trajectory that occurred in the analytical work. However, the nozzles that were used in that configuration required a greater amount of turning of the flow than these particular nozzle blades. These trajectories are selected because of their general nature.

Figure 38b shows some of the trajectories that bounce more as they enter these nozzles. Generally, these trajectories were typical of some of the worst bouncing particles that occurred, and yet the particles appear to pass through the nozzle passages quite easily. This figure also shows a particle in the scroll. This particle is accelerating and during the time that it was observed,

it accelerated uniformly from 0.85 of the gas velocity to 0.93 of the gas velocity.

Figure 38c shows some of the trajectories that were observed in the vortex. These particles have previously entered the vortex and are not moving about within the vortex region. The figures indicate the moderate angle impacts that seem to occur on the trailing edges of the nozzles. Measurements of the velocities of these particles indicated that maximum velocities in the vortex region were about 50 to 60% of the gas tangential velocity. This is lower than what would have been expected, and is probably caused by the plastic bounces that occur on the nozzle blades.

Measurements of the velocities of the particles at the end of the scroll and as the particles left the nozzle passages were made to compare with the previous analytical results. Figure 39 illustrates the curves that resulted from the previous study of the analytical turbine for the velocity lag as a function of the characteristic length. The difference between the analytic result at the scroll exit and the data that resulted from these experiments is probably caused by the fact that these particular particles had rather plastic impacts on surfaces, and therefore, lose a great deal of momentum when they strike the scroll contour.

The comparison of the data collected here and the results from the analytic turbine are closer and the differences could possibly be caused by the differences in the nozzle configuration of the two turbines. It is also worth noting that the data spread that occurs at these locations is similar to the data spread that occurred in the analytic turbine. This data spread is caused by the more random nature of the trajectories of the particles that bounce many times off the scroll and nozzle surfaces.

DISCUSSION OF THE RESULTS

The purpose of this research has been to study the trajectories of erosive particles in radial inflow turbines and to investigate the effectiveness of design modifications in removing these particles from the rotor tip region.

The first part of this study considered the trajectories of particles in a radial inflow turbine, and included trajectory patterns in the scroll, the nozzles, the vortex between the nozzles and the rotor, and in the rotor blade passages.

In order to describe the types of impacts that occur as the particles strike the surfaces of the turbine, the following terminology will be used. The incidence velocities of the particle with respect to the surface will be referred to as relatively low velocities, relatively moderate velocities, and relatively high velocities. The low velocities correspond to incidence velocities in the range from 0 to 46 meters/sec. The moderate velocities correspond to incidence velocities in the range from 46 to 122 meters/sec, and the high velocities correspond to incidence velocities in the range greater than 122 meters per second. Generally, the high velocities that the particle achieves are caused by the acceleration that occurs when the particle impacts the rotor blade. In this particular analytical turbine, the top speed of the equivalent cold gas turbine rotor is about 242 meters/sec. This represents an approximate upper limit on particle velocities.

A similar terminology will be used to describe the incidence angles. The term low incidence angles will correspond to incidence angles between 0° and about 15°. The term moderate incidence angles will correspond to incidence angles between approximately 15° and 60°, and the term high incidence angles will correspond to incidence angles greater than 60°.

Investigation of the trajectories in the scroll indicated that the particles with characteristic lengths of 30 cm or greater tended to move radially outward until they impacted the scroll with

relatively low velocity and small incidence angle impacts. Once the impact occurred, the smaller particles tended to scrape along the scroll surface bouncing many times and travelling very short distances between the bounces. As the particle size increased, the particles tended to travel longer distances between the bounces, and there were fewer bounces as a result as the particle travelled around the scroll. These larger particles, with characteristic lengths of 150 and 300 cm, were observed to strike the scroll contour with low velocity, but more moderate incidence angle impacts.

It was observed from these trajectories that most of the particles with characteristic lengths from 30 to 150 cm struct the portion of the scroll contour that is usually suppressed to prevent it from interfering with the scroll inlet. The more rapid change in the curvature at this location causes the particle to suddenly bounce with a more moderate impact angle at the location where the scroll contour and the suppressed contour intersect. Because most of the particles of this size range struck this relatively small area, this region of the scroll might sustain more erosion damage.

Reference 8 reported a series of experiments on a turbine engine with controlled injection of erosive sand particles. In this report, the authors indicate that their turbine scroll eroded through, even though the particle number densities in the air were quite moderate. Based on information included in the report, an estimate was made of the corresponding characteristic length of dust sizes that were used in that test program. This yielded approximate dust sizes with characteristic lengths in the range from 0 to 40 cm. This figure is in general agreement with the results indicated from the analytic trajectories presented here for the scroll.

As the particles enter the nozzles, the smaller ones, with characteristic lengths of 3 and 6 cm, tend to follow the streamlines and not strike the nozzle blades, while the larger particles, with characteristic lengths greater than 15 cm, tend to strike both the pressure and suction surfaces. Most of these impacts were of

relatively small velocity, because the particle did not have sufficient time to accelerate to the high velocities that occur in this region, and the impacts occurred with moderate impact angles. In addition, because most of the particles of sizes sufficiently large to cause erosion on these blades, also follow the scroll contour until they strike the suppressed contour, most of the particles tended to enter only a few of the nozzles passages near the end of the scroll. These nozzle blades would then be more likely to experience erosion damage than most of the other nozzle blades. However, these impacts are of nominal interest because they are only capable of causing erosion by particles that pass through the nozzles a single time.

A more severe mechanism of erosion occurs on the trailing edges of the nozzle blades that face the rotor. Particles with characteristic lengths of 0.5 cm or larger do not pass through the rotor. These particles accumulate in the vortex region and have a tendency to strike the nozzle blade trailing edges. Some of the particles with characteristic lengths of 3 cm that reenter the nozzle passage flow field from the free vortex strike the trailing edges of the nozzles with velocities that are relatively high and with relatively small incidence angles. Other particles of this size were small incidence angles. Other particles of this size were turned away from the nozzle blades and reentered the free vortex without striking the nozzle trailing edge.

In addition, some particles with characteristic lengths between 6 and 150 cm tended to enter the rotor, while other particles passed through the vortex to reenter the nozzle flow field without penetrating to the rotor. Most of the particles with characteristic lengths greater than 150 cm tended to enter the rotor. However, all of these particles exhibited the same types of trajectories as they struck the trailing edges of the nozzle blades. They all strike this surface with relatively high velocity, moderate angle impacts.

These results are in agreement with comments in References 7 and 8 which report on experimental programs that used real turbine engines with controlled ingestion of erosive particles. These reports indicated that the greatest amount of erosion damage occurred on the trailing edges of the nozzle blades. The results presented in the present study indicate that these surfaces of the nozzle blades were subjected to impacts from particles that did not strike the scroll surfaces, and also from particles that failed to enter the rotor. In addition, the larger particles that are moving relatively slow as they enter the vortex region have a tendency to penetrate to the rotor which then accelerates these particles to relatively high velocities.

As the particles leave the nozzles, they enter the vortex region. The study of the particles passing all the way through the scroll, nozzles, and then the vortex revealed that most of the smaller particles, in the range of characteristic lengths from 3 to 15 cm, did not tend to penetrate to the rotor, while larger particles with characteristic lengths greater than 15 cm did have a tendency to enter the vortex in such a way that these larger particles penetrated to the rotor. This was caused by the fact that these particles tended to enter the vortex at smaller angles than the gas flow due to bounces off the suction surface of the nozzle blades. These more massive particles with smaller inlet angles were then not able to accelerate to the large tangential velocities that are required for outward motion.

In the rotor, the trajectories of these larger particles that penetrate through the vortex and enter the rotor, are modified as the rotor overtakes the slower moving particle. Because of the relatively slow velocity of the particle and the quite high velocity of the rotor blades, these impacts occur with relatively high incidence velocities and at relatively high incidence angles. After impact, the particle suddenly has a very large tangential velocity, and this causes centrifugal forces that are large enough

to cause the particle to move radially outward quite soon after the impact. These particles continue their radial motion until they strike the trailing edges of the nozzle blades.

Data on the velocity lag that occurred as a set of particles passed through various stations of the flow indicated that the velocity lag could be related to the particle characteristic length. This data was used to evaluate the limit characteristic length, and the results indicated that the characteristic length was always greater than the limit characteristic length. In addition, the data indicated trends that imply that this would always be so over a very wide range of particle sizes. The implication of these results is that the limit characteristic length is not a worthwhile parameter in determining the sizes of the particles that will not penetrate the radial turbine. A more realistic term would be the orbit characteristic length.

Several possible design modifications that might lead to a reduction in the amount of erosion that occurs in the radial inflow turbine by removing erosive particles that accumulate in the vortex-rotor tip region were investigated.

One design modification that seems to lend itself to the removal of particles in the turbine is the use of a turning vortex. Such a design would allow the installation of a pocket that might capture particles which became accumulated in the vortex region. A study of the trajectories in such a flow region revealed that particles with characteristic lengths of 60 cm and smaller could be expected to penetrate this turning vortex region and enter the rotor blades. In addition, particles with characteristic lengths of about 150 cm or larger could be expected, if they entered the rotor, to be bounced outward by the rotor, and to travel against the gas flow back into the turning vortex. However, there appeared to be a range of particle sizes, with characteristic lengths between 60 and 150 cm, where the particles could not be successfully removed if they penetrated into the free vortex region before the rotor. Particles with characteristic lengths between about 60 and

0.5 would probably orbit the axis in this region, accumulating until the flow became blocked. Particles with characteristic lengths smaller than about 0.5 cm would probably pass through the rotor without striking the rotor blades.

In addition, the study revealed that in this particular turning vortex, a slot as indicated on Figure 32 would have a 50% probability of capturing particles with characteristic lengths greater than 150 cm at all times, and in addition, would capture about half the particles with characteristic lengths between 6 and 60 cm that entered the turning vortex region. The particles that were not captured would then tend to accumulate in the free vortex before the turbine rotor.

Another design modification that has been proposed for helping to reduce the erosion problem is a forward swept rotor blade. Such a configuration would tend to deflect particles toward the axis of the rotor where they would be more likely to pass out of the rotor exit. A study of this effect revealed that particles of larger sizes, with characteristic lengths in the range greater than about 150 cm, could be deflected to about 75% of the tip radius regardless of their inlet direction. This suggests that the forward swept rotor tip may be beneficial for the removal of some of the particles that collect in the vortex region of the turbine.

Experimental results in the form of high speed motion pictures that show the motion of particles in the nozzle, vortex, and rotor tip regions of a radial inflow turbine confirm the results that have been presented for the analytical turbine. Data from one of these films also indicates the same general trend predicted by the analytical study for the ratio of the particle velocity and the gas velocity at the exit from the nozzles.

Figure 40 illustrates the general sizes of particles that will cause erosion in the various areas of the turbine, and in addition, shows the sizes of particles that would probably benefit from the use of the turning vortex and the forward swept rotor blade.

These results apply to the particular model turbine used in this study, and different turbine sizes and geometries might yield slightly different results on the sizes of particle that could be expected to cause erosion. However, most radial inflow turbines are relatively small, and therefore, these results should provide the designer with an approximate understanding of the sizes of particles that will probably cause erosion damage and the nature of the impacts that occur.

CONCLUSIONS

The purpose of this research has been to study the trajectories of particles in radial inflow turbines and to investigate the possible value of several design modifications that might be used to reduce the severity of erosion.

The study of trajectory patterns in the scroll revealed that particles with characteristic lengths greater than 30 cm tended to move radially outward and would strike the outer edges of the scroll contour with a large number of low velocity, low angle impacts. In addition, most of these particles would impact with low velocity, moderate angle impacts on the portion of the scroll that is suppressed to prevent interference with the scroll inlet. This relatively small area of the scroll contour would be subject to a more severe erosion problem.

Investigation of the trajectories in the nozzles indicated that most of the particles with characteristic lengths greater than 30 cm would cause erosion of a few of the nozzle blade passages near the scroll exit. These particles appear to strike the pressure and suction surface of the nozzle blades with a low velocity and moderate angle impacts. The study also indicated that the trailing edges of the nozzle blades would be subjected to a very large number of high velocity, moderate angle impacts by any particles with characteristic lengths greater than 0.5 cm. This results because these particles tend to accumulate in the vortex region, and

the larger particles that do enter the rotor are struck by it and accelerated to very high tangential velocities.

The study indicated that the particles with characteristic lengths greater than about 60 cm tended to enter the rotor passages with very small velocities, about 10% of the gas velocity at the rotor inlet, but were quickly overtaken by the rotor and suddenly accelerated to very high tangential velocities. These particles struck the rotor tip with very high velocities, with respect to the rotor tip, and with very high incidence angles.

Finally, the study of the trajectories of particles in the turning vortex and the influence of a forward swept blade revealed that although not completely effective in removing particles from the rotor tip regions, these modifications would help to remove some of the particles that accumulate at this location.

REFERENCES

1. Clevenger, W.B., and Tabakoff, W., "Erosion in Radial Inflow Turbines - Volume I: Erosive Particle Trajectory Similarity," NASA CR-134589, Lewis Research Center, 1974.
2. Clevenger, W.B., and Tabakoff, W., "Erosion in Radial Inflow Turbines - Volume II: Balance of Centrifugal and Radial Drag Forces on Erosive Particles," NASA CR-134616, Lewis Research Center, 1974.
3. S.L. Soo, "Gas Dynamic Processes Involving Suspended Solids," AIChe Journal, September, 1961.
4. W.S. Bailey, E.N. Nilson, R.A. Serra, and T.F. Zipnik, "Gas Particle Flow in an Axisymmetric Nozzle," ARS Journal, June, 1961.
5. M.F. Hussein and W. Tabakoff, "Gas-Particle Suspension Properties on a Blade-to-Blade Stream Surface of a Cascade Nozzle," Project Themis Report No. 70-17, University of Cincinnati, December 1970. AD-715971.
6. W. Tabakoff and M.F. Hussein, "Trajectories of Particles Suspended in Fluid Flow Through Cascades," Journal of Aircraft, Volume 8, No. 1, January 1971.
7. G. Grant and W. Tabakoff, "Erosion Prediction in Turbomachinery Due to Environmental Solid Particles," AIAA Paper No. 74-16, 1974.
8. J.E. Montgomery and J.M. Clark, Jr., "Dust Erosion Parameters for Gas Turbines," SAE Paper No. 538, 1962.
9. H.E. Shoemaker and C.P. Shumate, "Techniques for Reducing Sand and Dust Erosion in Small Gas Turbine Engines," SAE Paper No. 700706, September 1970
10. T. Katsanis, "Use of Arbitrary Quasi-Orthogonals for Calculating Flow Distribution in the Meridional Plane of a Turbomachine," NASA TN D-2546, 1964.
11. Shepherd, Principles of Turbomachinery, The MacMillan Company, Toronto, Ontario, Canada, 1956.

LIST OF SYMBOLS

A	Area - meters^2.
$\bar{a}$, a	Acceleration - meters/second^2.
C_D	Drag coefficient.
$\bar{D}$	Drag force - newtons.
D	Diameter - meters.
d/dt	Rate of change with respect to the inertical reference frame - 1/second.
$\bar{e}$	Unit vector.
F	Centrifugal force - newtons.
$\bar{F}$	General force vector - newtons.
g	Acceleration of gravity - meters/second^2.
m	Mass - kilograms.
$\bar{q}$	General vector of arbitrary orientation.
$\bar{r}$, r	Vector and scalar forms of radius - meters.
$Re=\frac{\rho_g V D_p}{\mu_g}$	Reynolds number.
t	Time - seconds.
$\bar{V}$, V	Vector and scalar forms of velocity of the gas with respect to the particle - meters/second.
w	Velocity of the gas with respect to the rotating reference frame - meters/second.
$\bar{W}$	Weight force - newtons.
z	Axial distance - meters.

Greek Symbols

α	Angle of meridion l velocity vector with respect to radial direction, shown in Figure 10 - degrees.

β	Angle of velocity vector with respect to meridional velocity, shown in Figure 10 - degrees.
T	Ratio of specific heats.
$\delta/\delta t$	Rate of change with respect to the rotating reference frame - 1/seconds.
$\delta=\frac{10}{3}\frac{\rho_p D_p}{\rho_g}$	Characteristic length - meters.
δ_o	Orbit characteristic length, defined by Equation 27 - meters.
δ_L	Limit characteristic length, defined by Equation 29 - meters.
ζ	Velocity lag, the ratio of the velocity of the particle at a location to the velocity of the gas at the same location.
θ	Angular position - radians.
ρ	Density - kilograms/meter^3.
σ	Angular position of the verticle axis of the turbine with the gravitational verticle axis. Indicated in Figure 11 - degrees.
ϕ	Angular position of the turbine's axis with respect to the gravitational horizonal axis, indicated in Figure 3 - degrees.
$\bar{\Omega}$	Rotational velocity vector - radians/second.
ω	Rotational speed - radians/second.

Subscripts

cr	Represents property evaluated at critical conditions.
g	Represents gas property.
p	Represents particle property.
r	Component in the radial direction.
θ	Component in the tangential direction.
t	Represents stagnation conditions.

tip	Represents term evaluated based on properties at the rotor tip.
u	Component in the tangential direction.
z	Component in the axial direction.

Superscripts and other Symbols

*	Represents properties evaluated at critical conditions.
-	Bar - Indicates vector quantity.

Table 1. Description of the Model Turbine Used in the Analytic Study

Description	Station (See Fig 2)	Radius cm	Axial Span cm	Radial Span cm
Scroll Inlet - Mean	1	17.1145	12.1920	12.1920
Contoured Vortex Inlet	2	11.0185	2.2053	-
Nozzle Inlet	3	9.7993	0.8053	-
Free Vortex Inlet	4	8.3567	0.8053	-
Rotor Inlet	5	7.5209	0.8053	-
Rotor Exit - Mean	6	3.5177	-	2.4637

Table 2. Description of the Model Turbine Used in the Experimental Study

Description	Station (See Fig 7)	Radius cm	Axial Span cm	Radial Span cm
Scroll Inlet - Mean	1	17.996	8.458	8.458
Contoured Nozzle Inlet	2	13.767	1.905	-
Nozzle Inlet	3	11.227	1.270	-
Free Vortex Inlet	4	8.689	1.270	-
Rotor Inlet	5	8.382	1.270	-
Rotor Exit	6	5.842	1.270	-

Table 3. Characteristics of Particles Used in the Analytic Study

Code Designation	Characteristic Length cm	Velocity Lag at Scroll Inlet V_p/V_g	Initial Radial Position cm
3- 50- 25	3	50	14.0665
3- 50- 50	3	50	17.1145
3- 50- 75	3	50	20.1625
6- 50- 25	6	50	14.0665
6- 50- 50	6	50	17.1145
6- 50- 75	6	50	20.1625
15- 50- 25	15	50	14.0665
15- 50- 50	15	50	17.1145
15- 50- 75	15	50	20.1625
30- 50- 25	30	50	14.0665
30- 50- 50	30	50	17.1145
30- 50- 75	30	50	20.1625
60- 50- 25	60	50	14.0665
60- 50- 50	60	50	17.1145
60- 50- 75	60	50	20.1625
150- 50- 25	150	50	14.0665
150- 50- 50	150	50	17.1145
150- 50- 75	150	50	20.1625
300- 50- 25	300	50	14.0665
300- 50- 50	300	50	17.1145
300- 50- 75	300	50	20.1625
3- 0- 50	3	0	17.1145
3-100- 50	3	100	17.1145
30- 0- 50	30	0	17.1145
30-100- 50	30	100	17.1145
300- 0- 50	300	0	17.1145
300-100- 50	300	100	17.1145

Table 4. Particle Velocity and Direction at Scroll Exit

Code Designation	Magnitude of Velocity V_p/V_g	Deviation Angle from Direction of Gas Degrees
3- 50- 25	1.000	0.31
3- 50- 50	1.000	0.31
3- 50- 75	1.000	0.31
3- 0- 50	1.000	0.31
3-100- 50	1.000	0.31
30- 50- 25	0.964	-29.05
30- 50- 50	0.965	-29.95
30- 50- 75	0.959	-31.44
30- 0- 50	0.976	-28.93
30-100- 50	0.955	-32.40
300- 50- 25	0.823	-21.65
300- 50- 50	0.832	-18.04
300- 50- 75	0.886	-67.87
300- 0- 50	0.750	-59.84
300-100- 50	0.950	-30.97

Table 5. Particle Velocity and Direction at Stator Exit

Code Designation	Magnitude of Velocity V_p/V_g	Deviation Angle from Direction of Gas Degrees
3- 50- 25	0.803	- 4.51
3- 50- 50	0.737	- 3.81
3- 50- 75	0.780	- 4.30
3- 0- 50	0.737	- 3.81
3-100- 50	0.738	- 3.86
30- 50- 25	0.290	-13.46
30- 50- 50	0.291	-17.76
30- 50- 75	0.330	- 8.43
30-100- 50	0.266	-22.49
300- 50- 25	0.103	-14.17
300- 50- 75	0.090	-38.45
300- 0- 50	0.103	-20.97
300-100- 50	0.103	-50.30

Table 6. Particle Velocity and direction at Vortex Exit

Code Designation	Magnitude of Velocity V_p/V_g	Deviation Angle from Direction of Gas Degrees
3- 50- 25*	0.803	32.35
3- 50- 50*	0.737	31.26
3- 50- 75*	0.780	31.53
3- 0- 50*	0.737	31.24
3-100- 50*	0.739	31.28
30- 50- 25*	0.259	7.91
30- 50- 50*	0.260	- 2.99
30- 50- 75	0.330	35.21
30-100- 50*	0.237	-10.16
300- 50- 25	0.092	5.24
300- 50- 75	0.080	-31.41
300- 0- 50	0.092	- 8.24
300-100- 50	0.091	-45.32

* Indicates particle that does not enter rotor.

Table 7. Comparison of Analytic Results and Assumption of Particle Motion at the Rotor Inlet

Particle Characteristic Length cm	Analytic Results		Assumed Values	
	Velocity Magnitude V_p/V_g	Deviation Angle Degrees	Velocity Magnitude V_p/V_g	Deviation Angle Degrees
3	0.75*	31*	0.50	0
6	0.65*	31*	0.50	0
15	0.43	2	0.50	0

* Data based on particle exit from the vortex into the nozzles because no particles of this size penetrated to the rotor.

Table 8. Blade Contour Used in Study of Forward Swept Blades

Radius cm	Angle θ Degrees
6.062	0.0
7.361	0.98
8.656	4.62

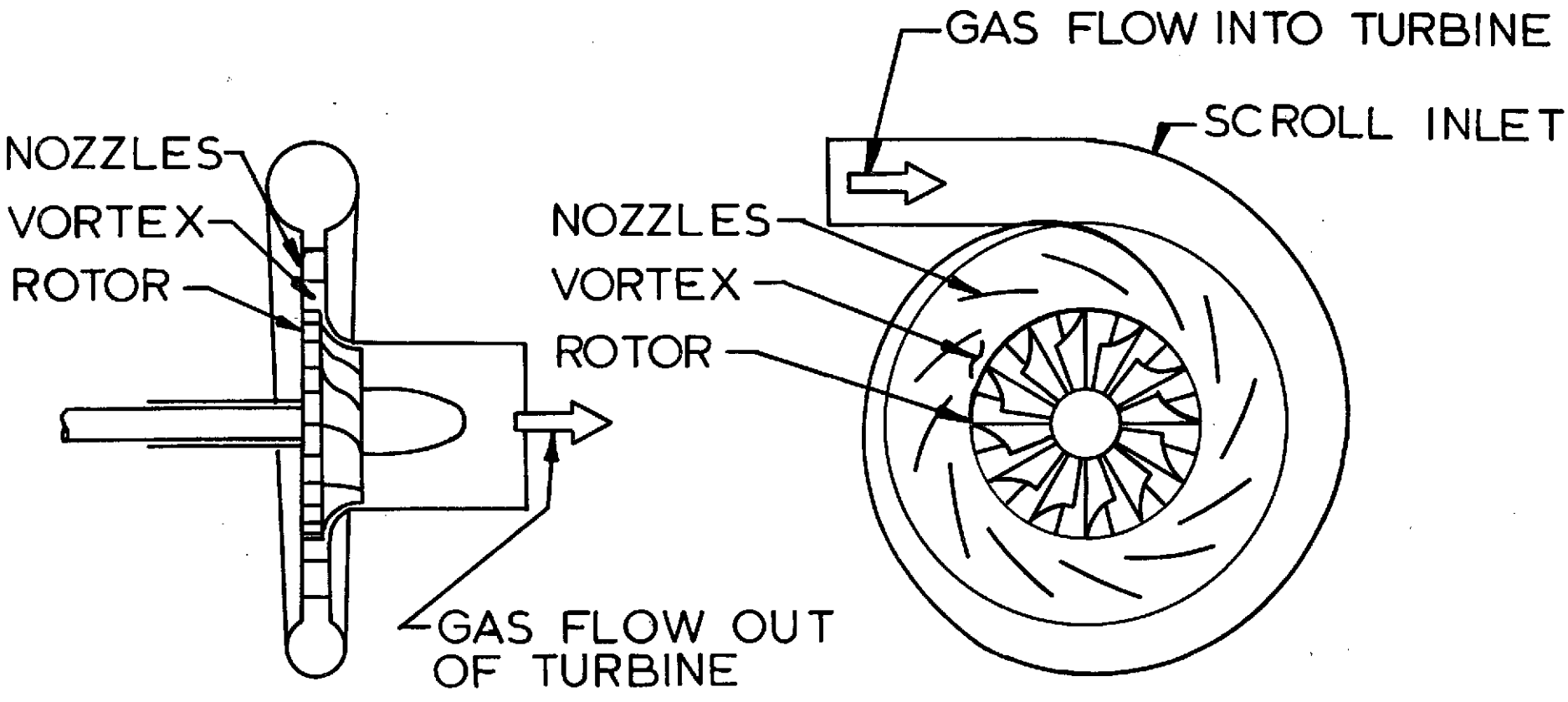

FIGURE 1. SCHEMATIC OF TYPICAL RADIAL INFLOW TURBINE.

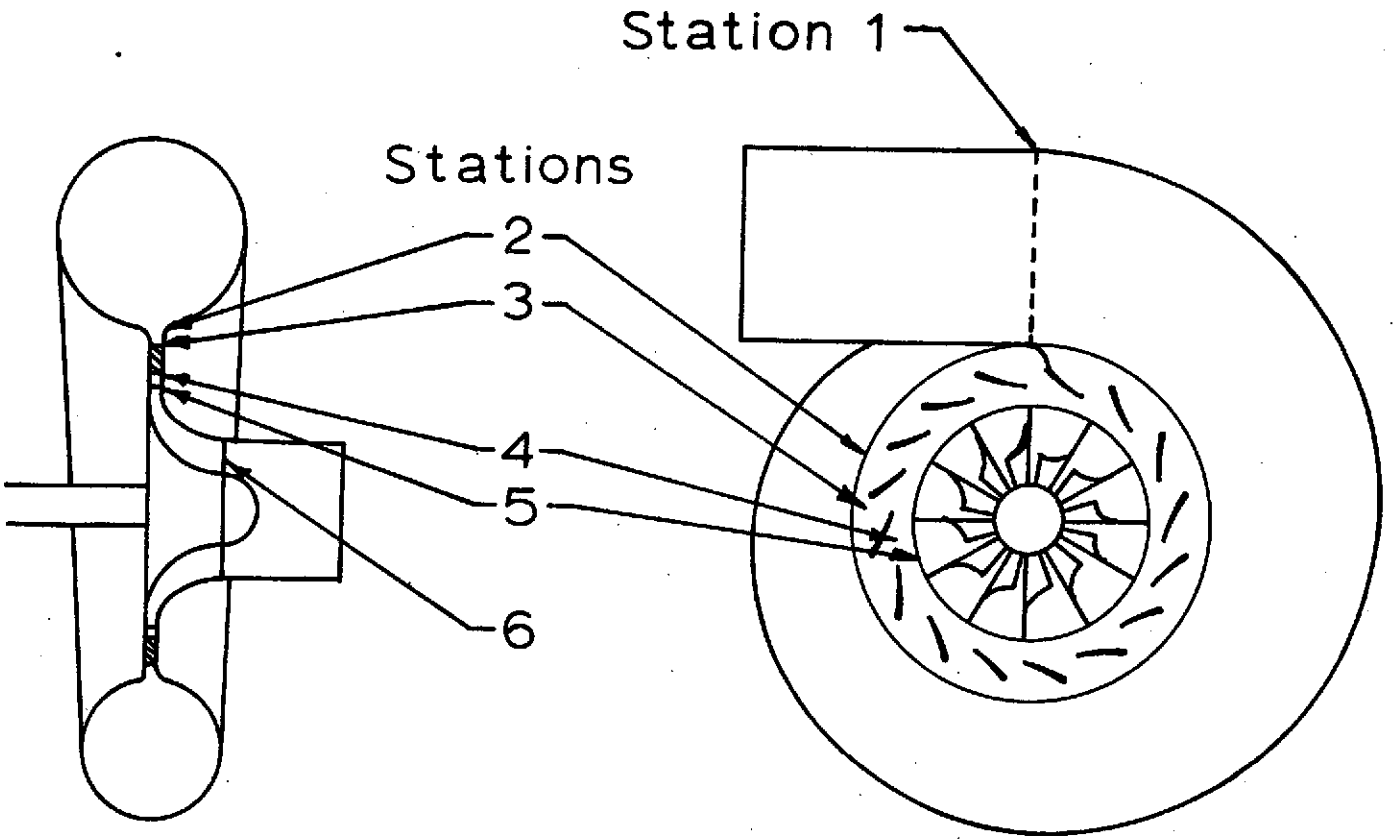

FIGURE 2 TURBINE MODEL USED IN ANALYTICAL STUDY

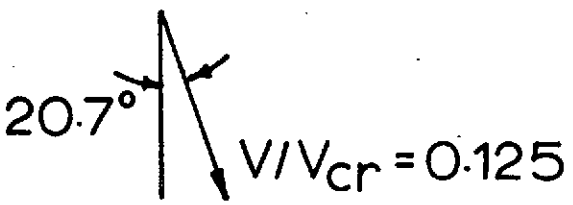

Nozzle Inlet R = 9.799 cm

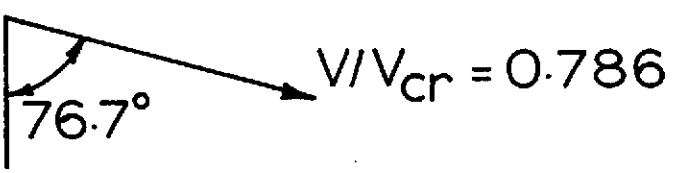

Nozzle Exit R = 8.357 cm

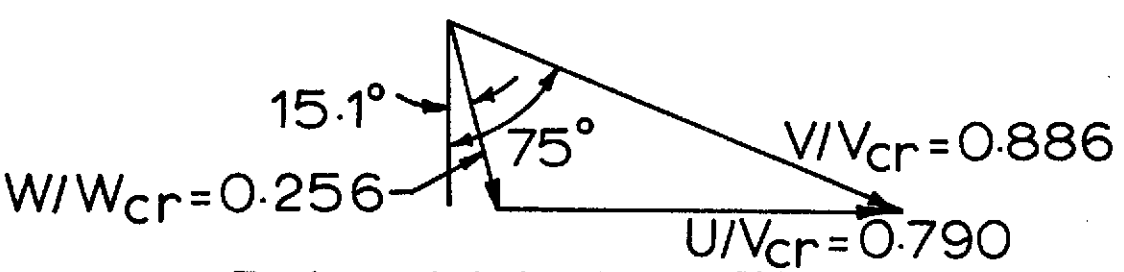

Rotor Inlet R = 7.521 cm

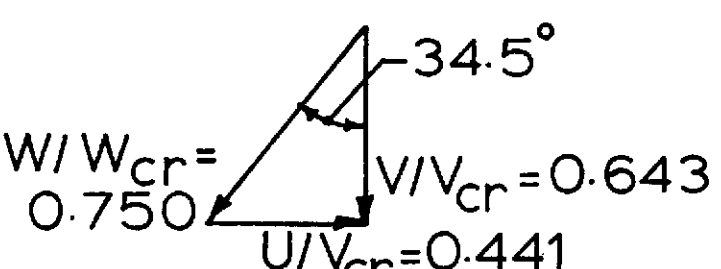

Rotor Exit Mean R = 3.518 cm

FIGURE 3 VELOCITY DIAGRAMS

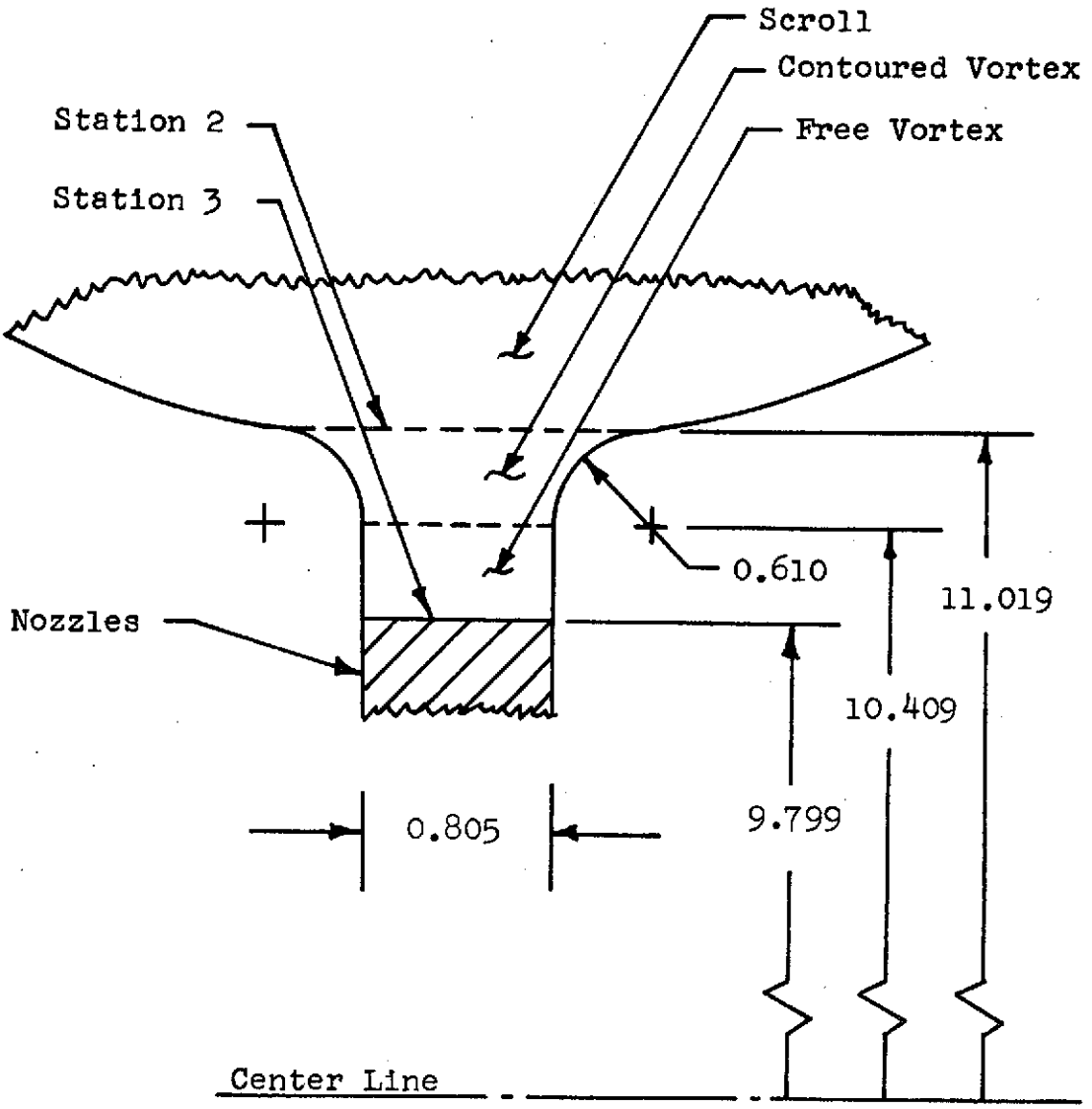

Dimensions in Centimeters

FIGURE 4. CONTOURED VORTEX REGION BETWEEN NOZZLES AND SCROLL

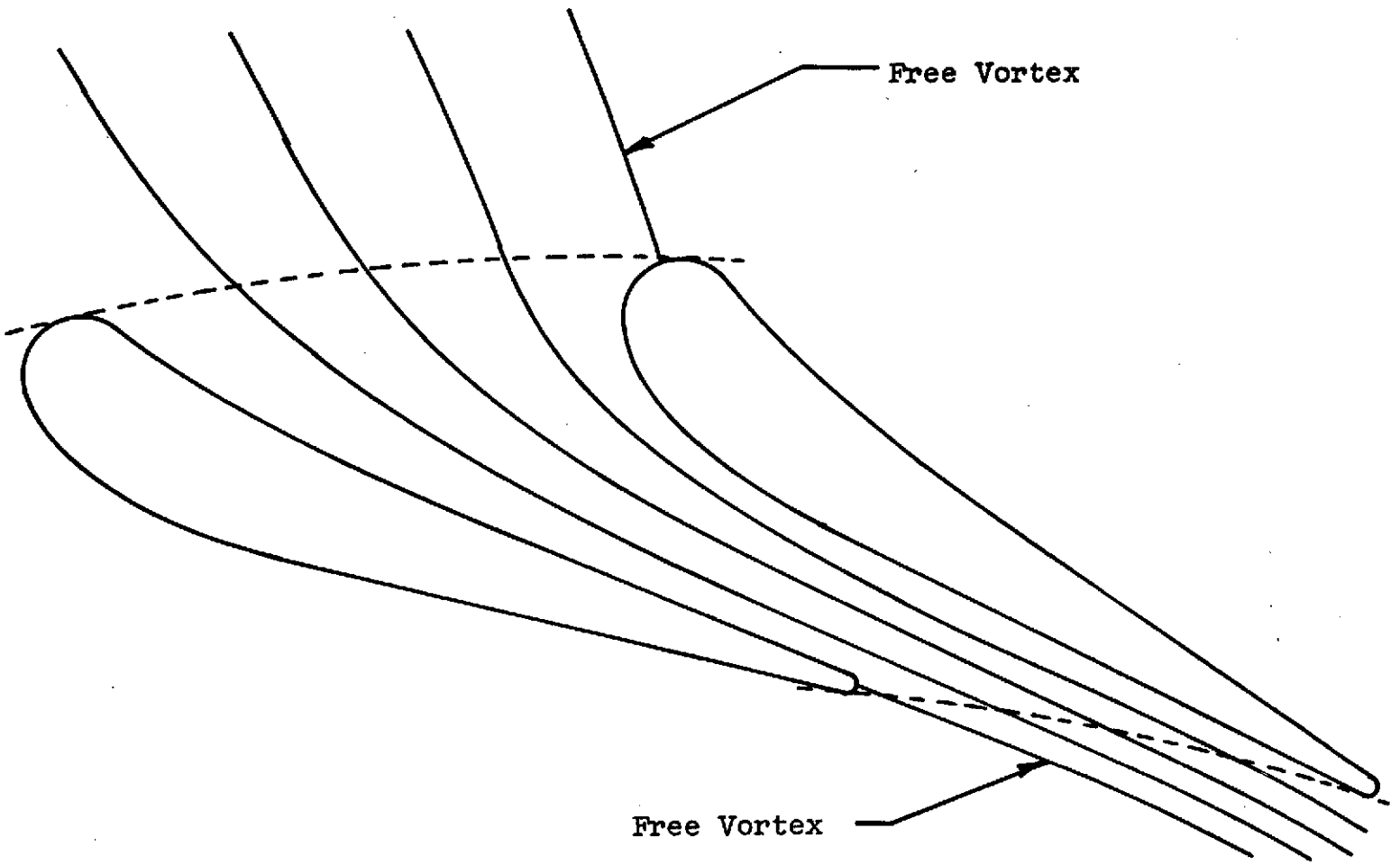

FIGURE 5. NOZZLE BLADE SHAPE AND SOLUTION STREAMLINES

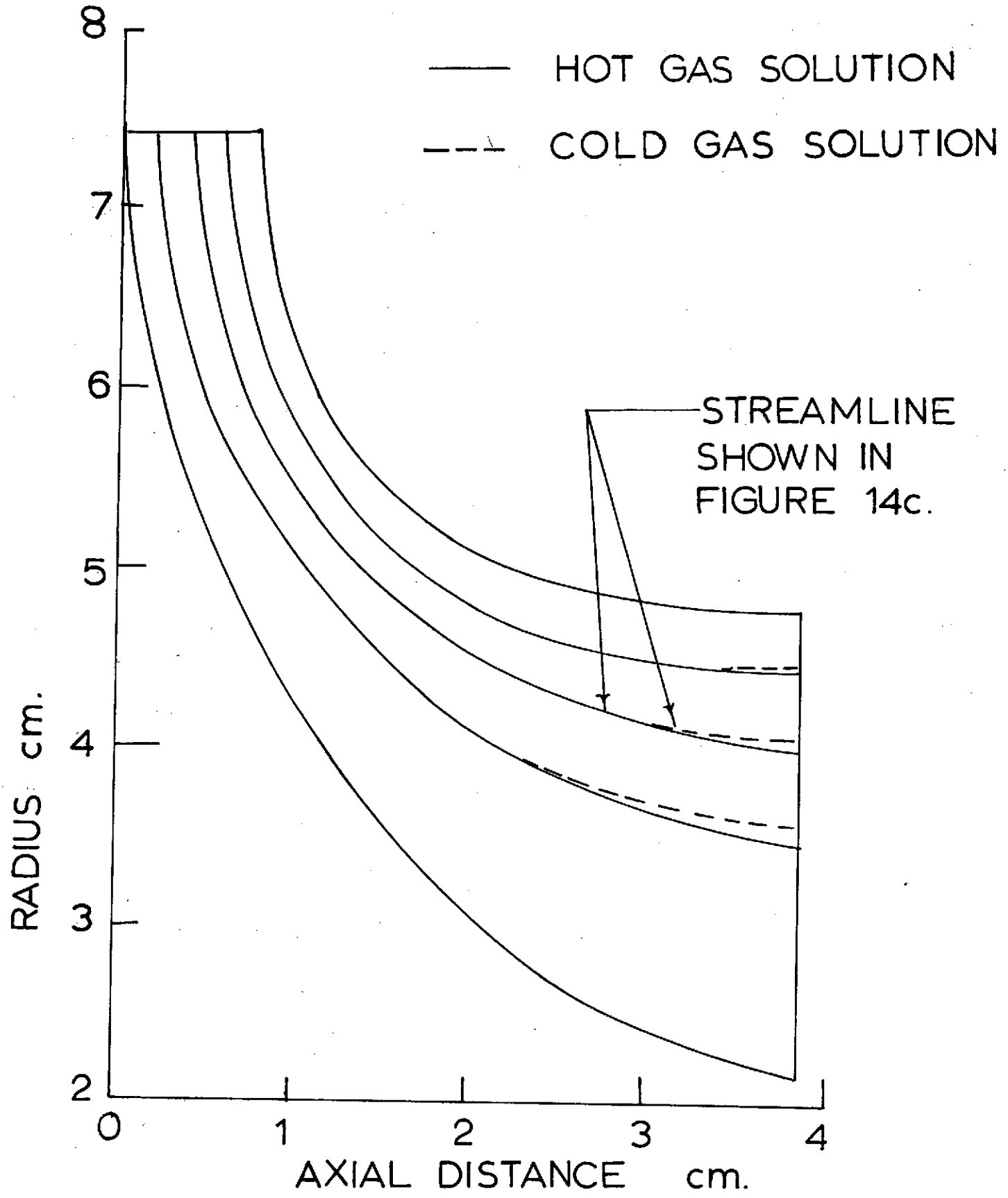

FIGURE 6a MERIDIONAL VIEW OF ROTOR

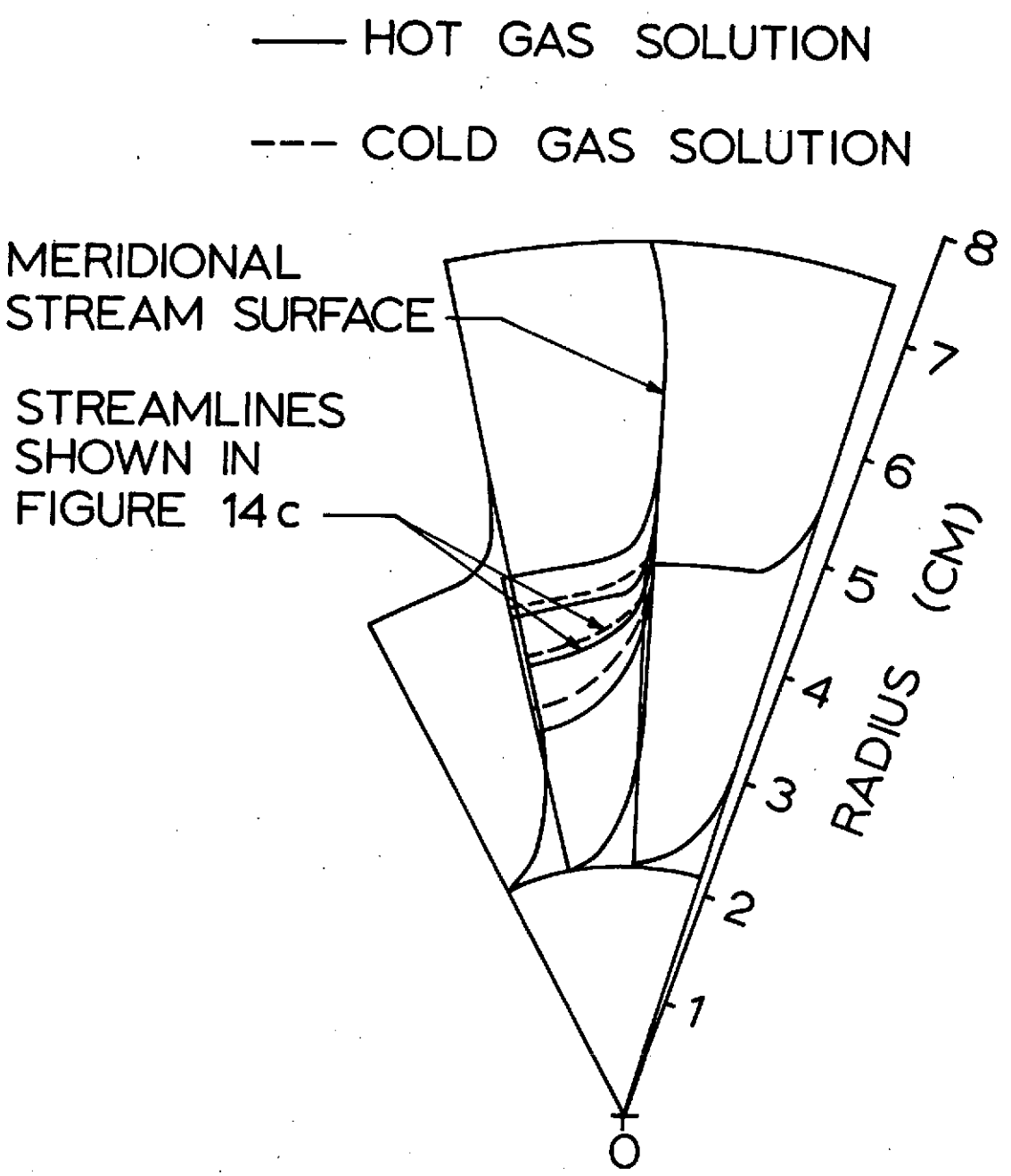

FIGURE 6b. AXIAL VIEW OF ROTOR WITH RESPECT TO ROTATING REFERENCE FRAME.

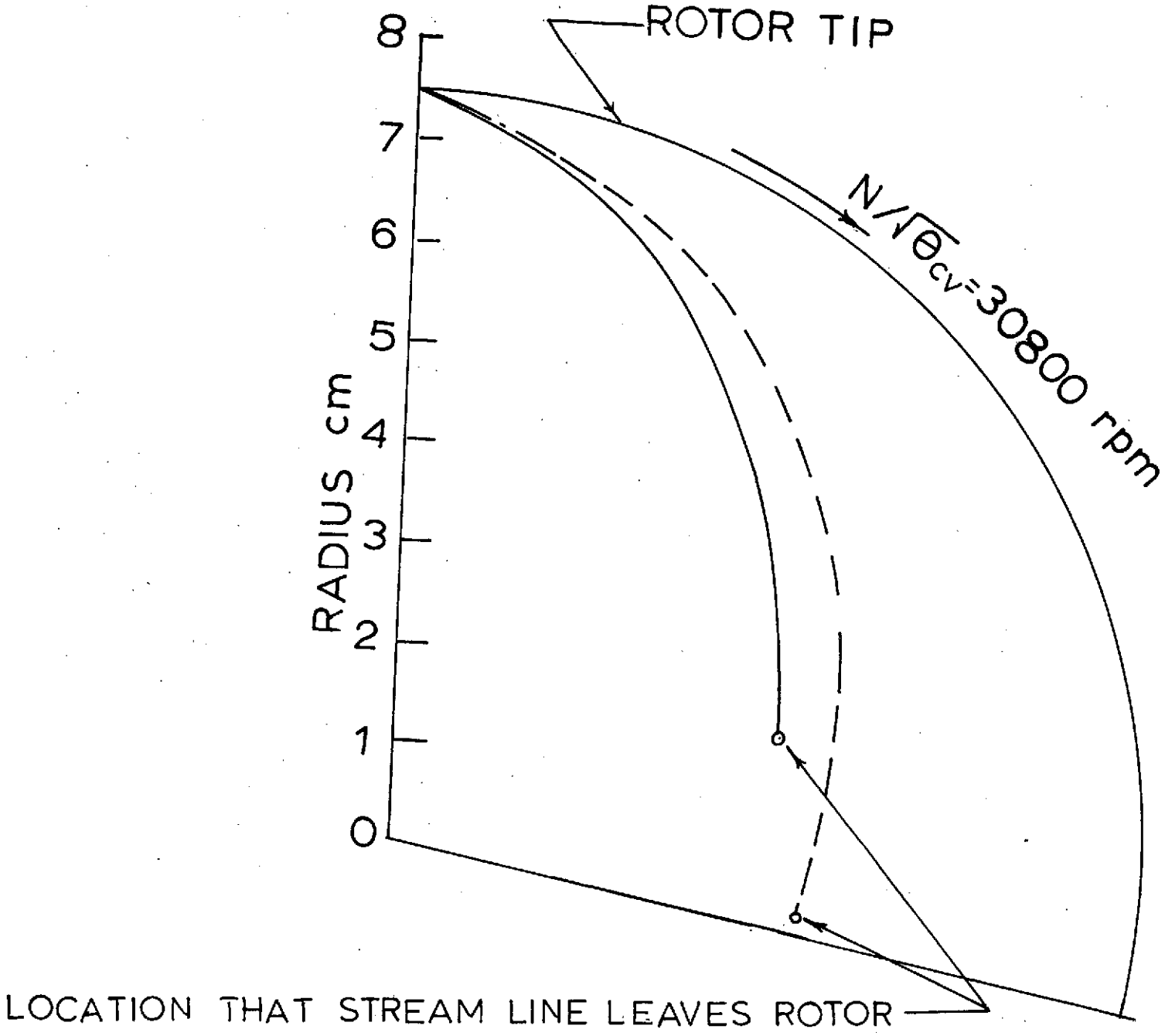

FIGURE 6c AXIAL VIEW OF ROTOR WITH RESPECT TO NON-ROTATING REFERENCE FRAME.

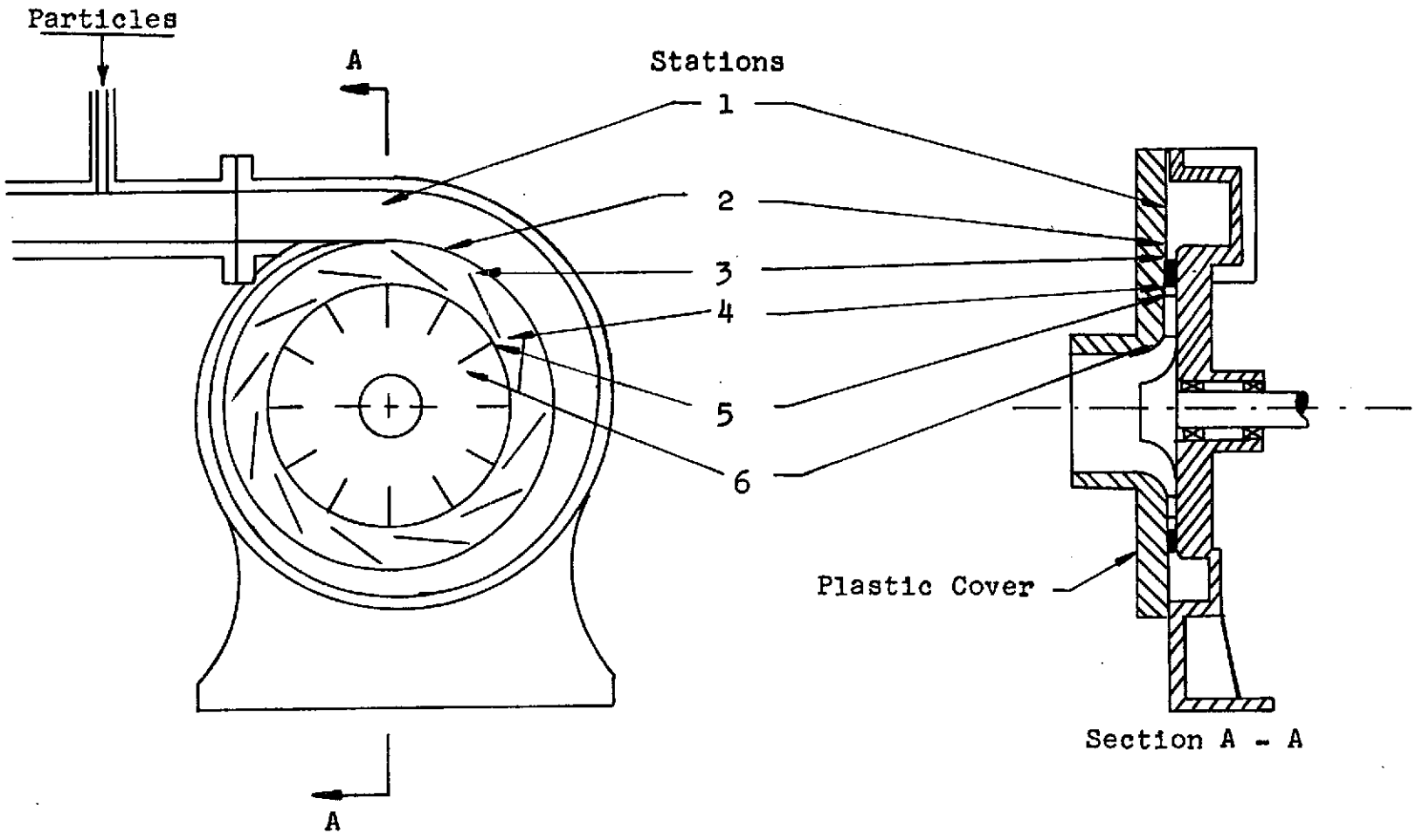

FIGURE 7. EXPERIMENTAL TURBINE CONFIGURATION.

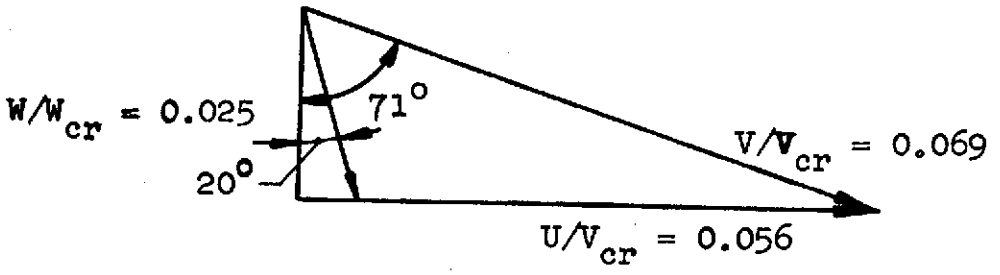

FIGURE 8. EXPERIMENTAL TURBINE VELOCITY DIAGRAM.

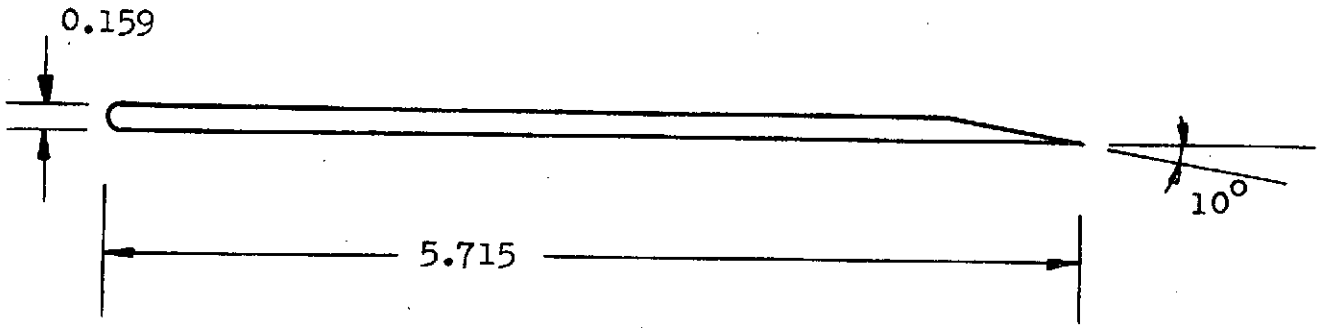

FIGURE 9. EXPERIMENTAL TURBINE NOZZLE BLADES.

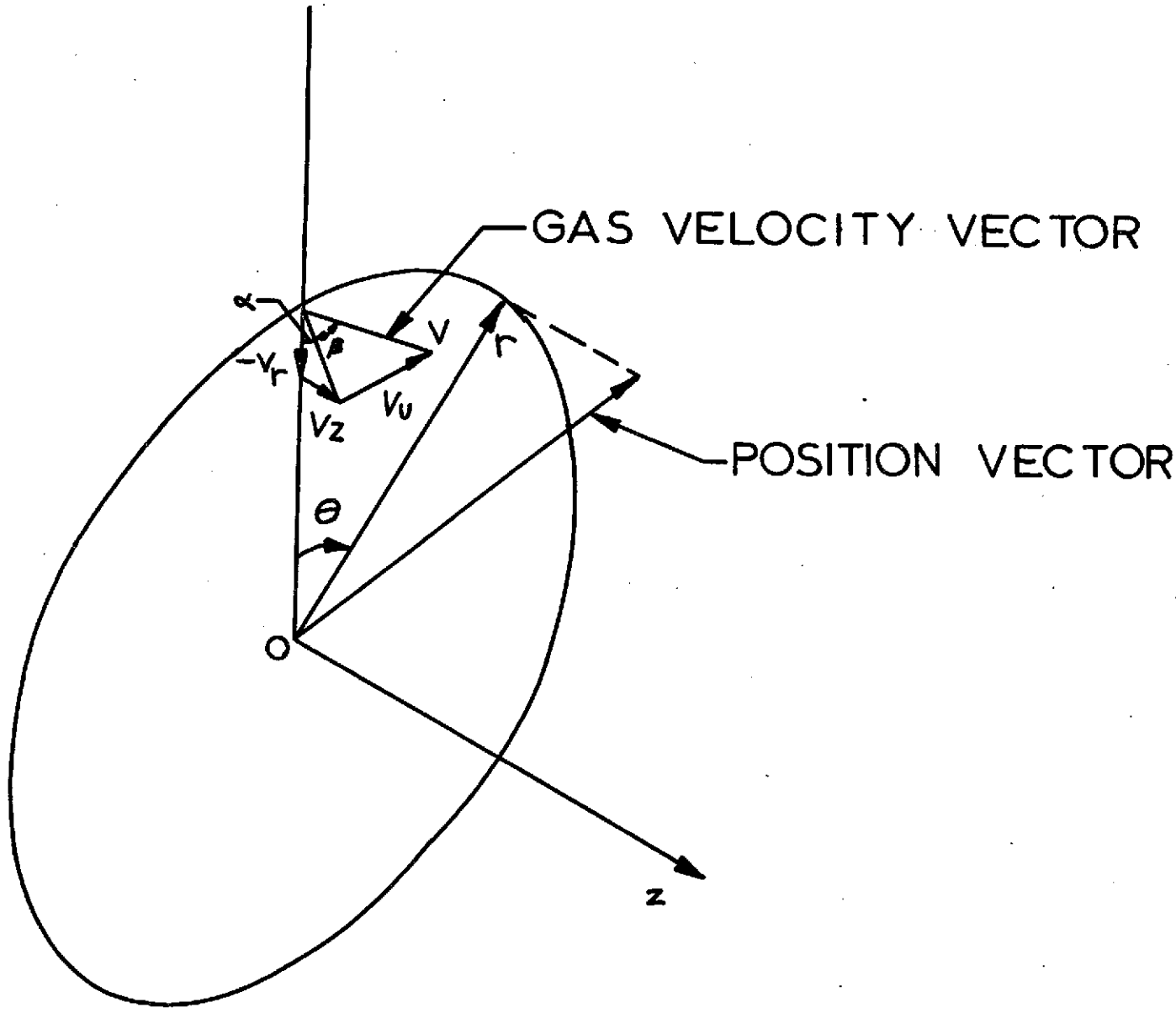

FIGURE 10. COORDINATE SYSTEM AND TYPICAL GAS VELOCITY COMPONENTS.

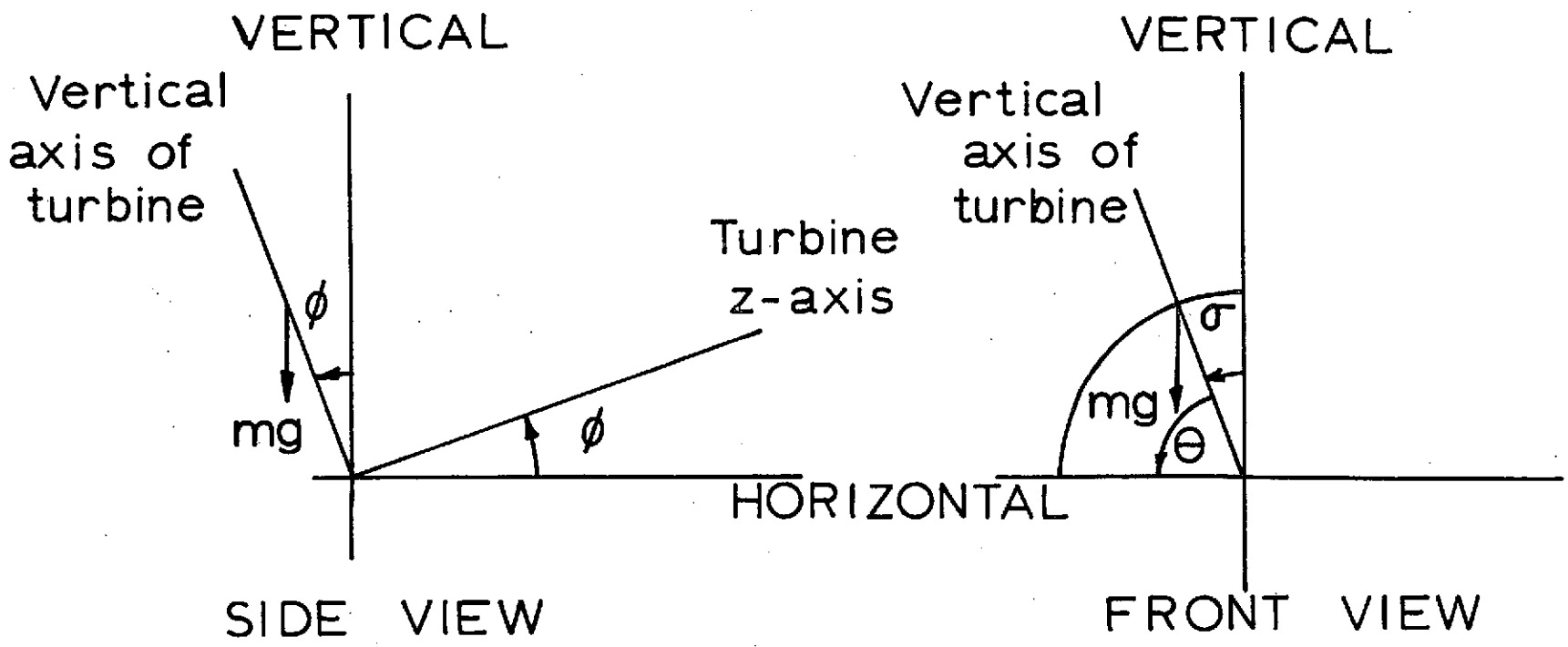

FIGURE 11 Orientation Coordinates

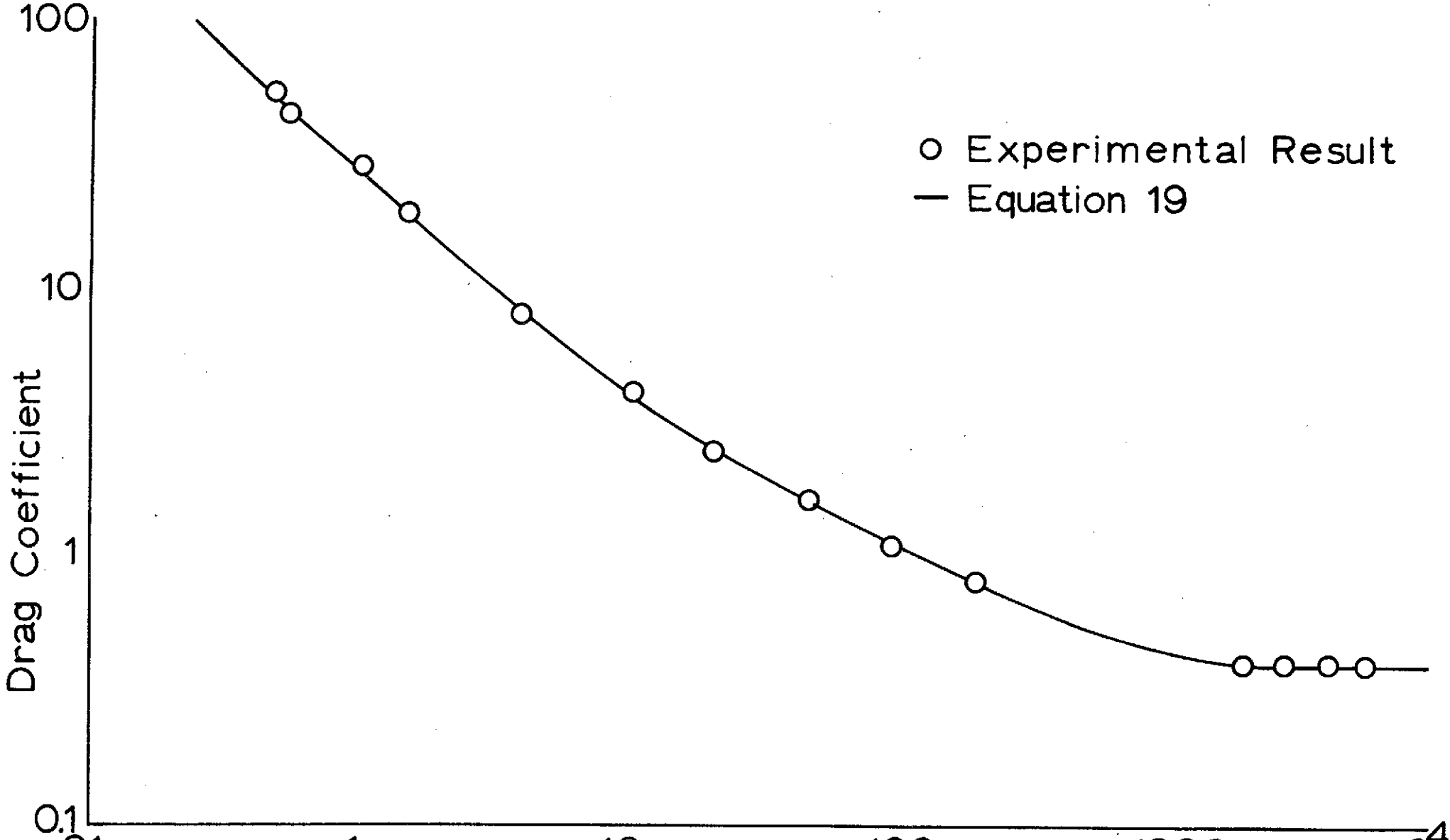

FIGURE 12 DRAG COEFFICIENT FOR SPHERICAL PARTICLE

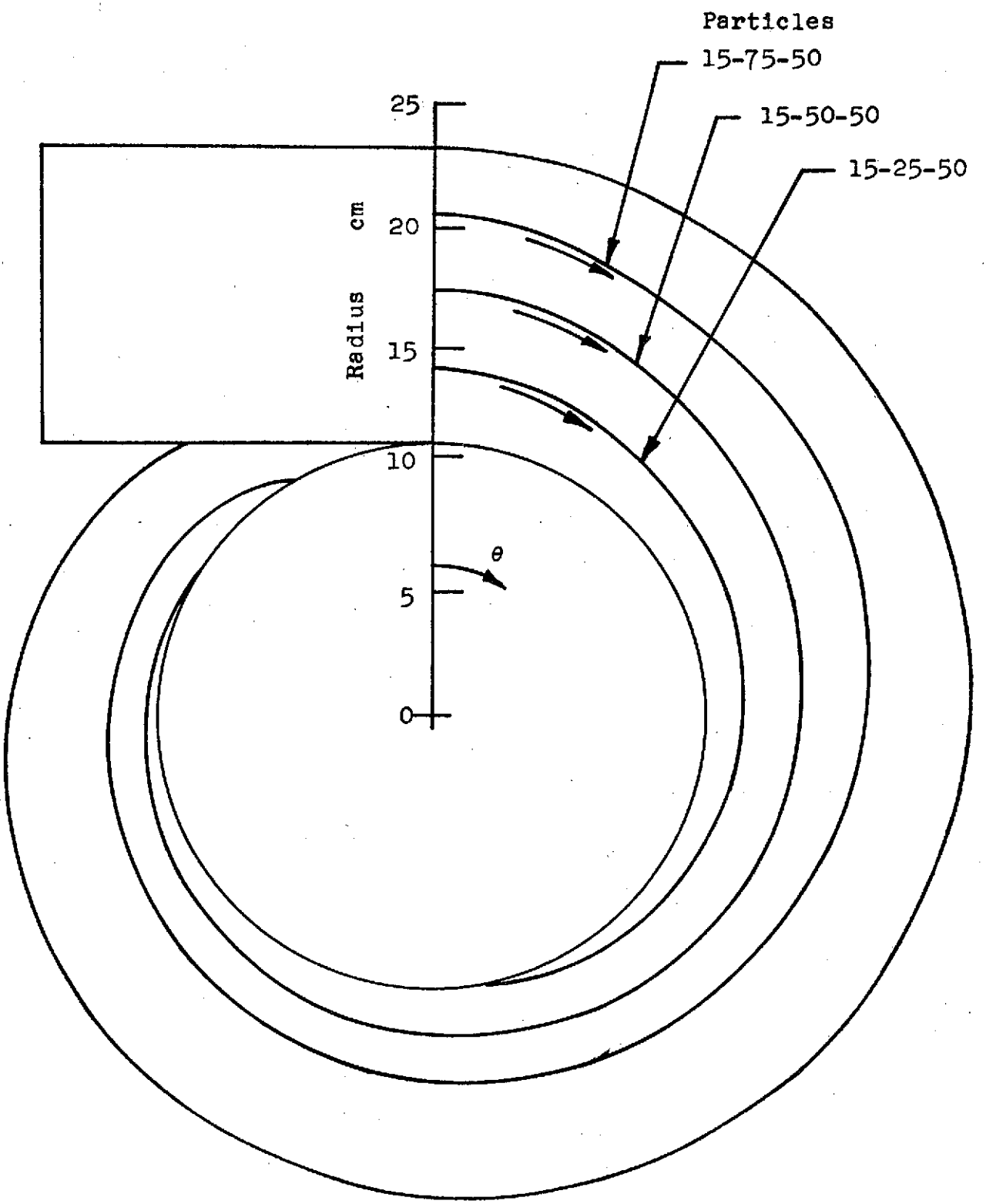

FIGURE 13a. TRAJECTORIES IN THE SCROLL, WITH $\delta = 15$ cm.

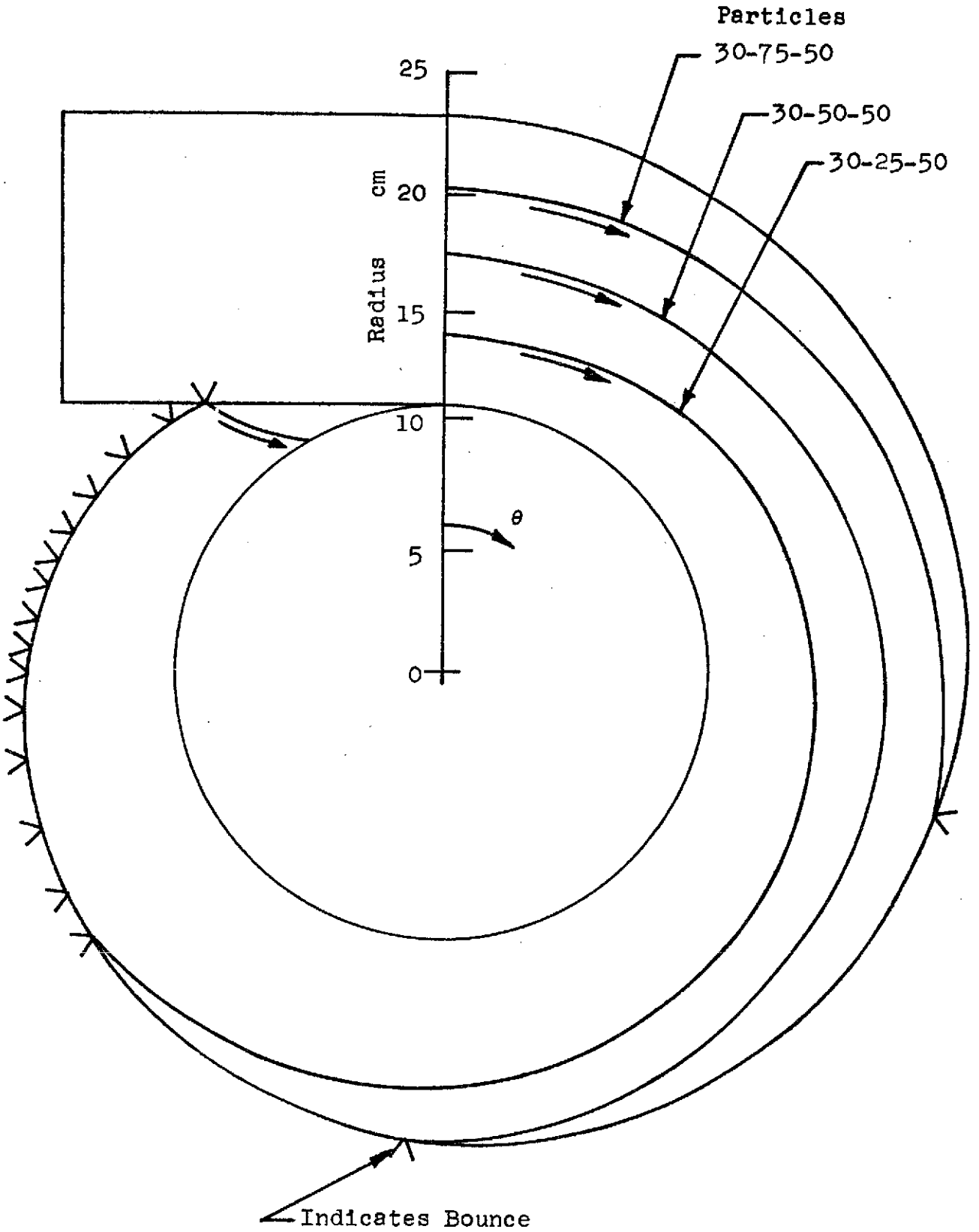

FIGURE 13b. TRAJECTORIES IN THE SCROLL, WITH δ = 30 cm.

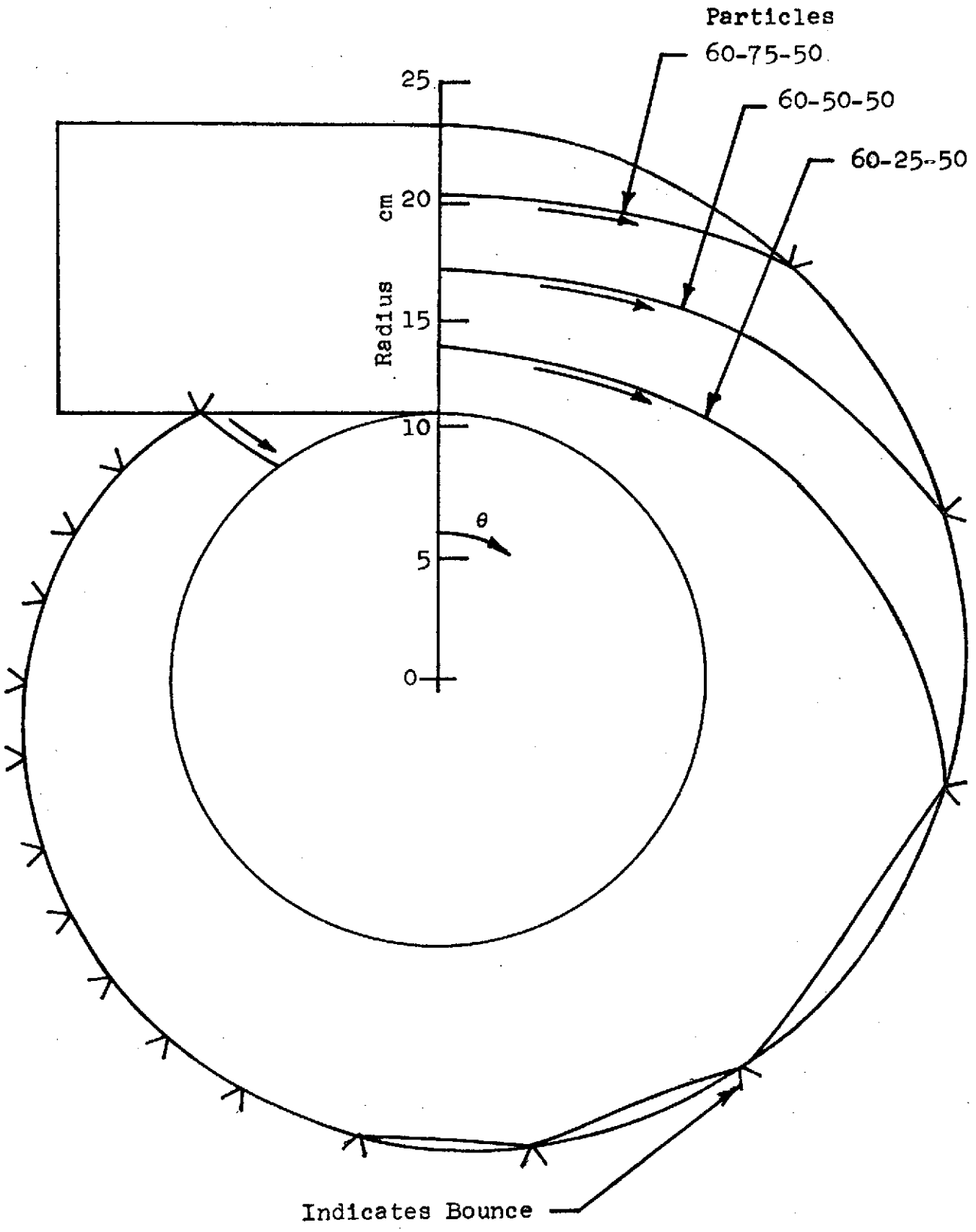

FIGURE 13c. TRAJECTORIES IN THE SCROLL, WITH $\delta = 60$ cm.

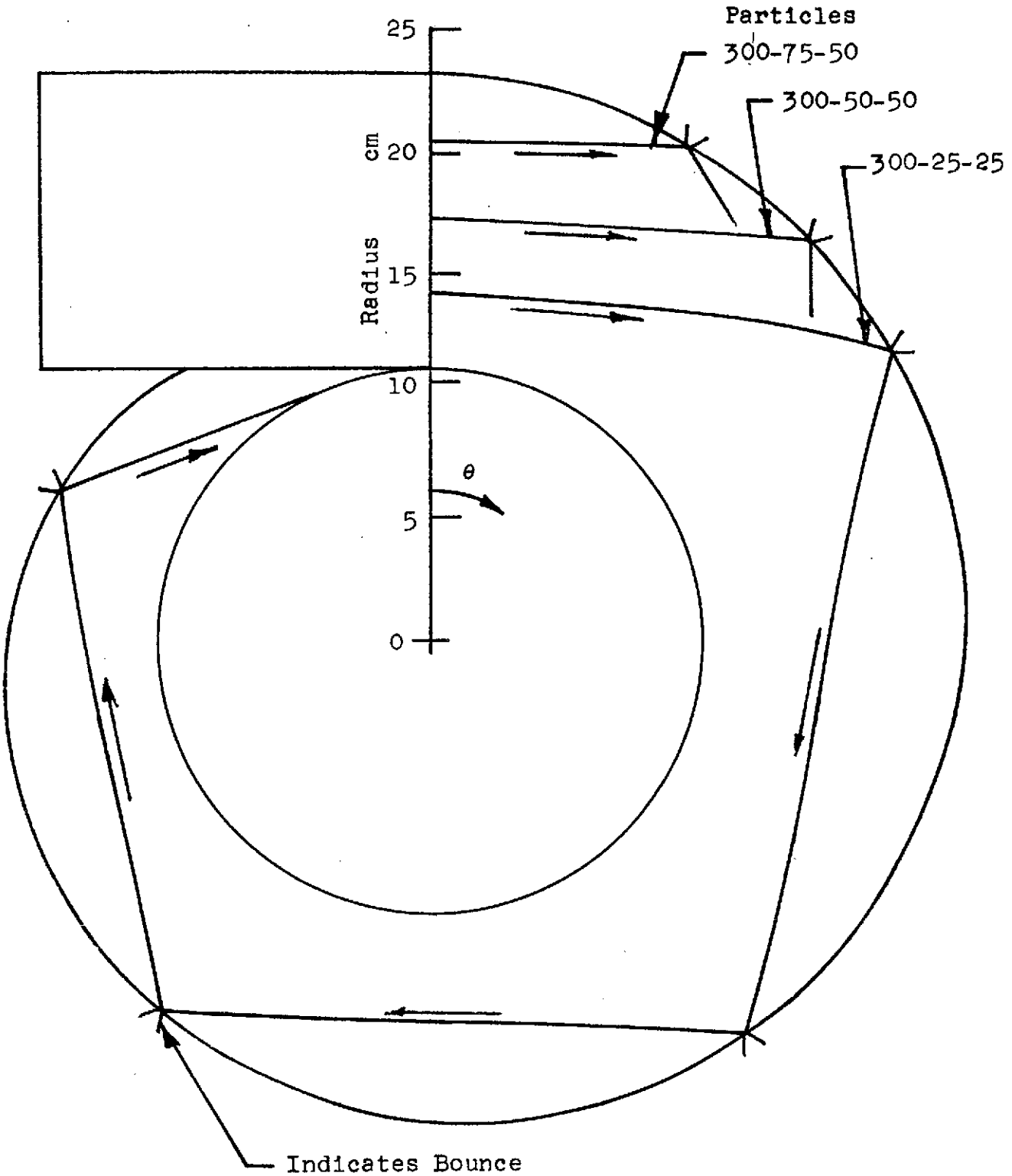

FIGURE 13d. TRAJECTORIES IN THE SCROLL, WITH δ = 300 cm.

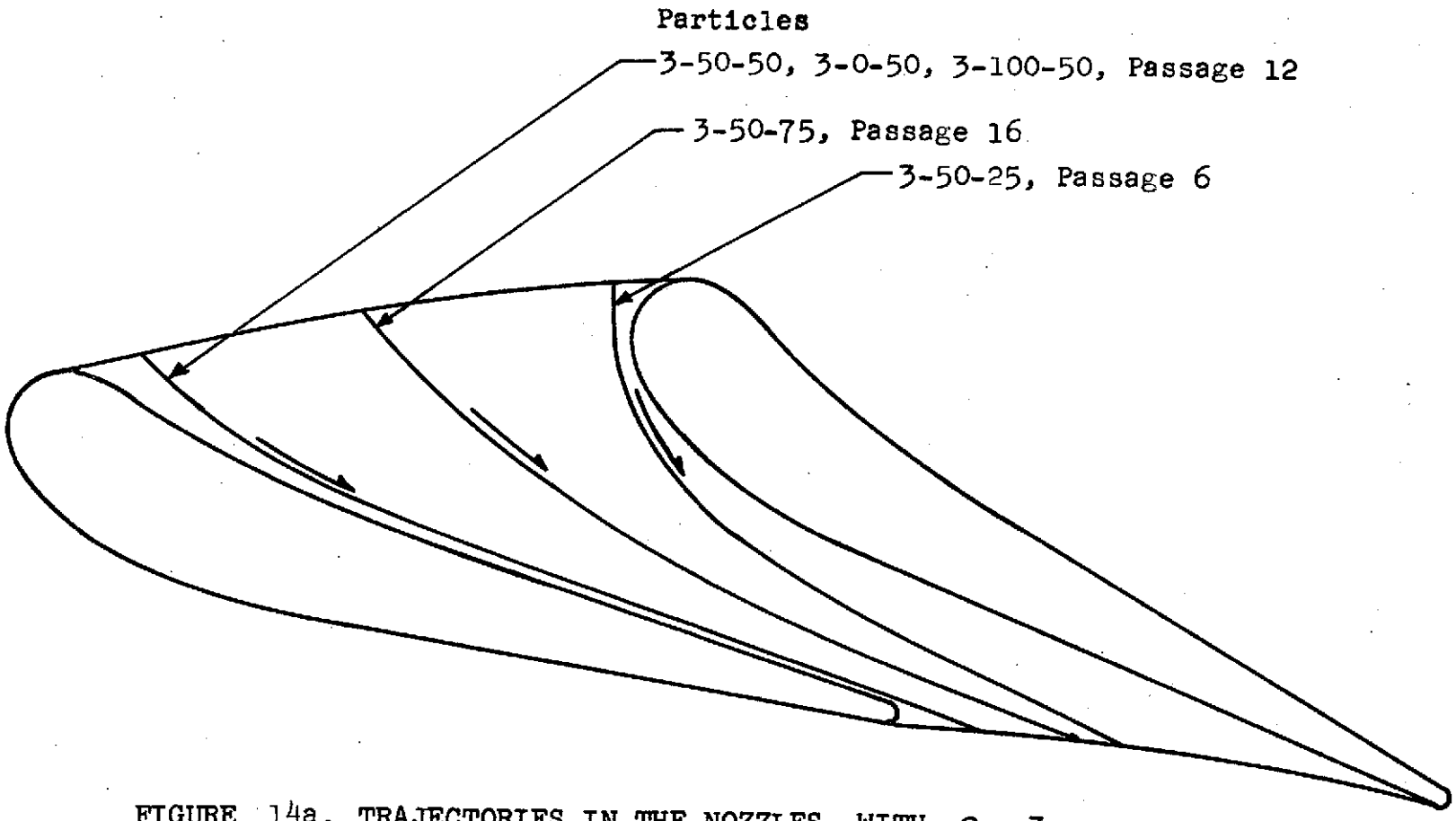

FIGURE 14a. TRAJECTORIES IN THE NOZZLES, WITH $\delta = 3$ cm.

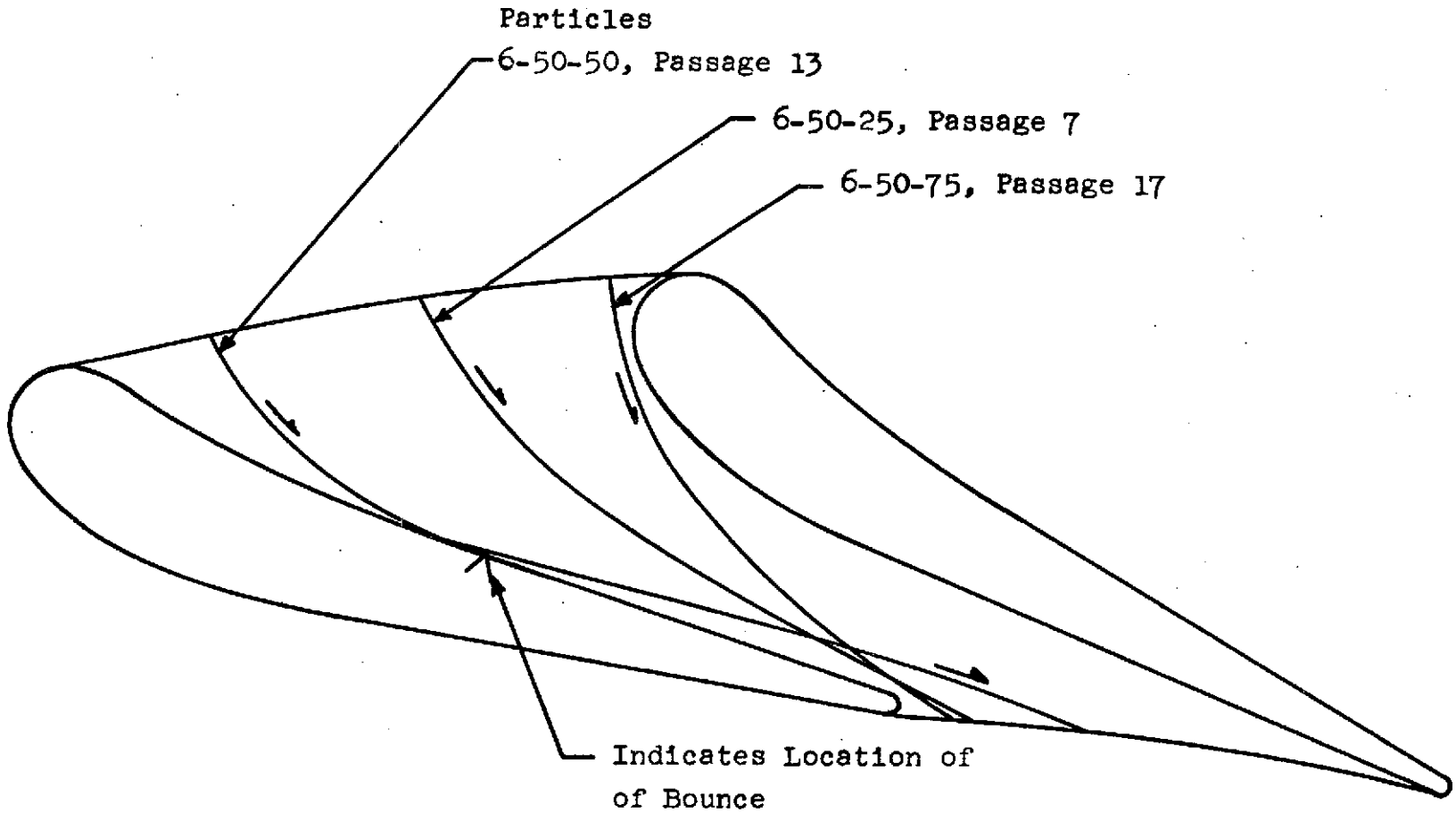

FIGURE 14b. TRAJECTORIES IN THE NOZZLES, WITH δ = 6 cm.

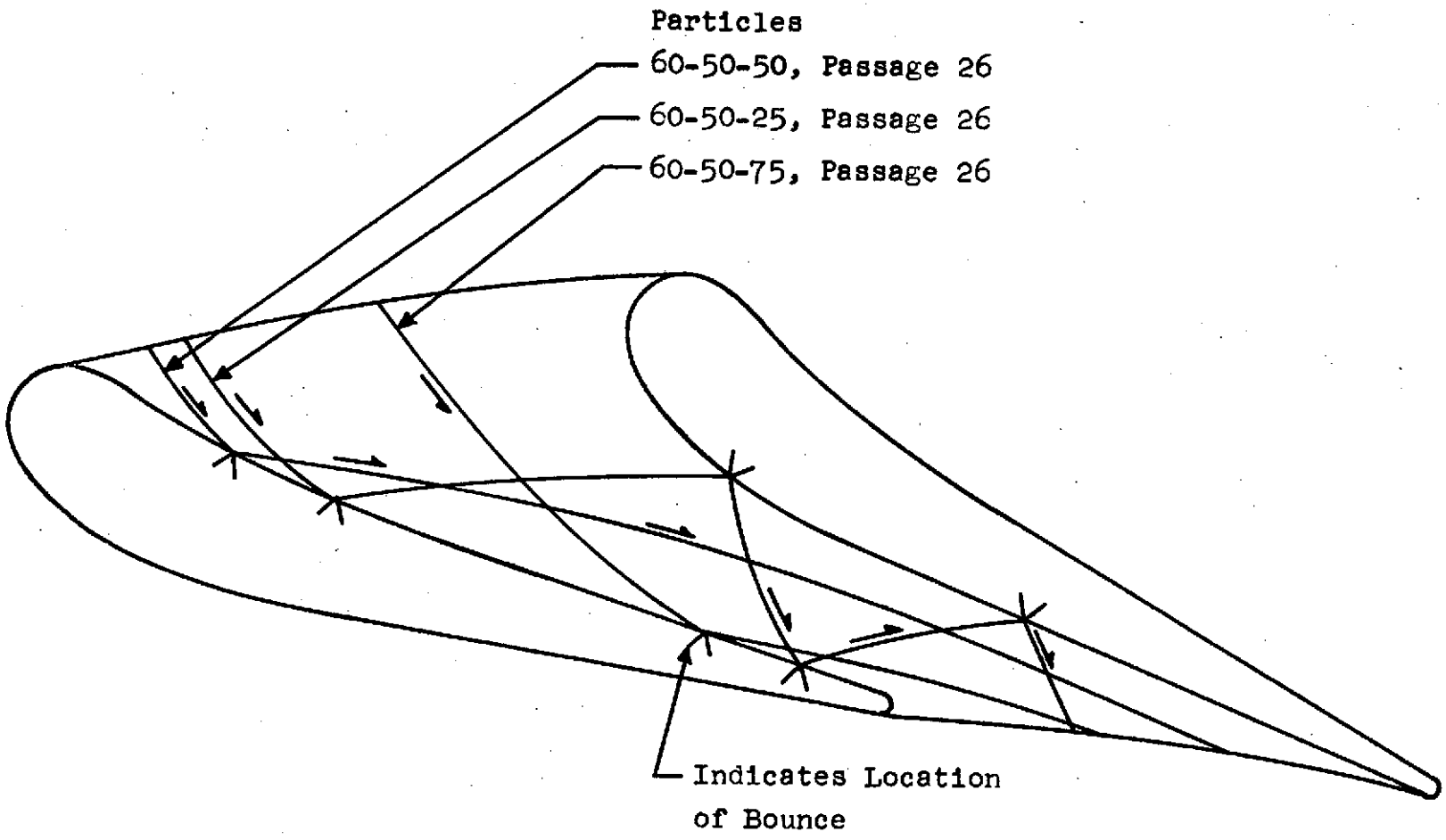

FIGURE 14c. TRAJECTORIES IN THE NOZZLES, WITH δ = 60 cm.

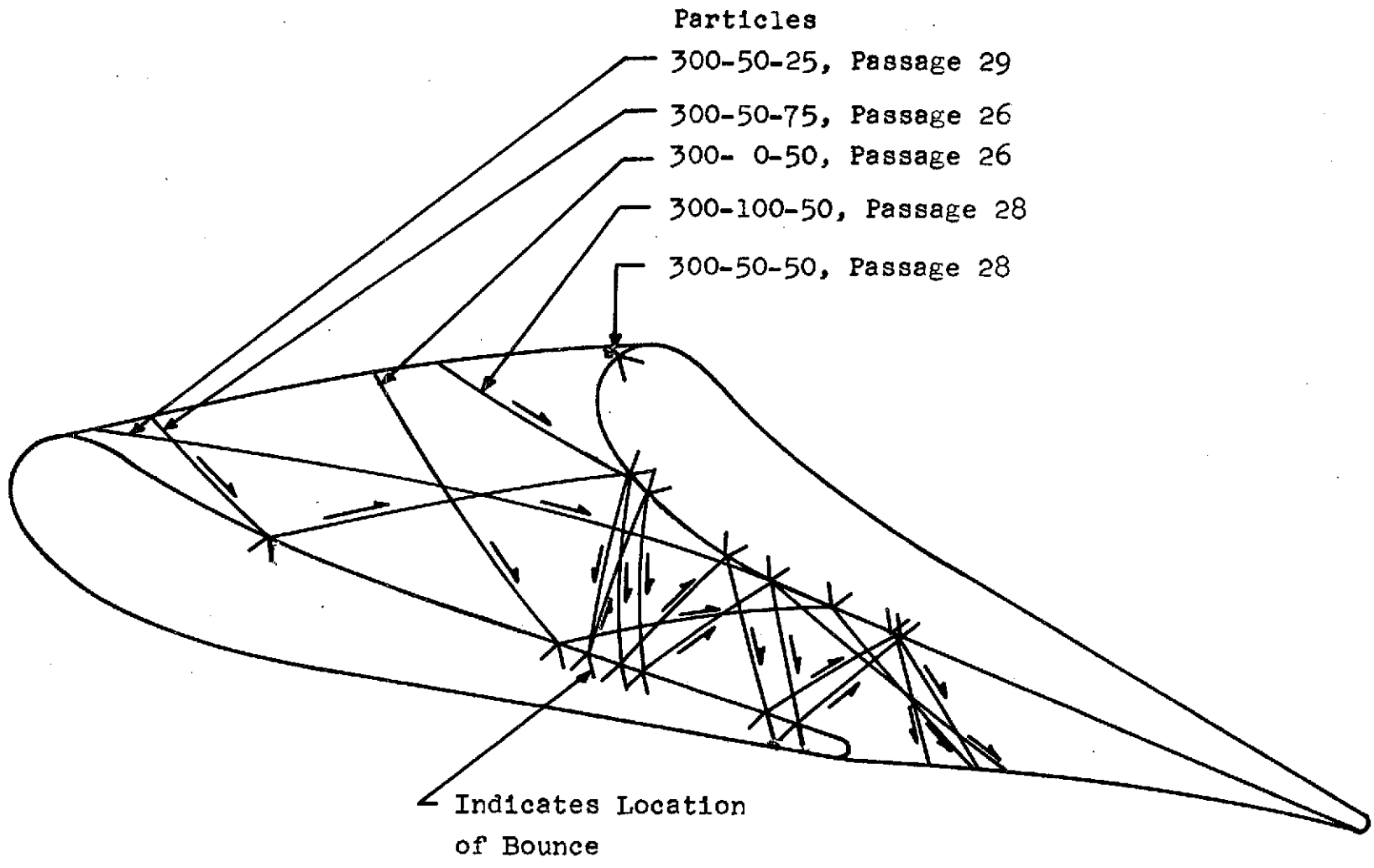

FIGURE 14d. TRAJECTORIES IN THE NOZZLES, WITH δ = 300 cm.

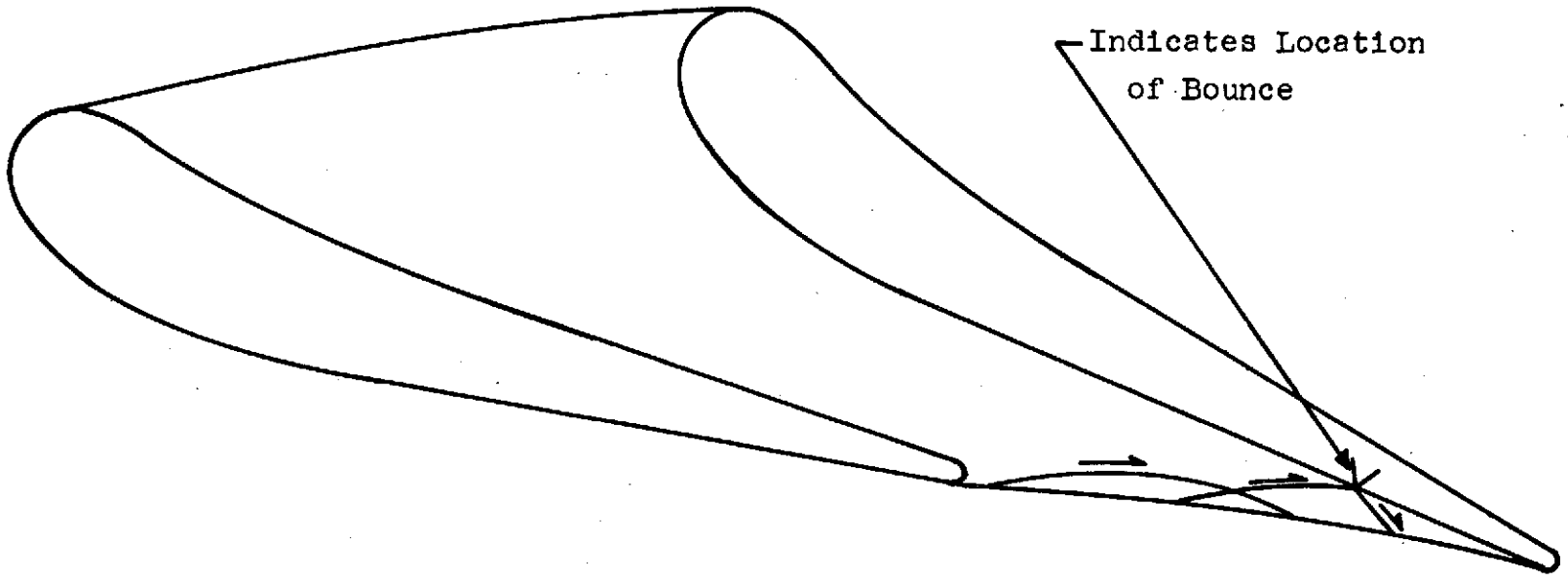

FIGURE 15a. TYPICAL TRAJECTORIES OF PARTICLES THAT RE-ENTER THE NOZZLES, WITH $\delta = 3$ cm.

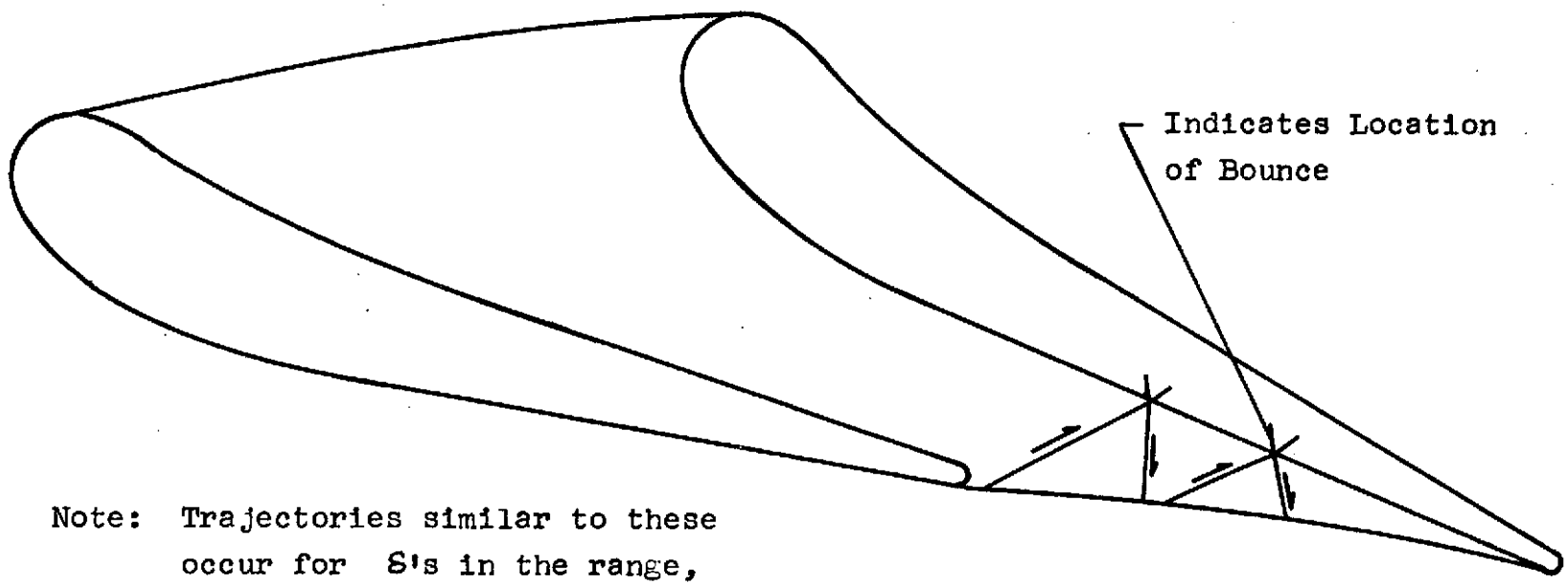

Note: Trajectories similar to these occur for δ's in the range, $\delta \geq 6$ cm.

FIGURE 15b. TYPICAL TRAJECTORIES OF PARTICLES THAT RE-ENTER THE NOZZLES, WITH $\delta = 30$ cm.

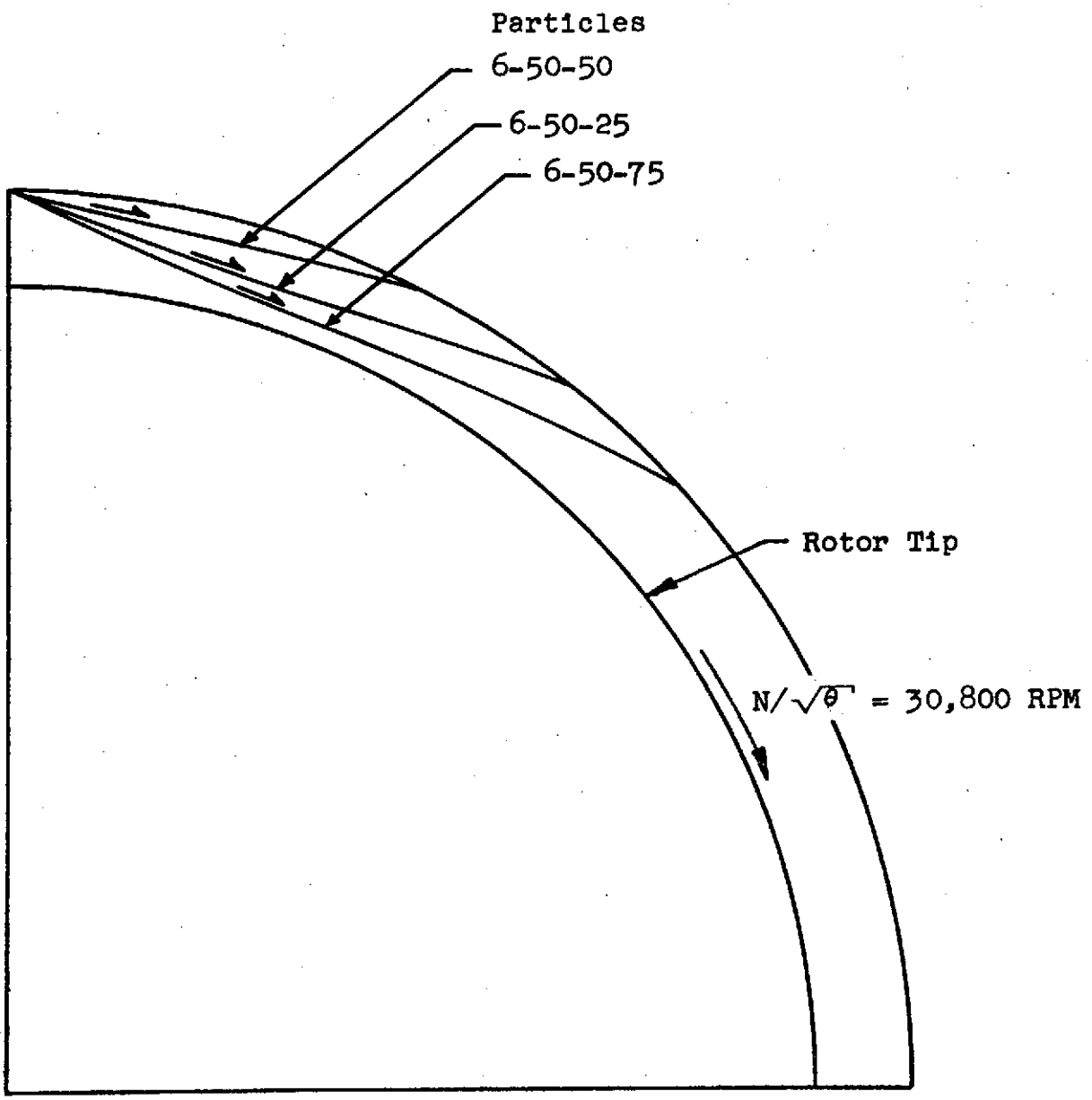

FIGURE 16a. TRAJECTORIES IN THE VORTEX, WITH δ = 6 cm.

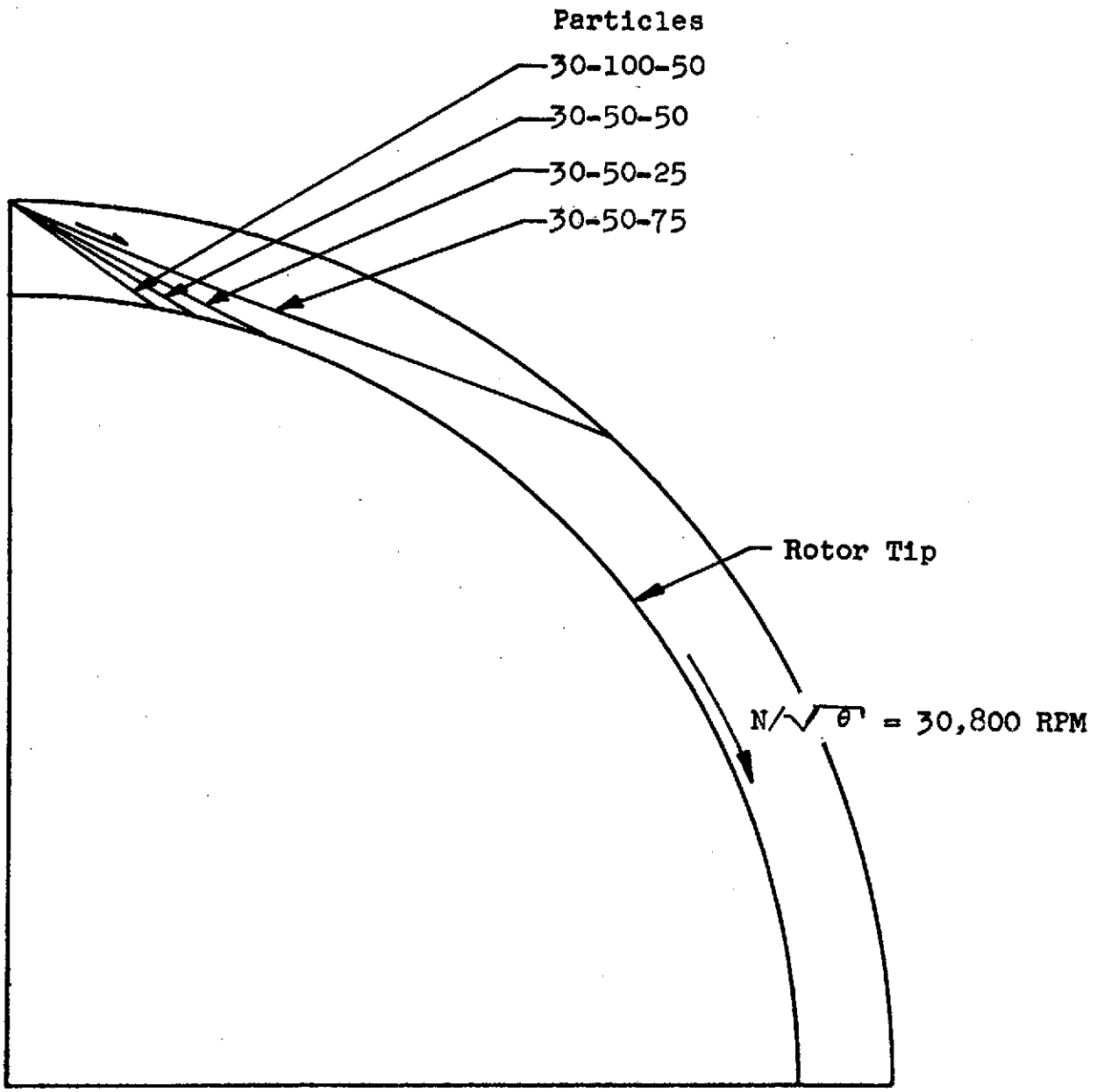

FIGURE 16b. TRAJECTORIES IN THE VORTEX, WITH δ = 30 cm.

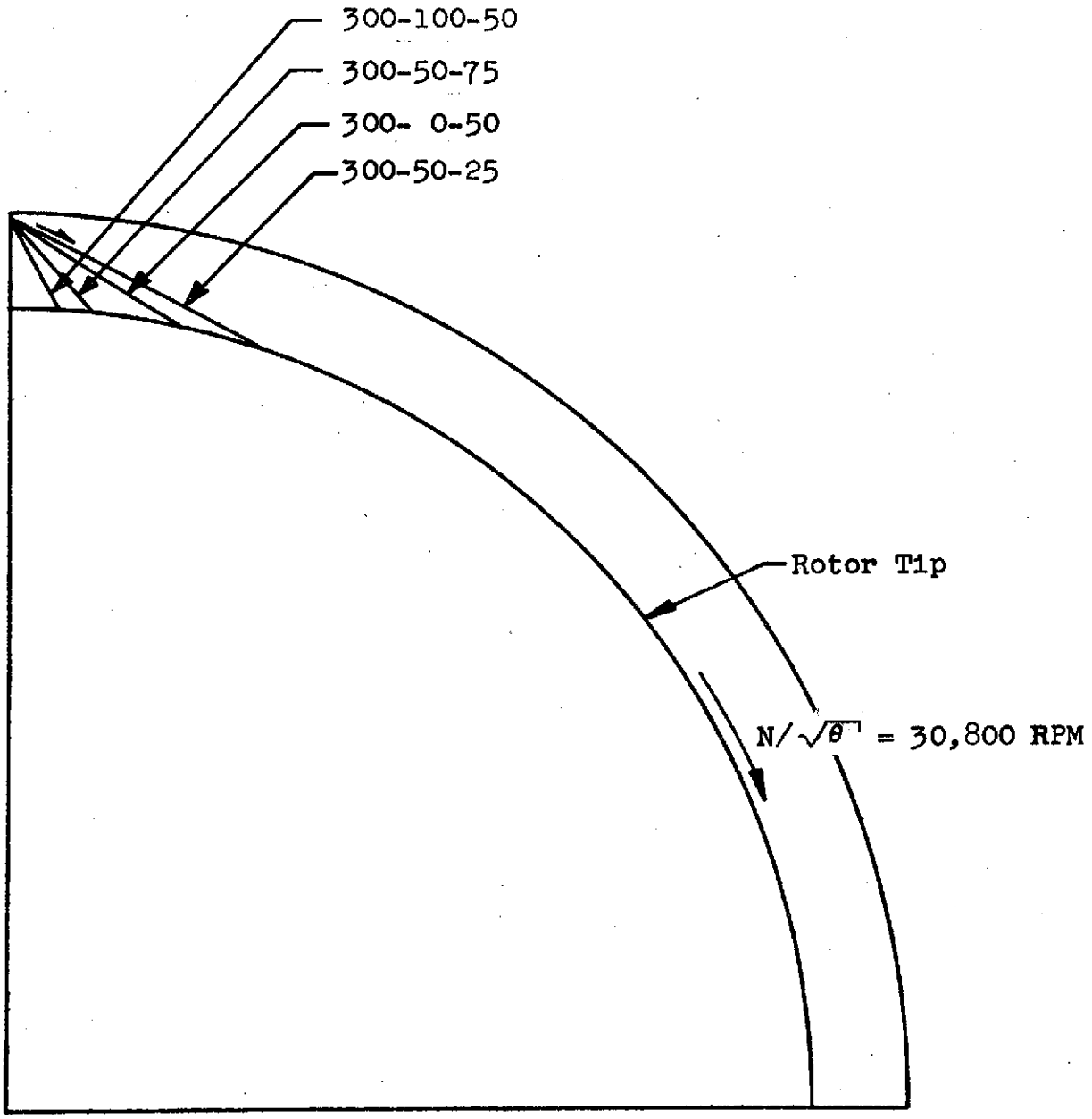

FIGURE 16c. TRAJECTORIES IN THE VORTEX, WITH δ = 300 cm.

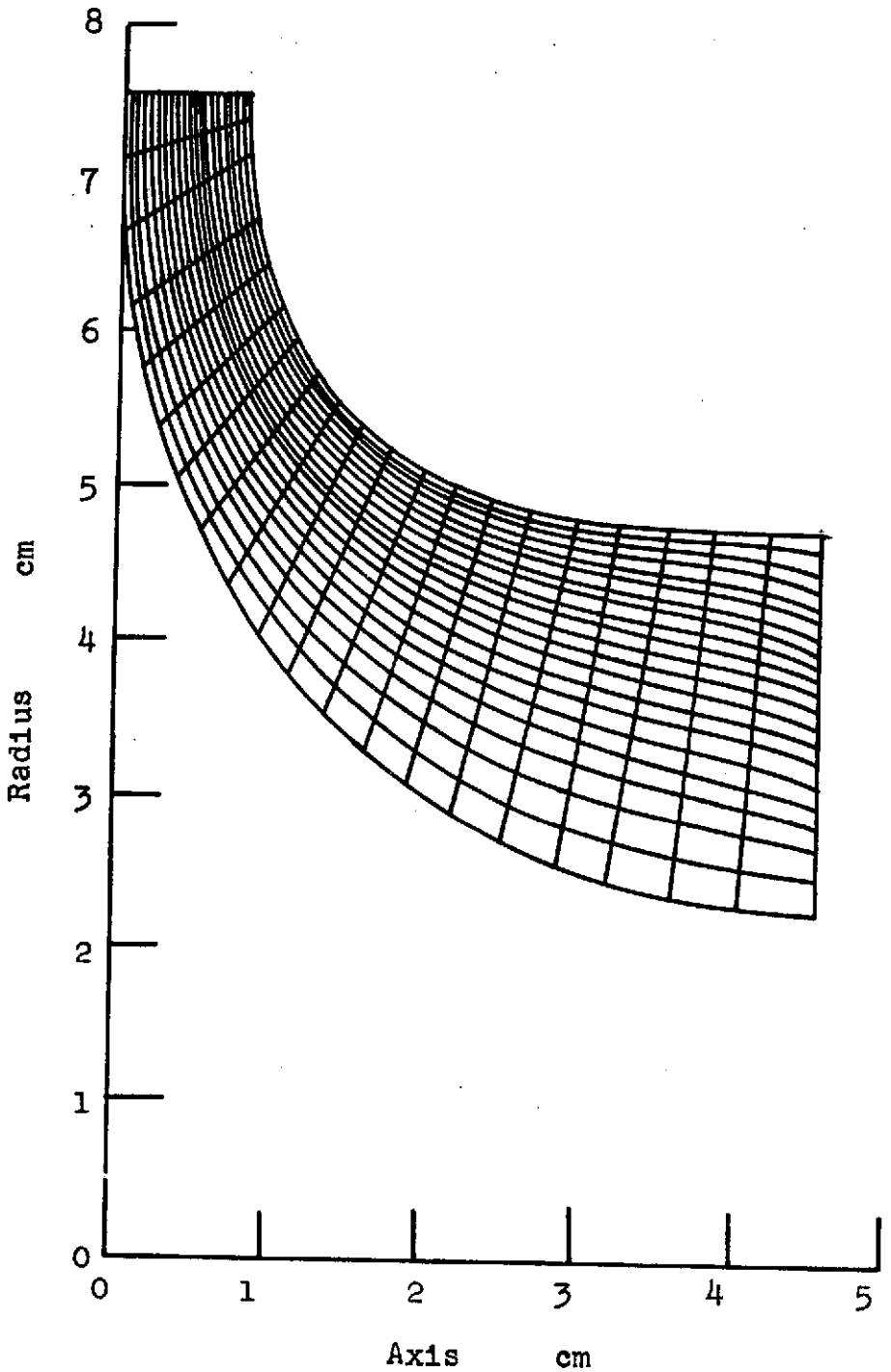

FIGURE 17. MERIDIONAL VIEW OF BLADE WITH STREAMLINE, QUASI-ORTHOGONAL MESH.

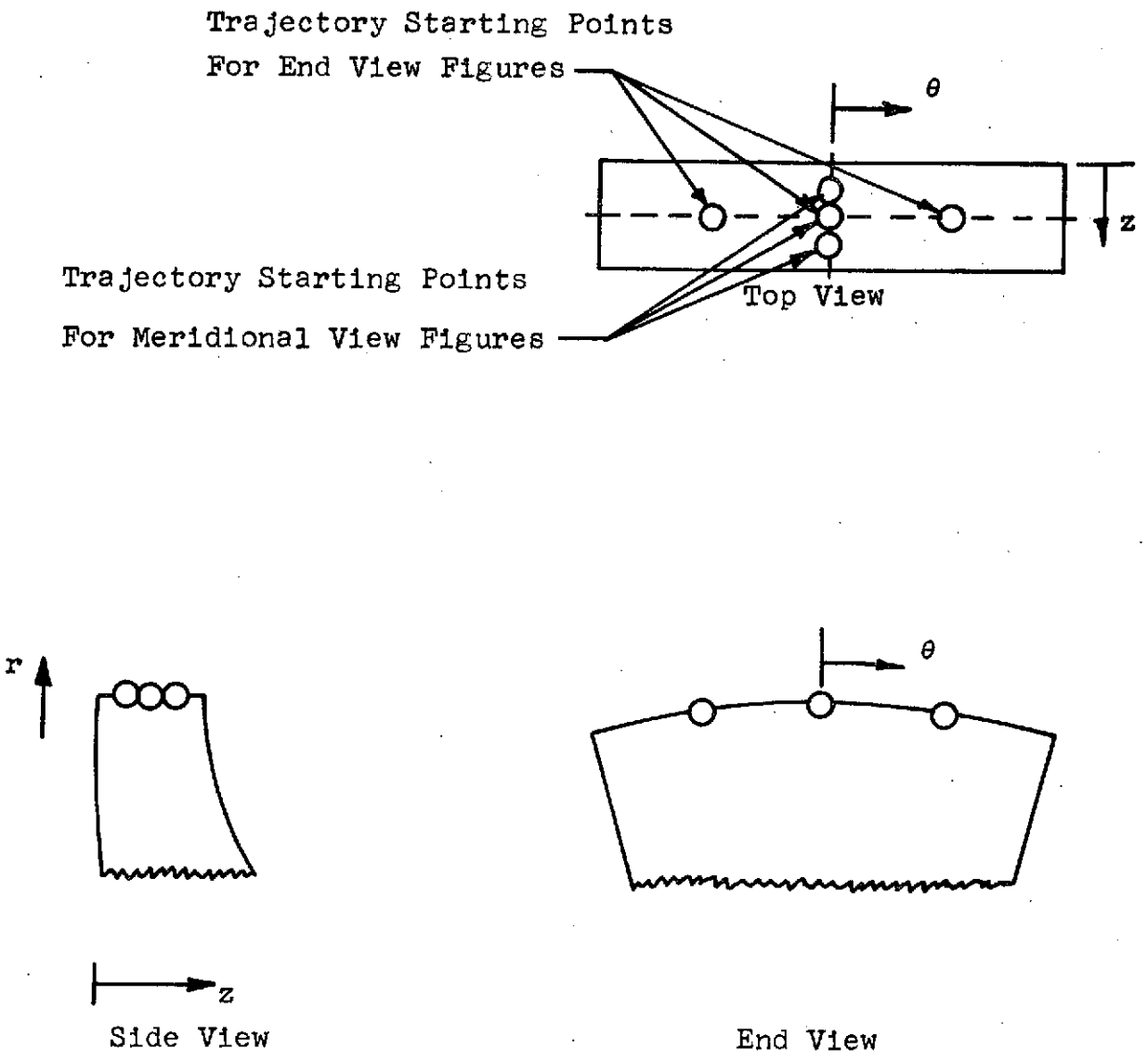

FIGURE 18. STARTING POINTS FOR PARTICLE TRAJECTORIES.

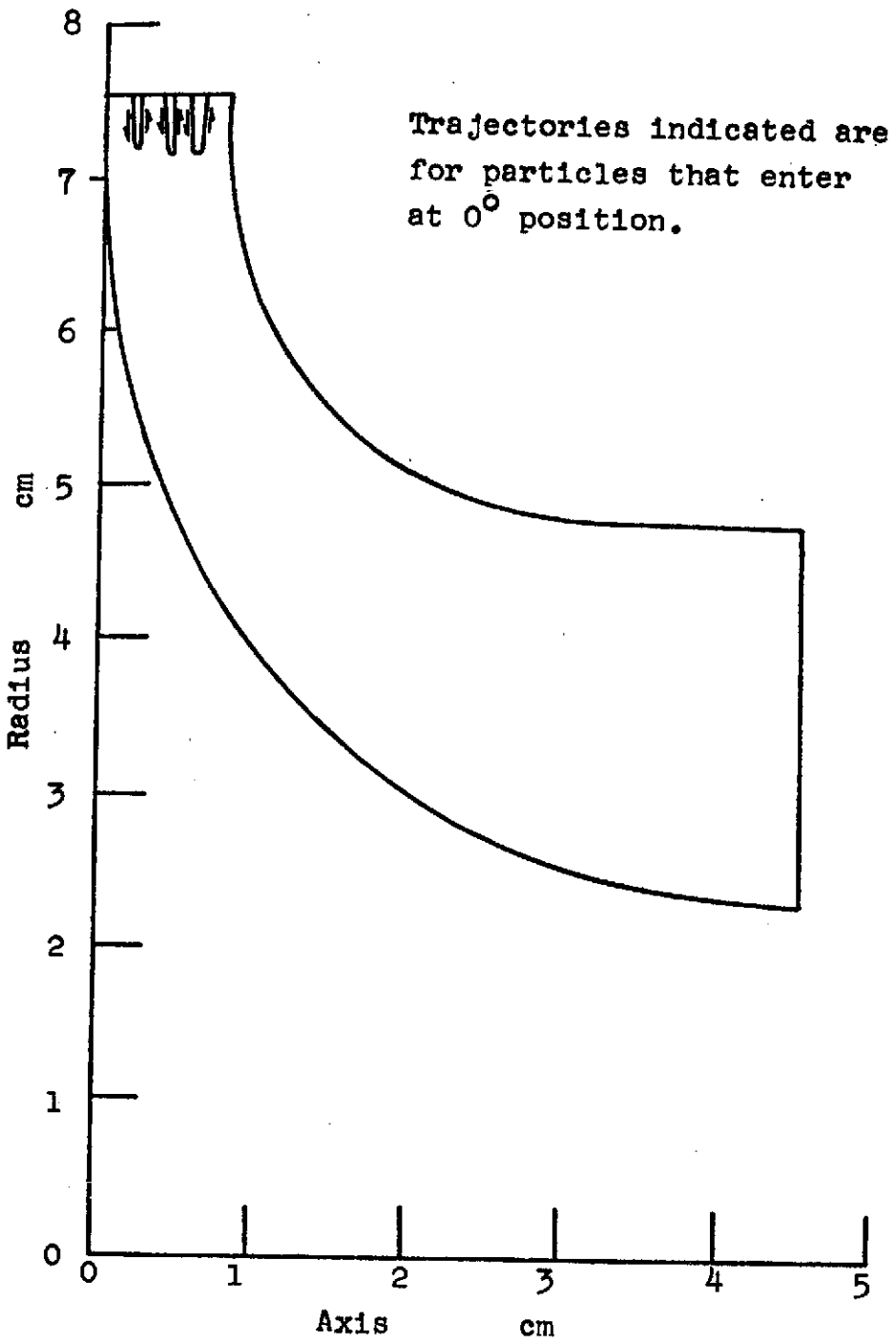

FIGURE 19a. MERIDIONAL VIEW OF PARTICLE TRAJECTORIES, WITH $\delta = 15$ cm.

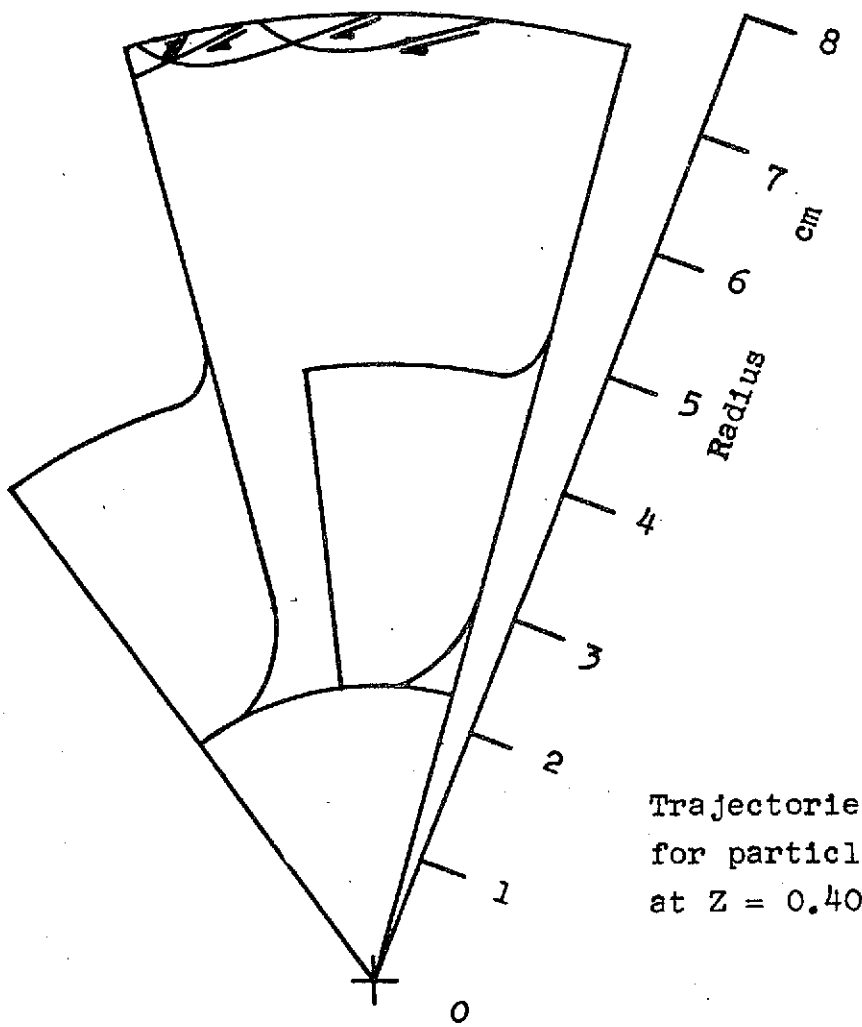

Trajectories indicated are for particles that enter at Z = 0.404 cm.

FIGURE 19b. AXIAL VIEW OF ROTOR WITH RESPECT TO ROTATING REFERENCE FRAME, WITH δ = 15 cm.

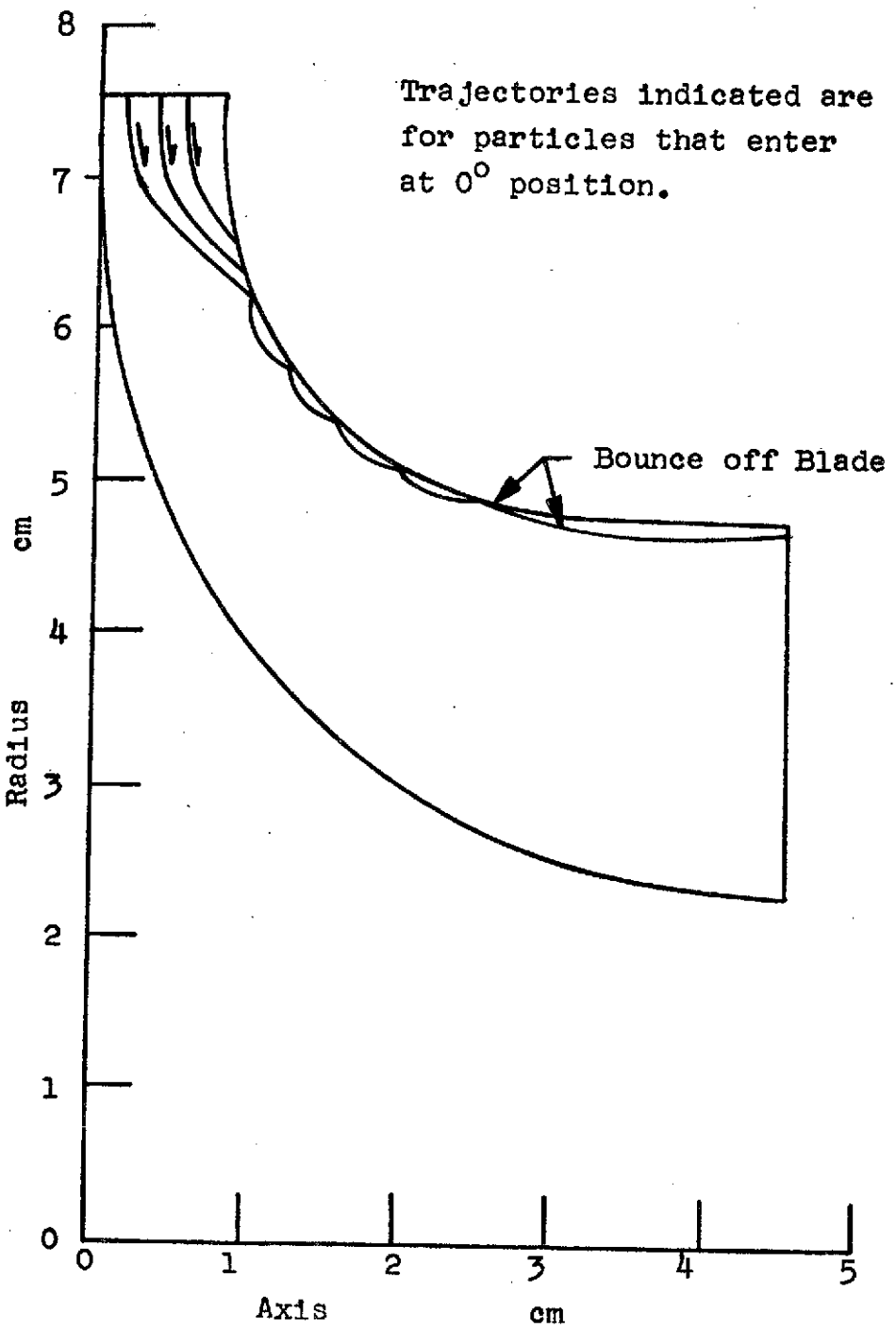

FIGURE 20a. MERIDIONAL VIEW OF PARTICLE TRAJECTORIES, WITH $\delta = 6$ cm.

C.2

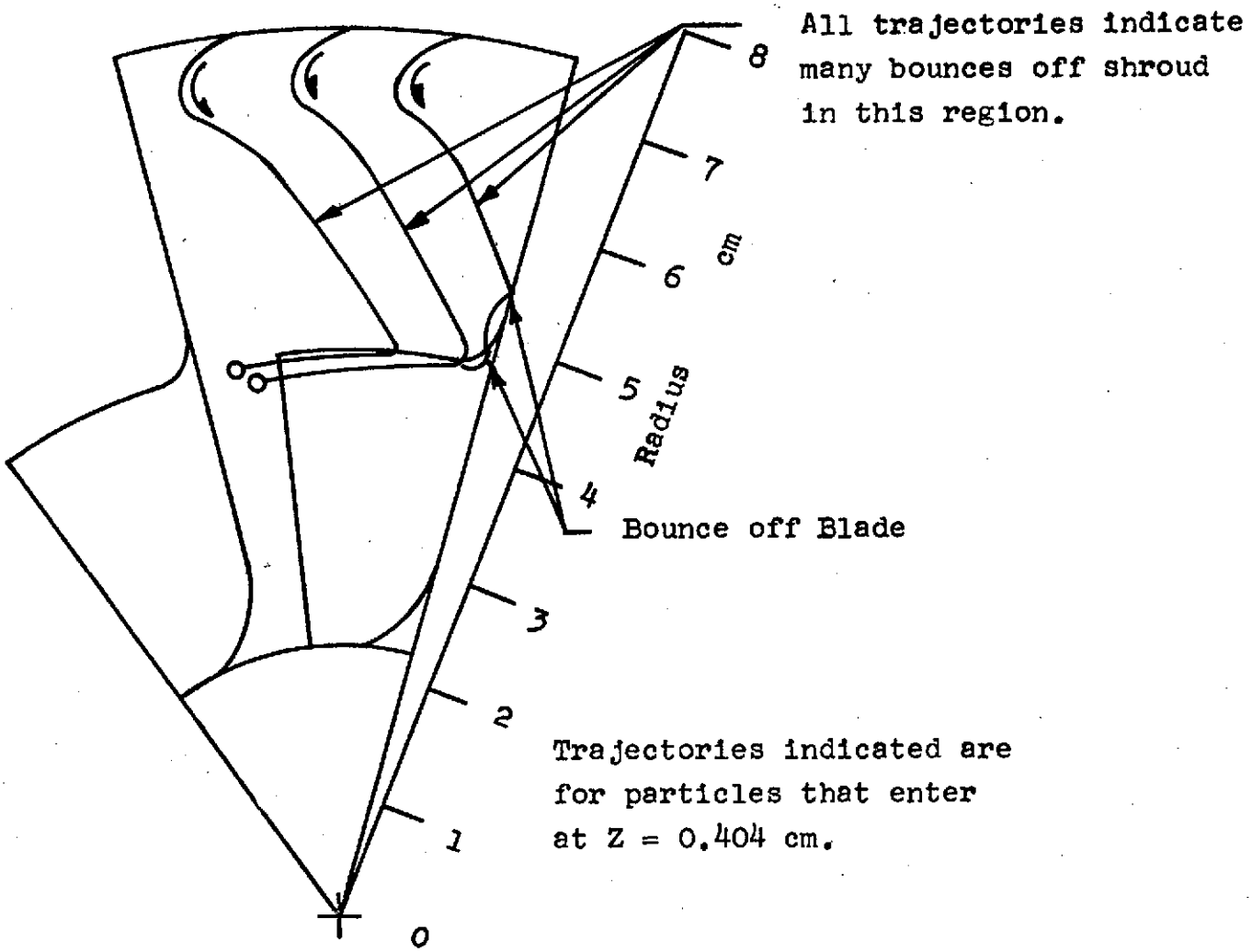

FIGURE 20b. AXIAL VIEW OF ROTOR WITH RESPECT TO ROTATING REFERENCE FRAME, WITH δ = 6 cm.

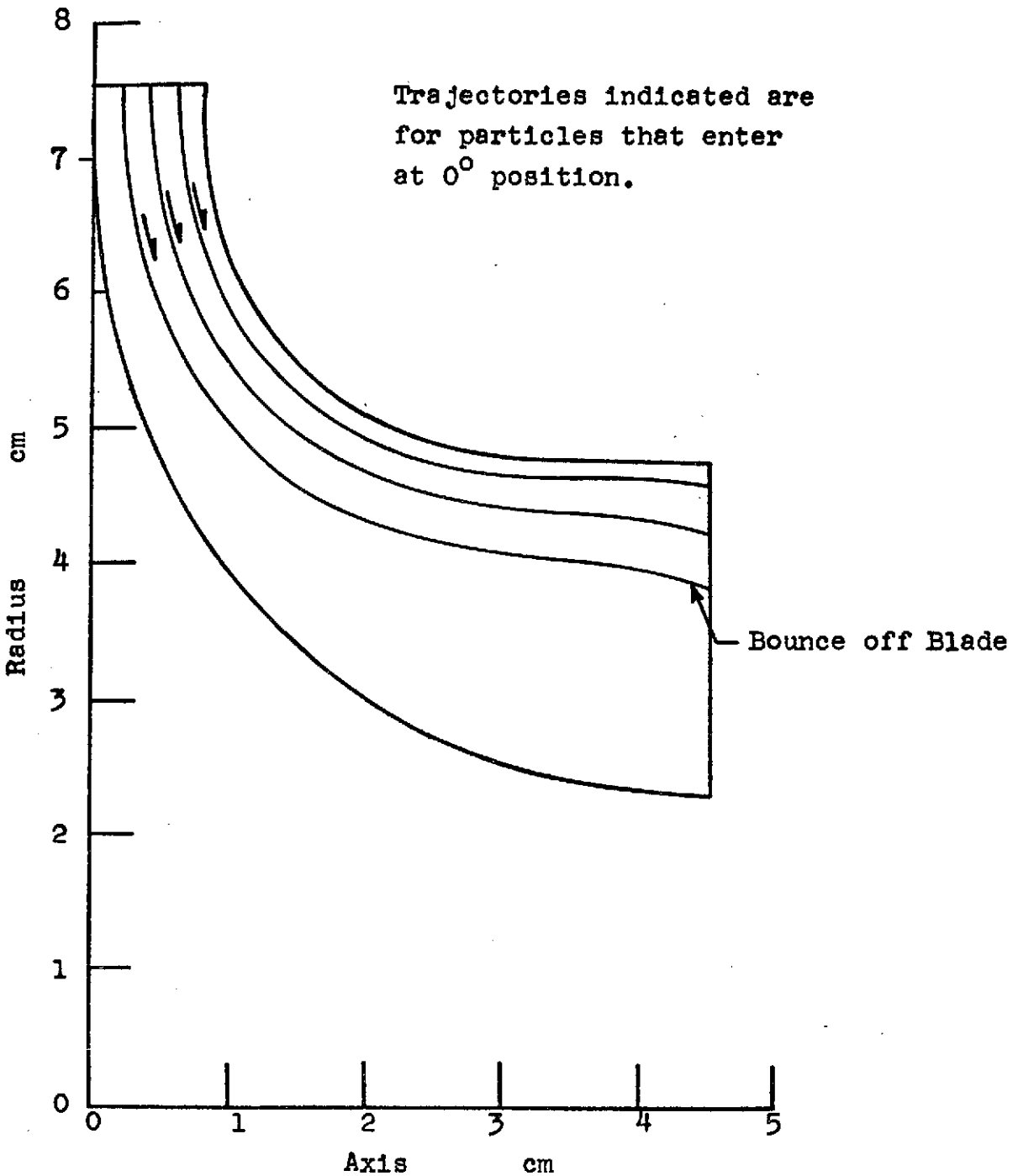

FIGURE 21a. MERIDIONAL VIEW OF PARTICLE TRAJECTORIES, WITH $\delta = 3$ cm.

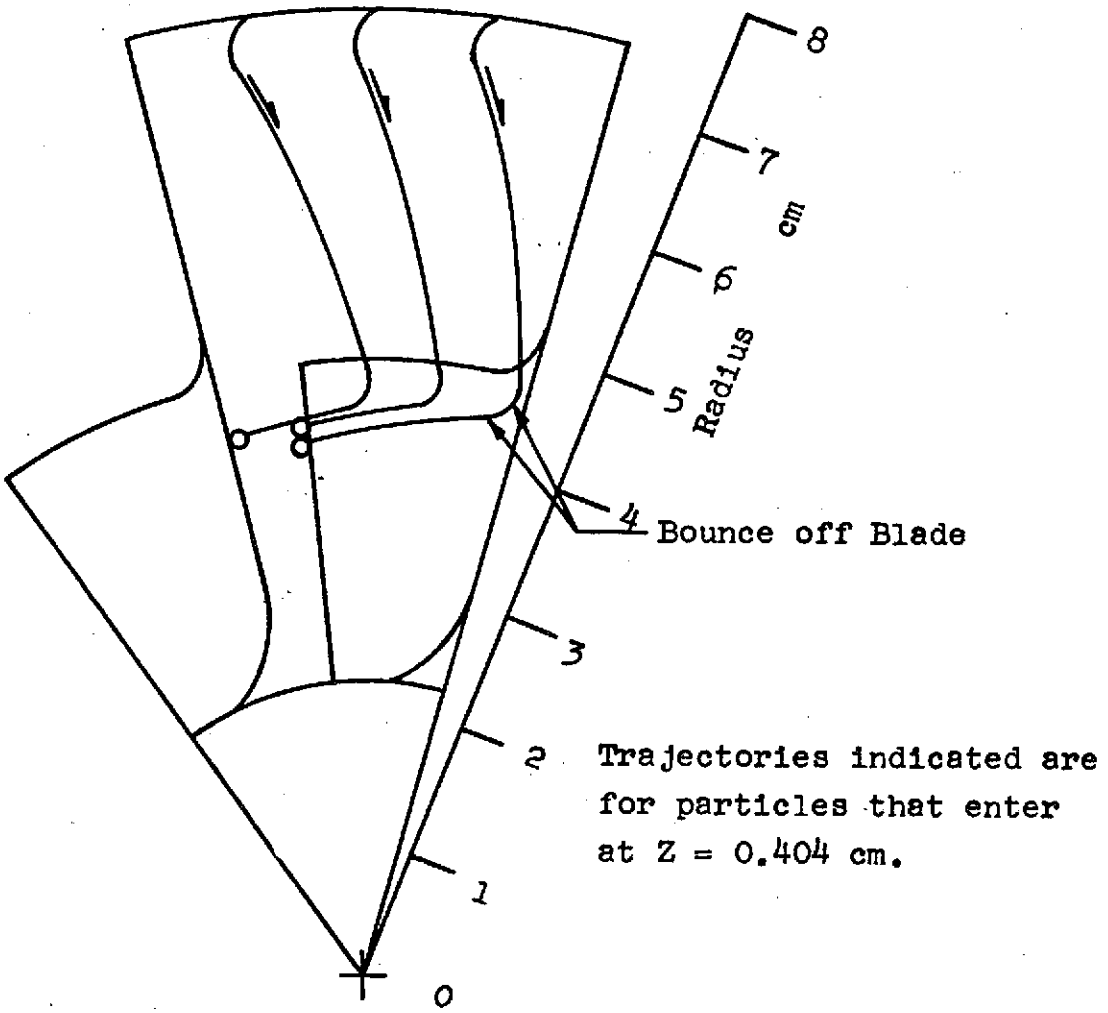

FIGURE 21b. AXIAL VIEW OF ROTOR WITH RESPECT TO ROTATING REFERENCE FRAME, WITH $\delta = 3$ cm.

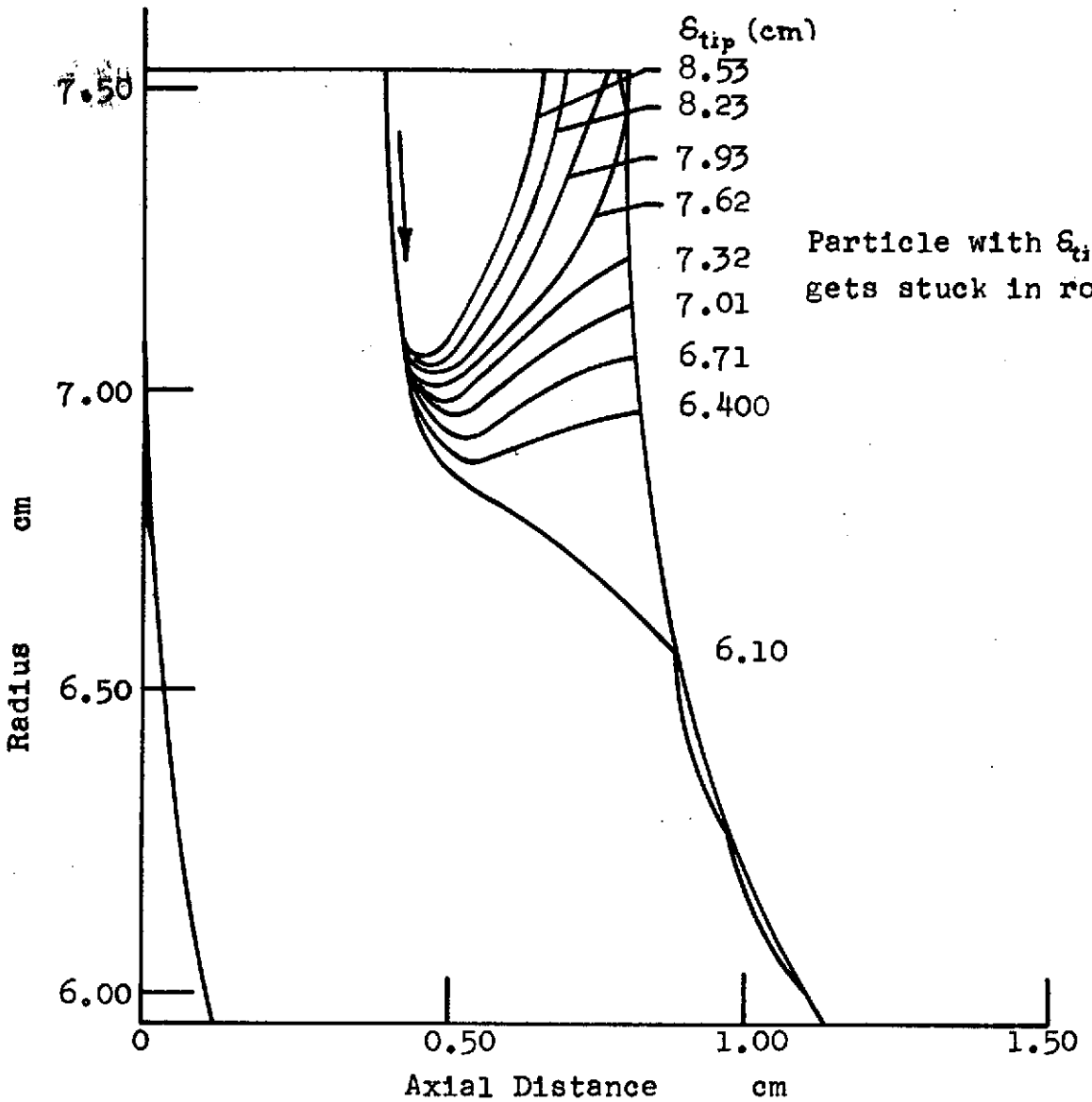

FIGURE 22. MERIDIONAL VIEW OF PARTICLE TRAJECTORIES FOR PARTICLES NEAR THE THRESHHOLD SIZE.

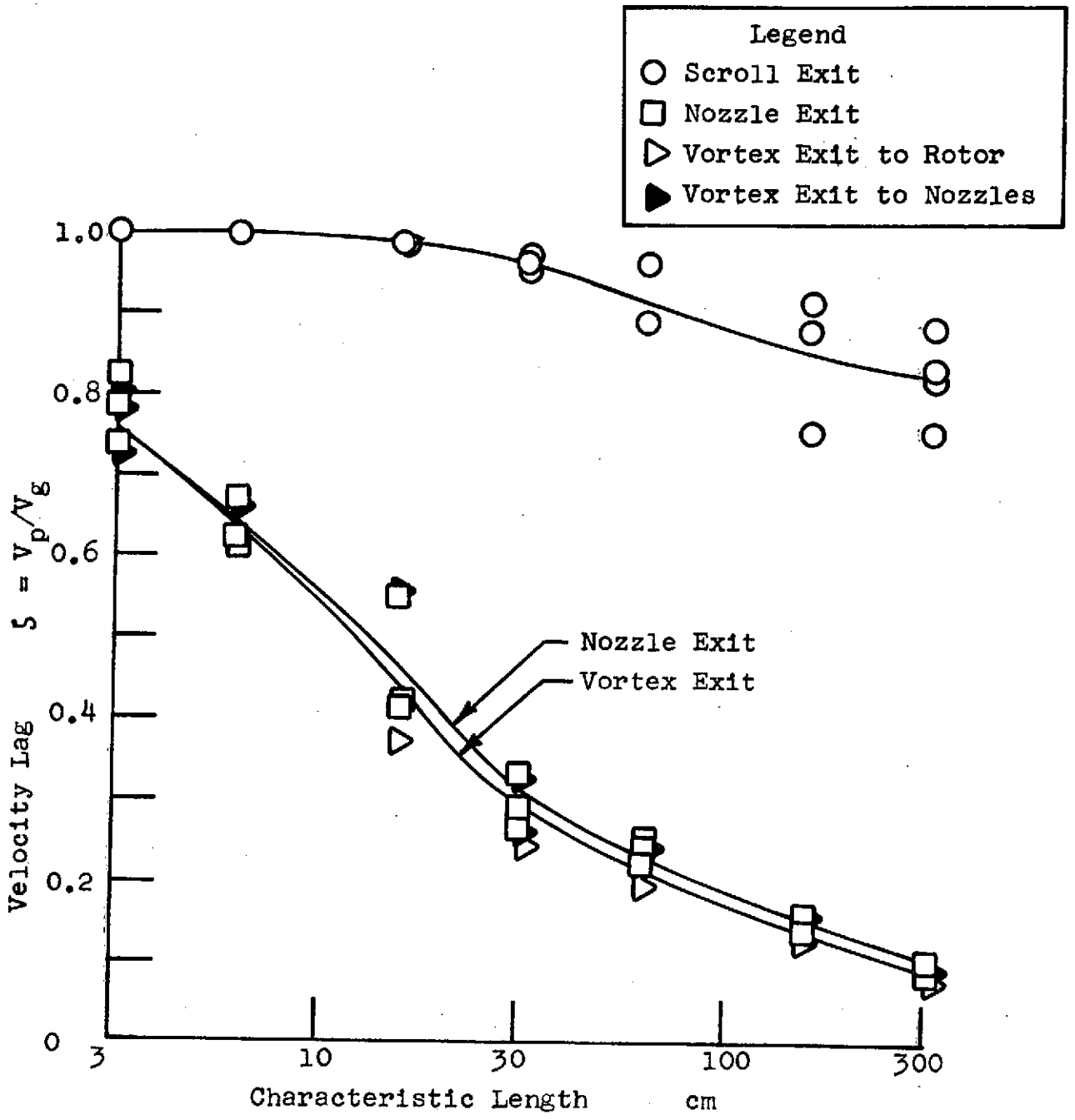

FIGURE 23. VELOCITY LAG IN ANALYTIC STUDY.

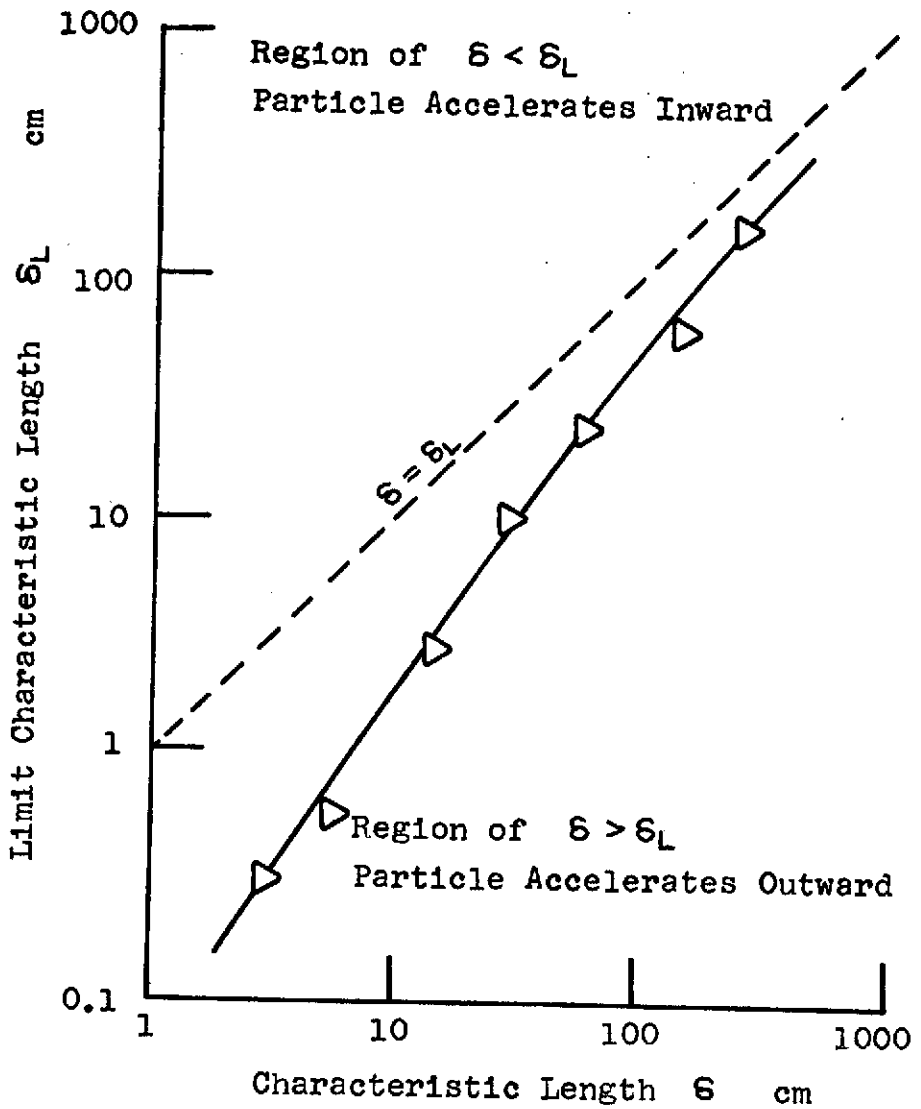

FIGURE 24. VARIATION OF LIMIT CHARACTERISTIC LENGTH WITH CHARACTERISTIC LENGTH

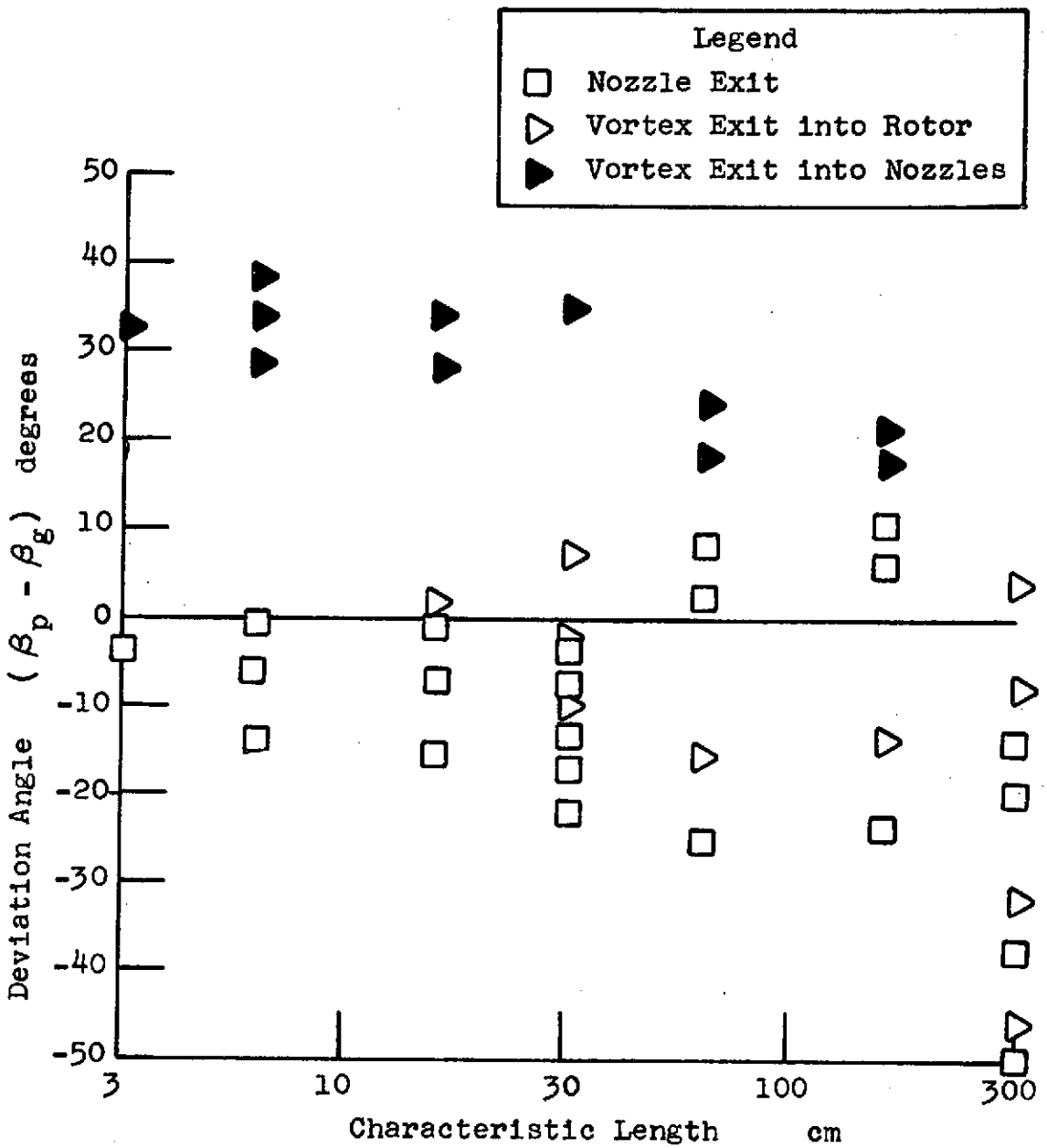

FIGURE 25. DEVIATION ANGLE VERSUS CHARACTERISTIC LENGTH.

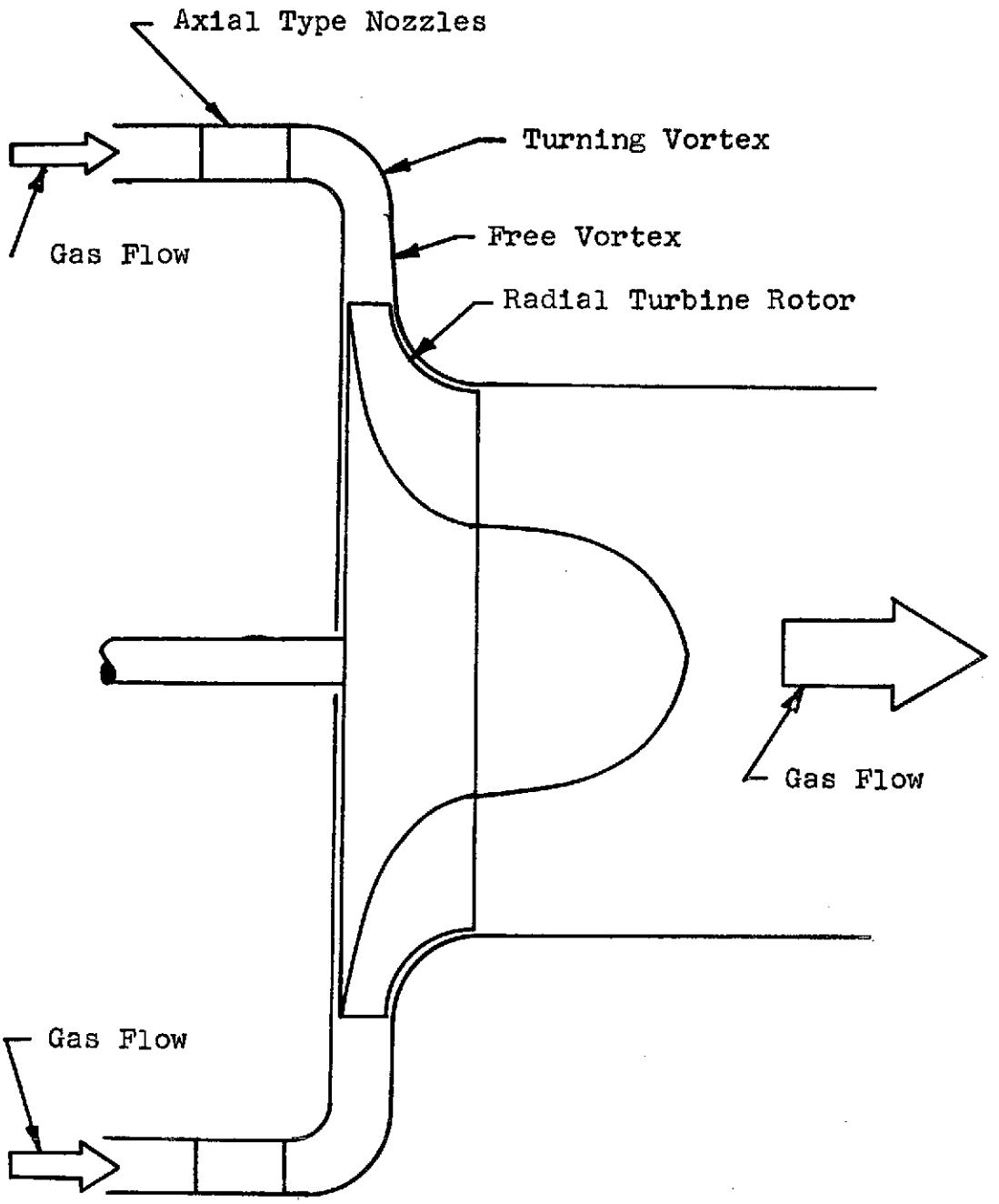

FIGURE 26. AXIAL NOZZLES COMBINED WITH RADIAL INFLOW TURBINE ROTOR.

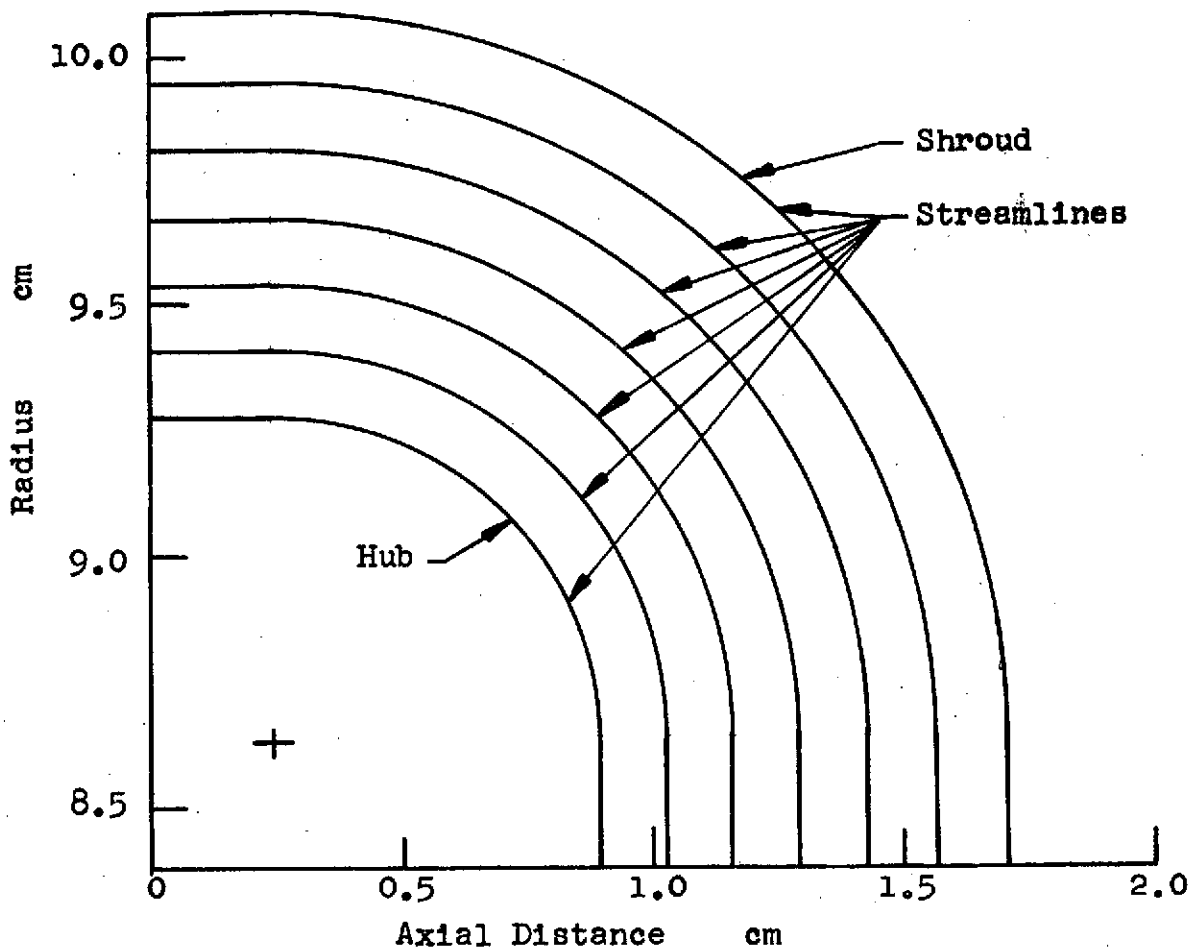

FIGURE 27a. TURNING VORTEX MERIDIONAL VIEW.

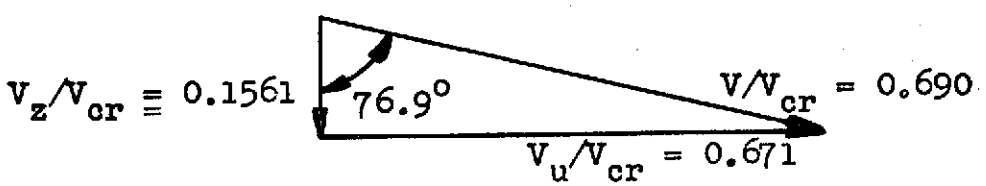

Inlet Mean

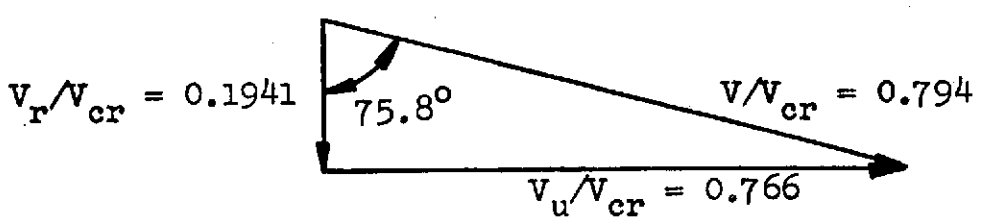

Exit Mean

FIGURE 27b. TURNING VORTEX VELOCITY DIAGRAM.

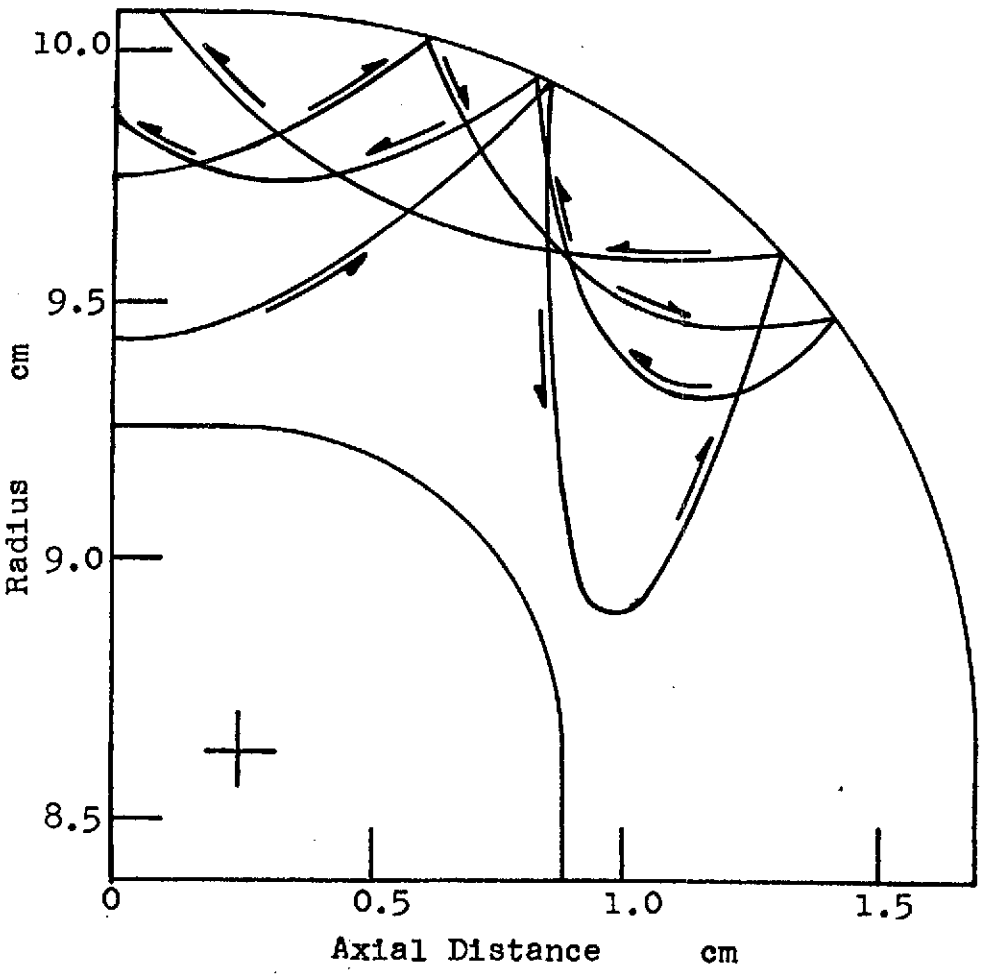

FIGURE 28a. TRAJECTORIES WITH $\delta = 300$ cm.

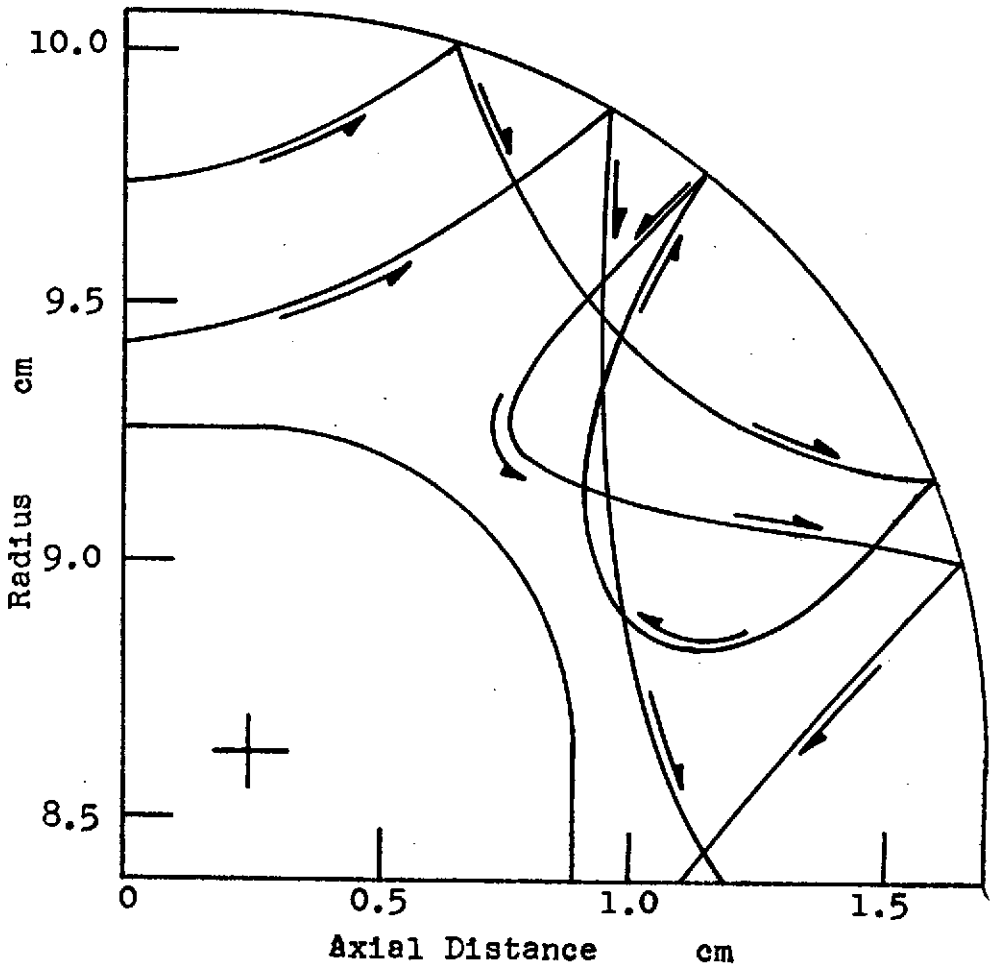

FIGURE 28b, TRAJECTORIES WITH $\delta = 150$ cm.

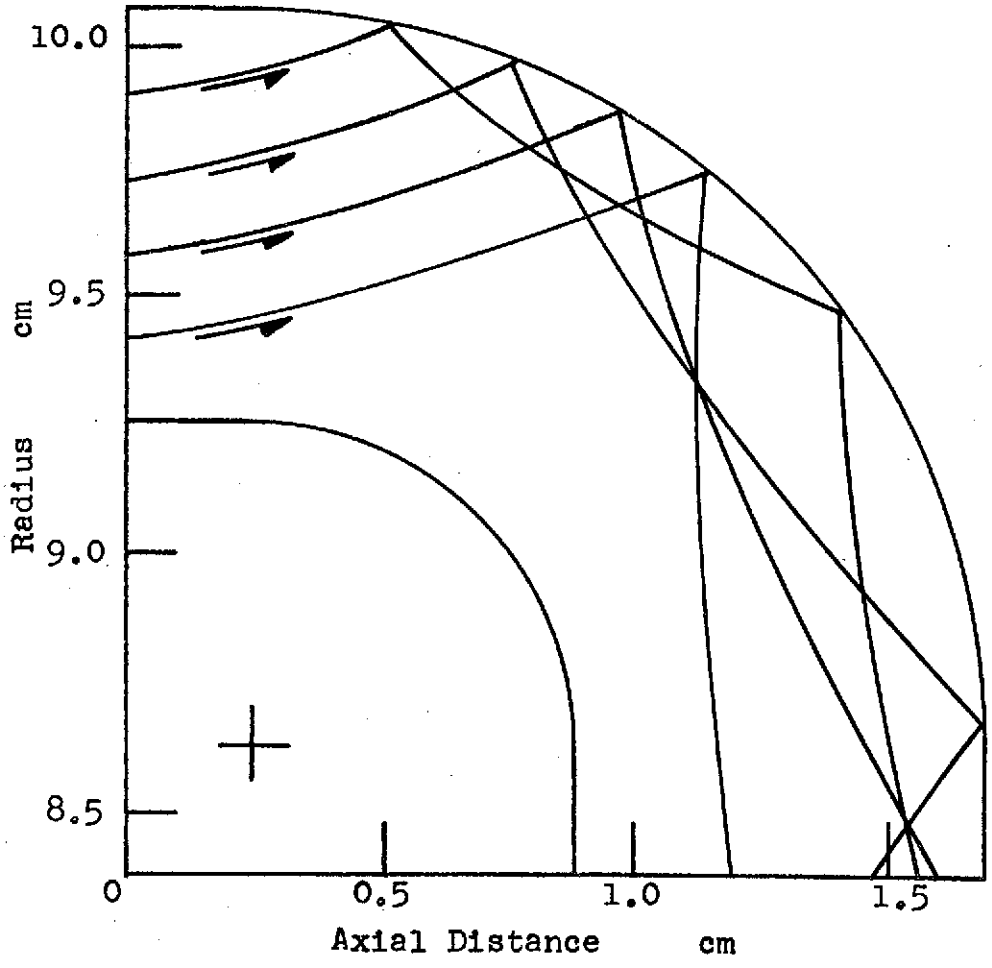

FIGURE 28c. TRAJECTORIES WITH δ = 60 cm.

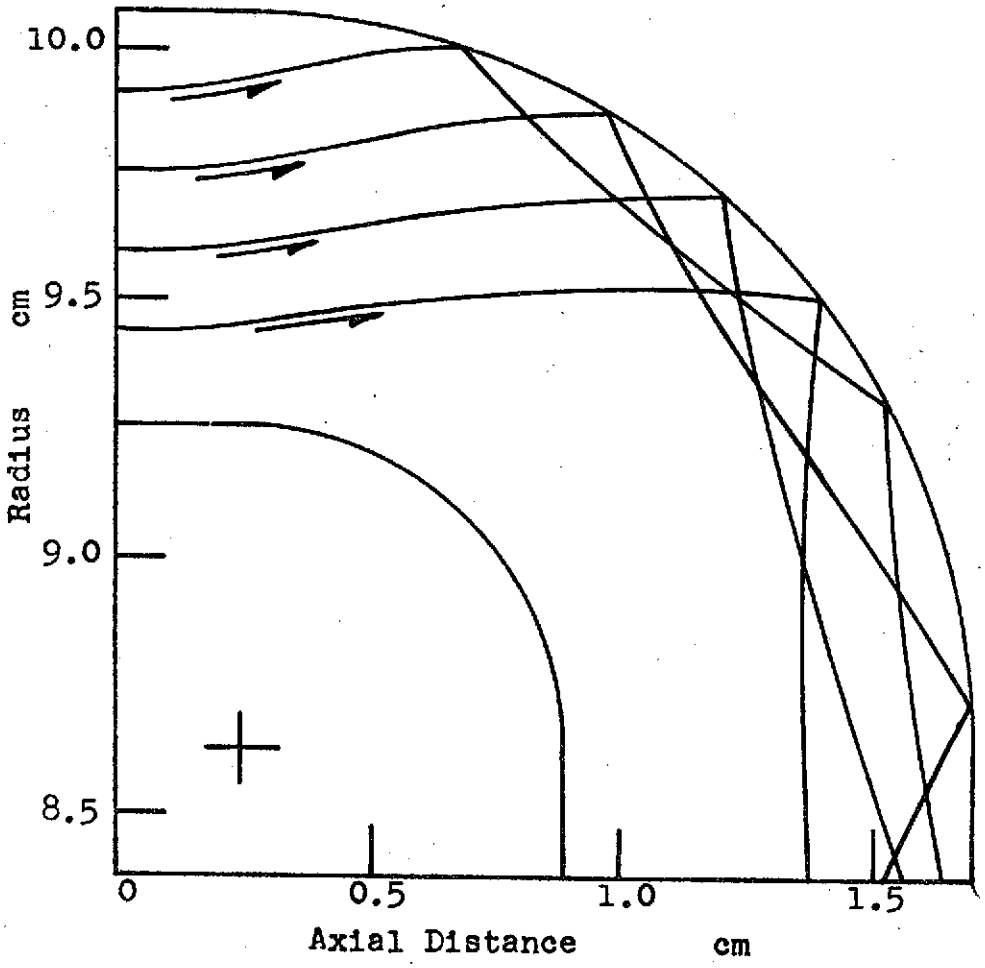

FIGURE 28d. TRAJECTORIES WITH δ = 30 cm.

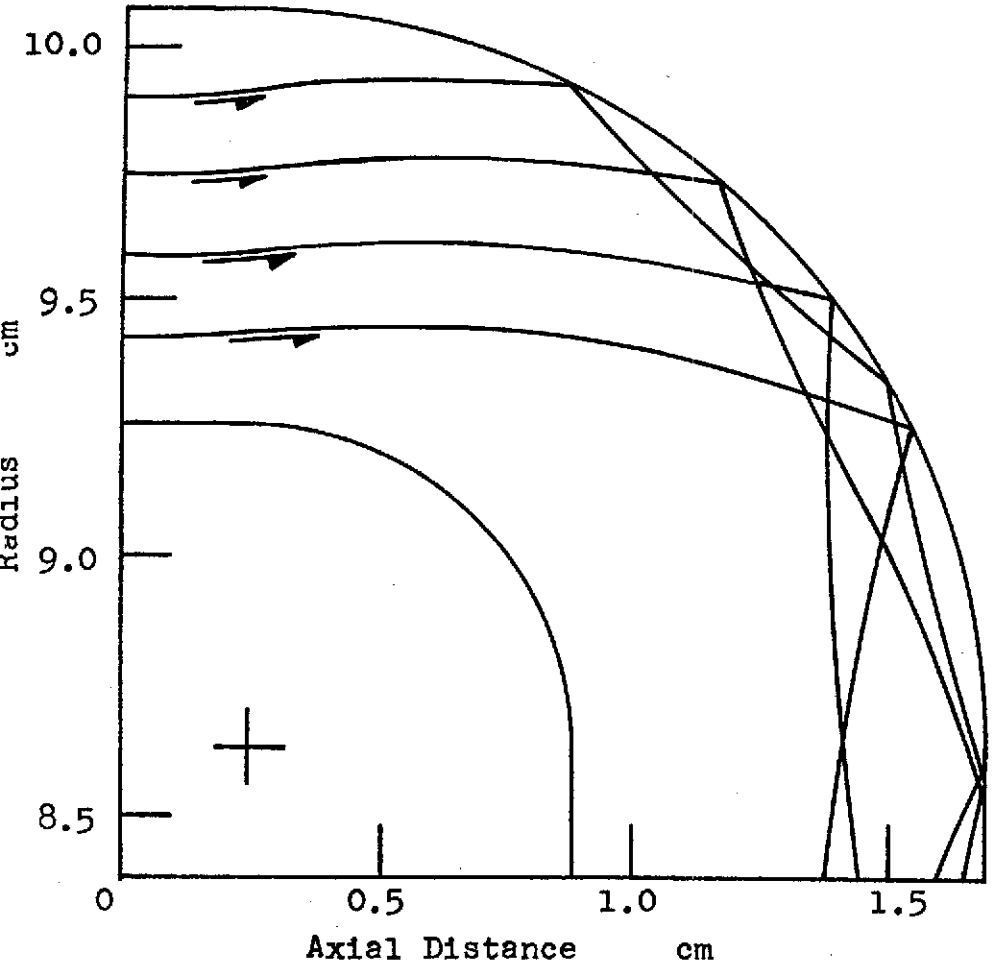

FIGURE 28e. TRAJECTORIES WITH δ = 15 cm.

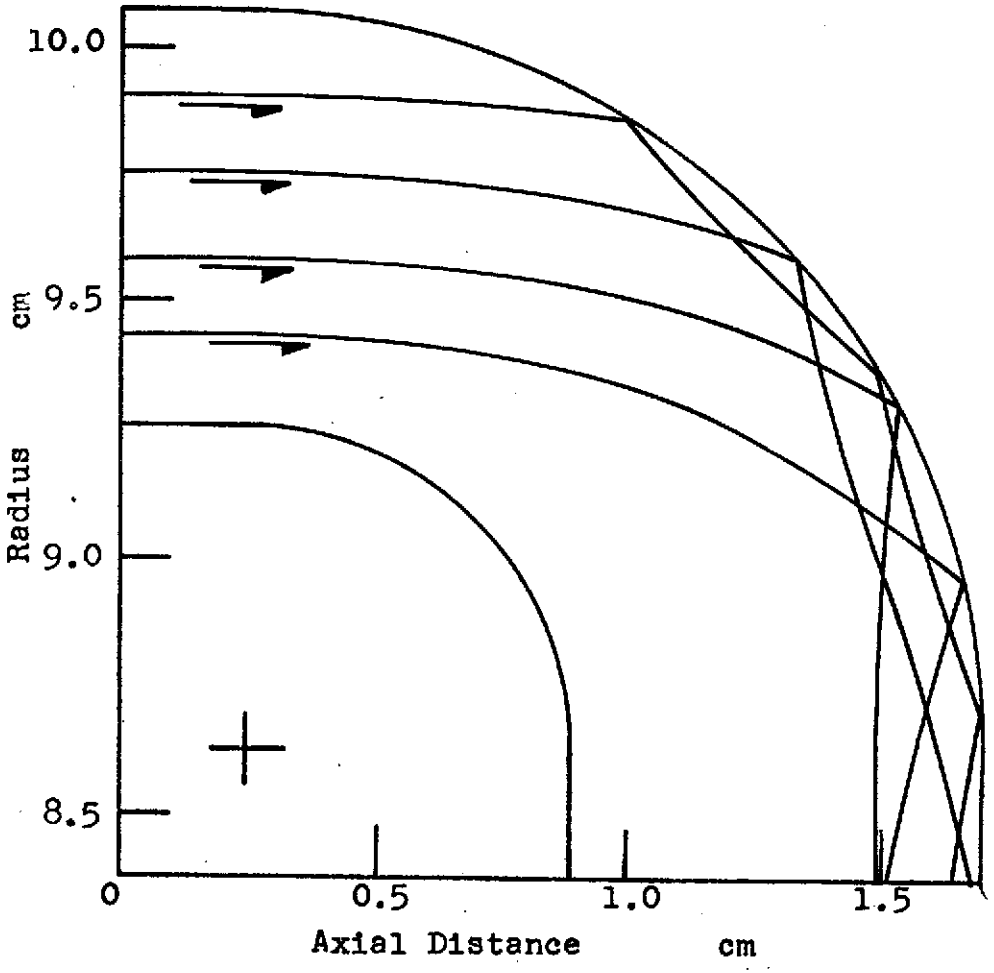

FIGURE 28f. TRAJECTORIES WITH δ = 6 cm.

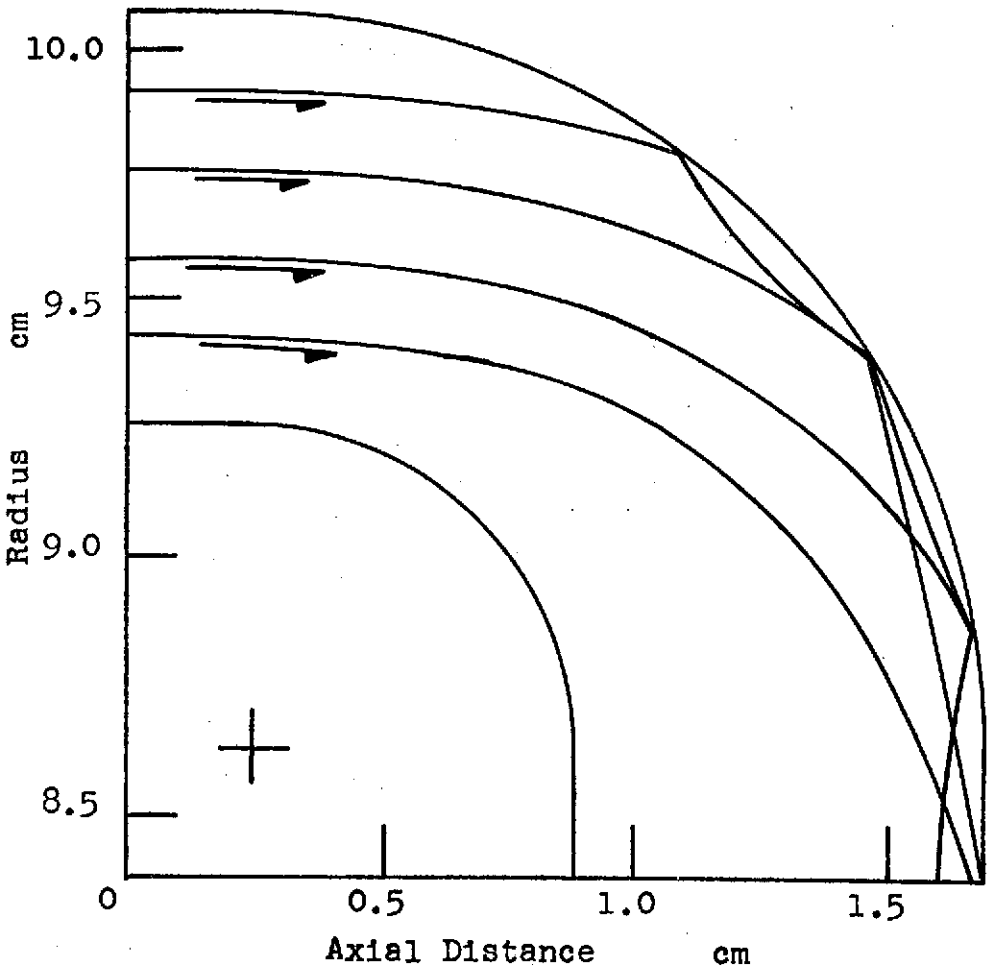

FIGURE 28g. TRAJECTORIES WITH $\delta = 3$ cm.

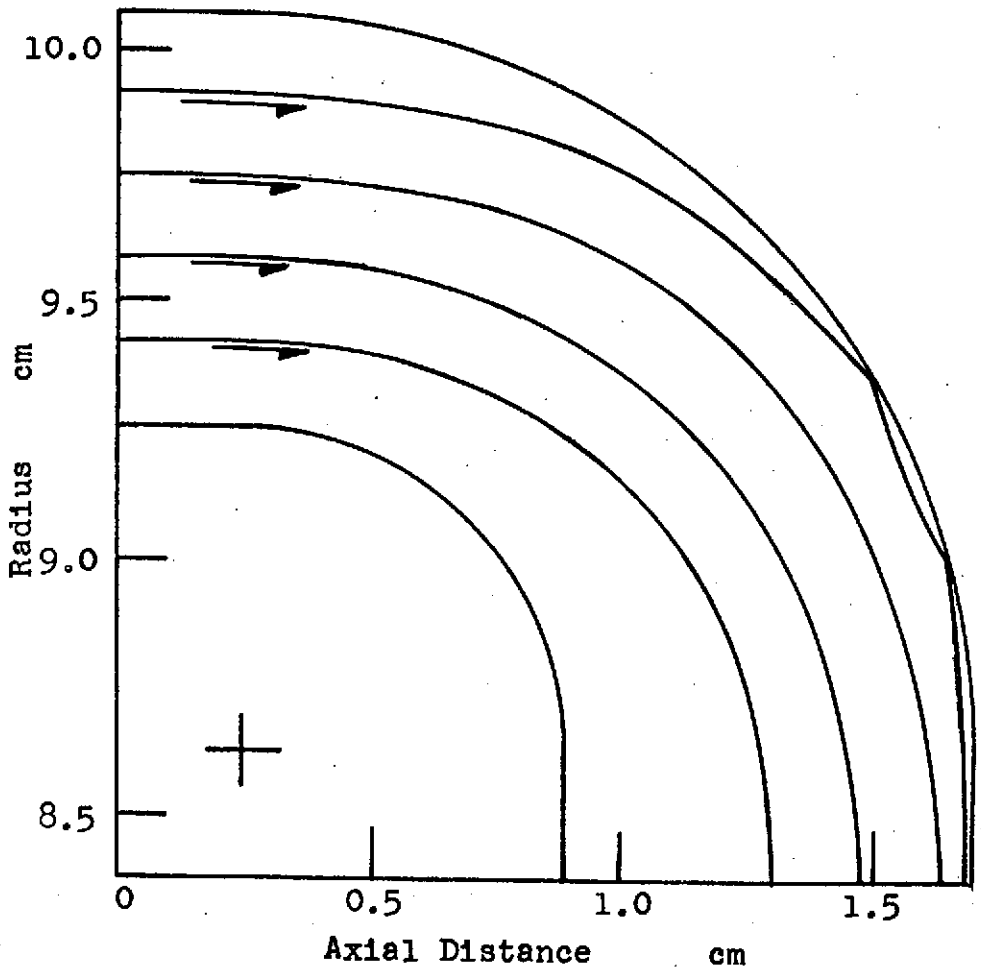

FIGURE 28h TRAJECTORIES WITH $\delta = 1.5$ cm.

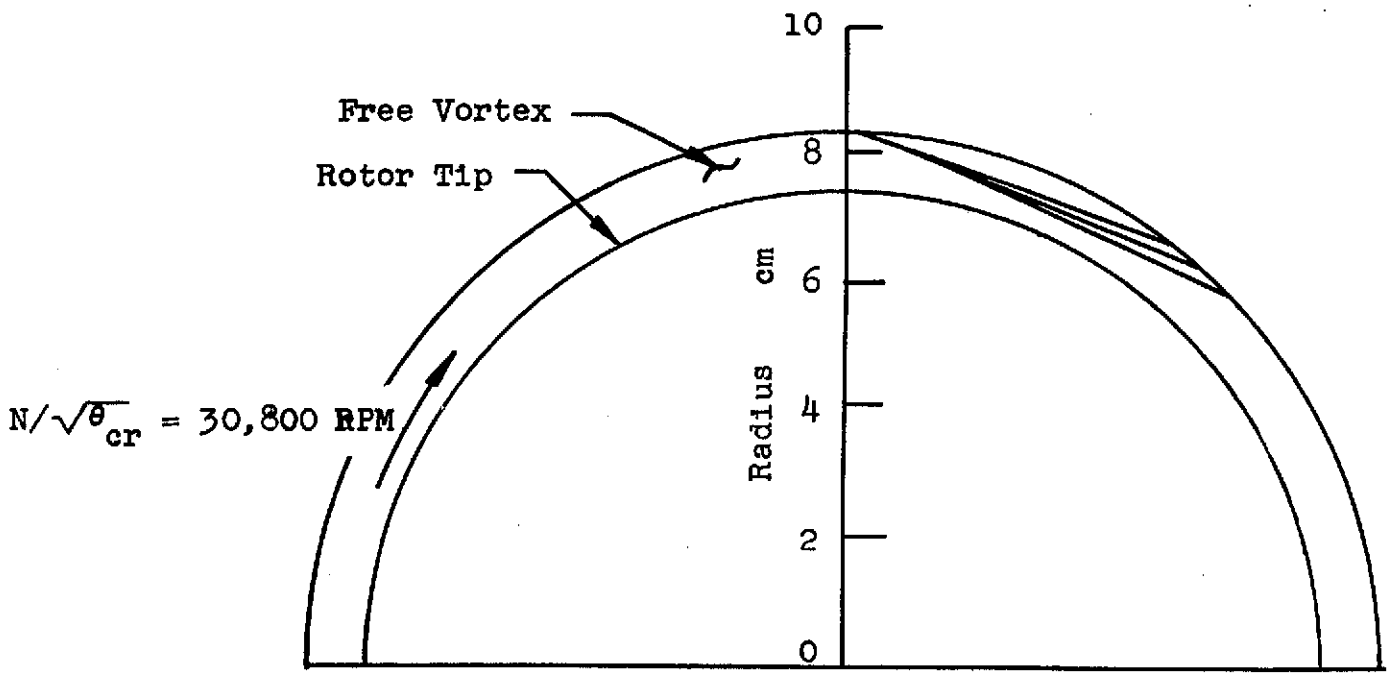

FIGURE 29a. TRAJECTORIES CONTINUED FROM FIGURE 28b. INTO FREE VORTEX, WITH δ = 150 cm.

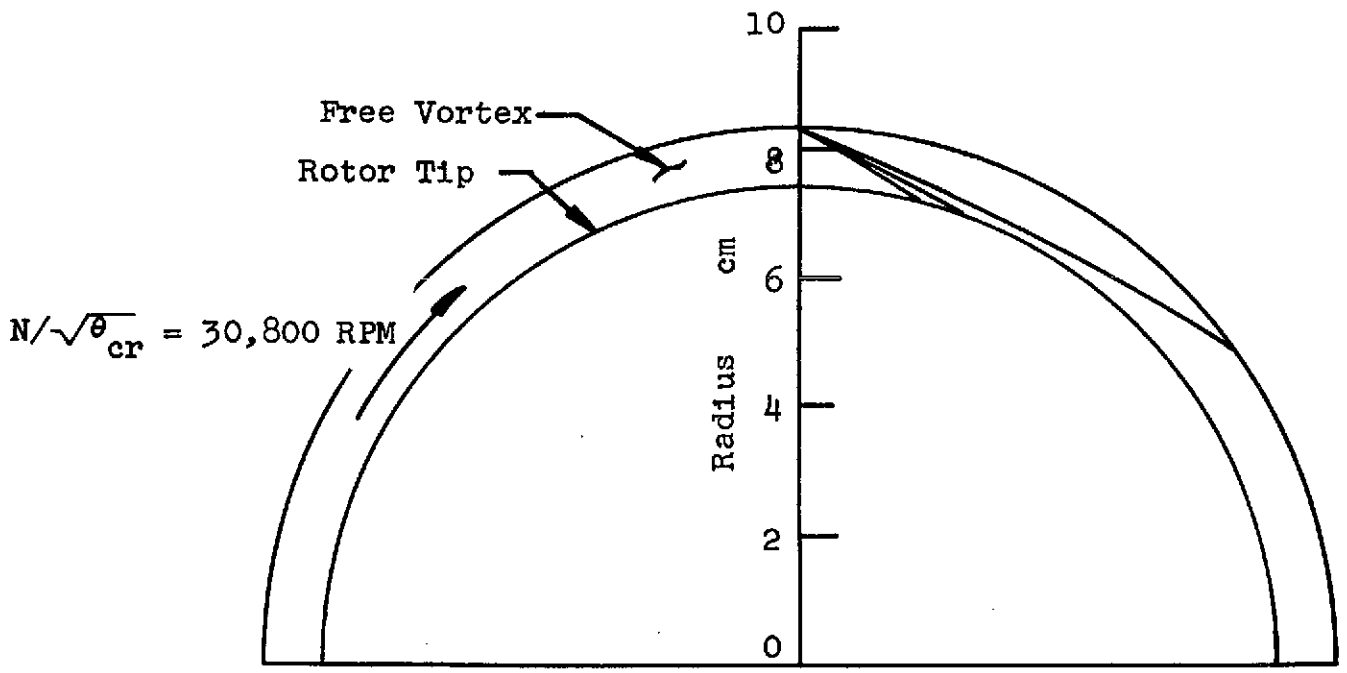

FIGURE 29b. TRAJECTORIES CONTINUED FROM FIGURE 28c. INTO FREE VORTEX, WITH δ = 60 cm.

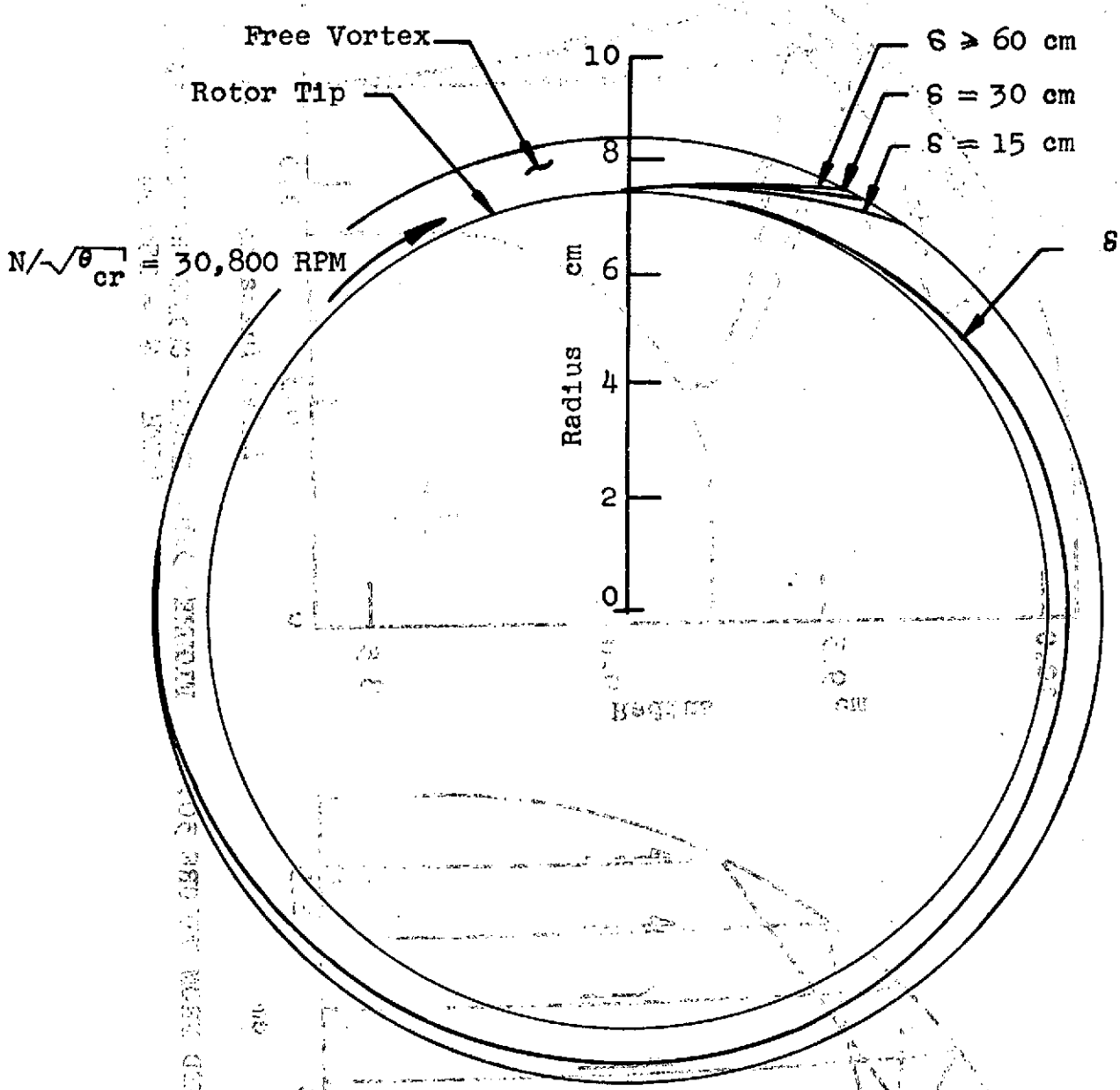

FIGURE 30. TRAJECTORIES OF PARTICLES THROWN OUT OF ROTOR INTO FREE VORTEX REGION.

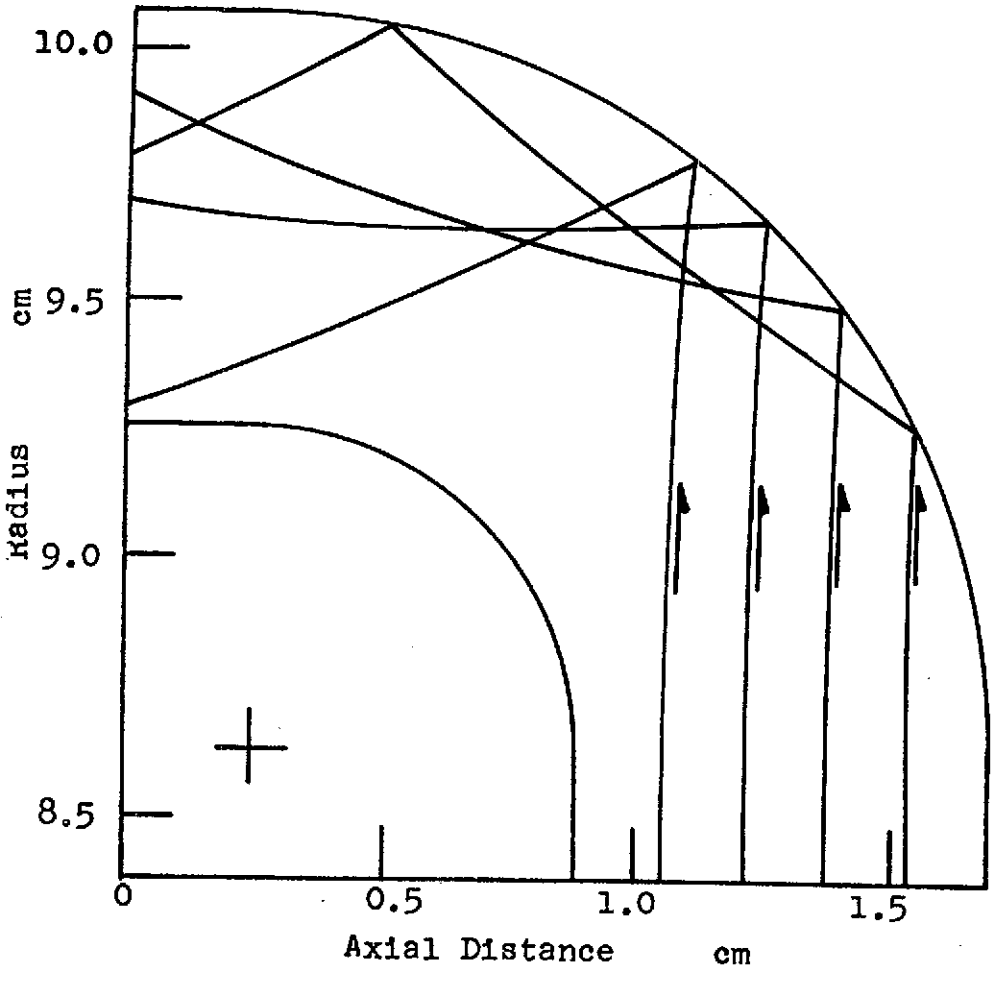

FIGURE 31a. TRAJECTORIES CONTINUED FROM FIGURE 30, WITH δ = 300 cm.

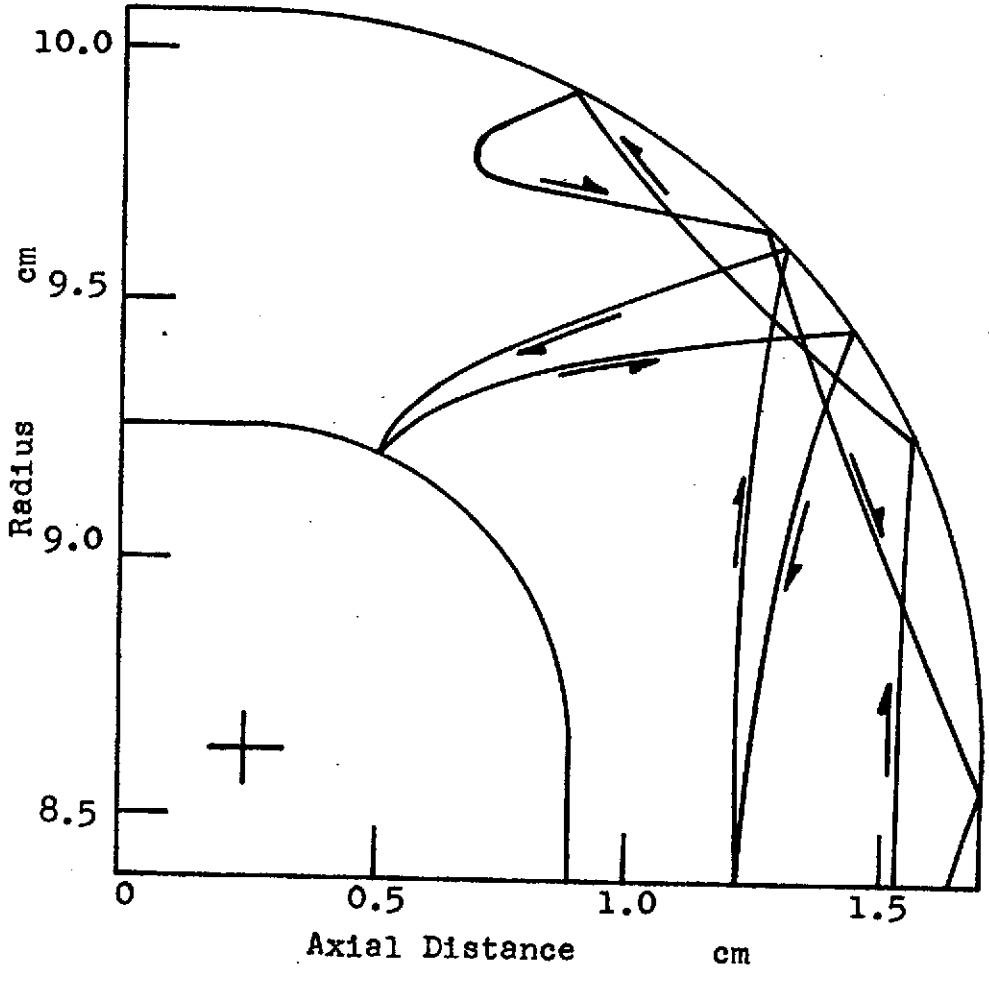

FIGURE 31b. TRAJECTORIES CONTINUED FROM FIGURE 30 WITH δ = 150 cm.

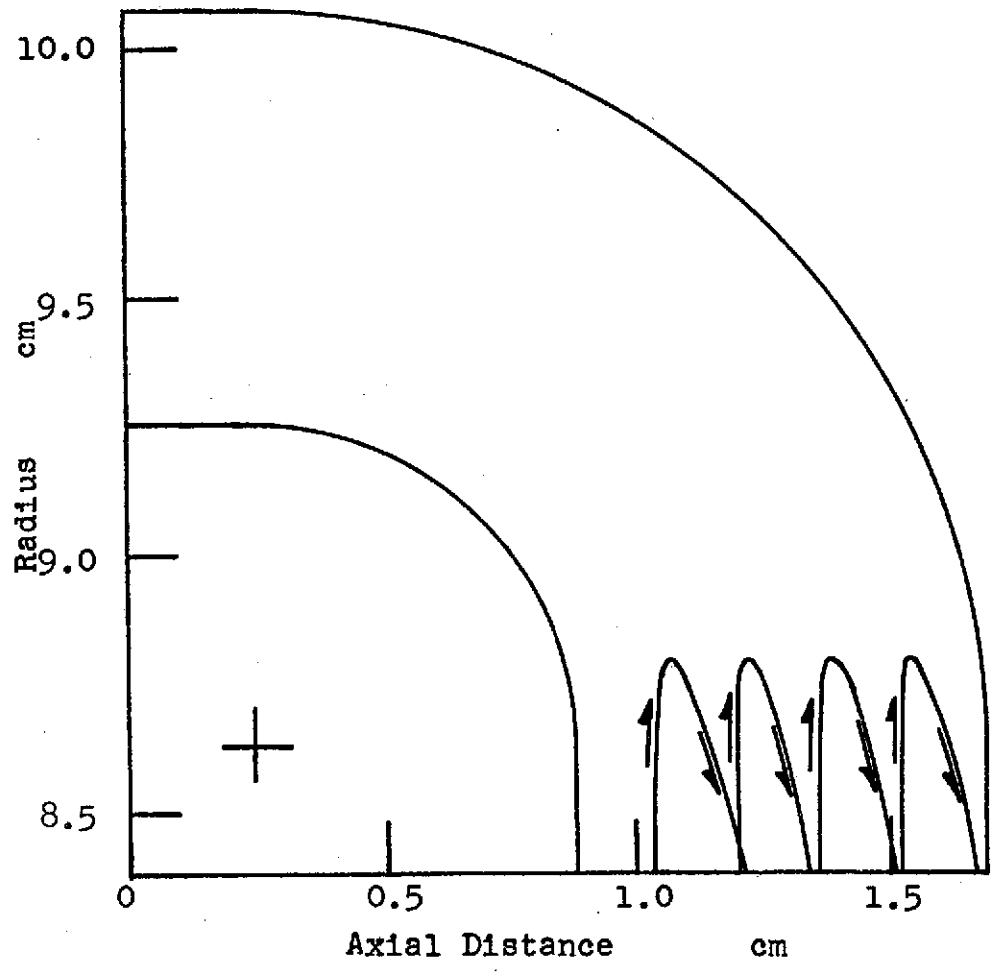

FIGURE 31c. TRAJECTORIES CONTINUED FROM FIGURE 30, WITH δ = 60 cm.

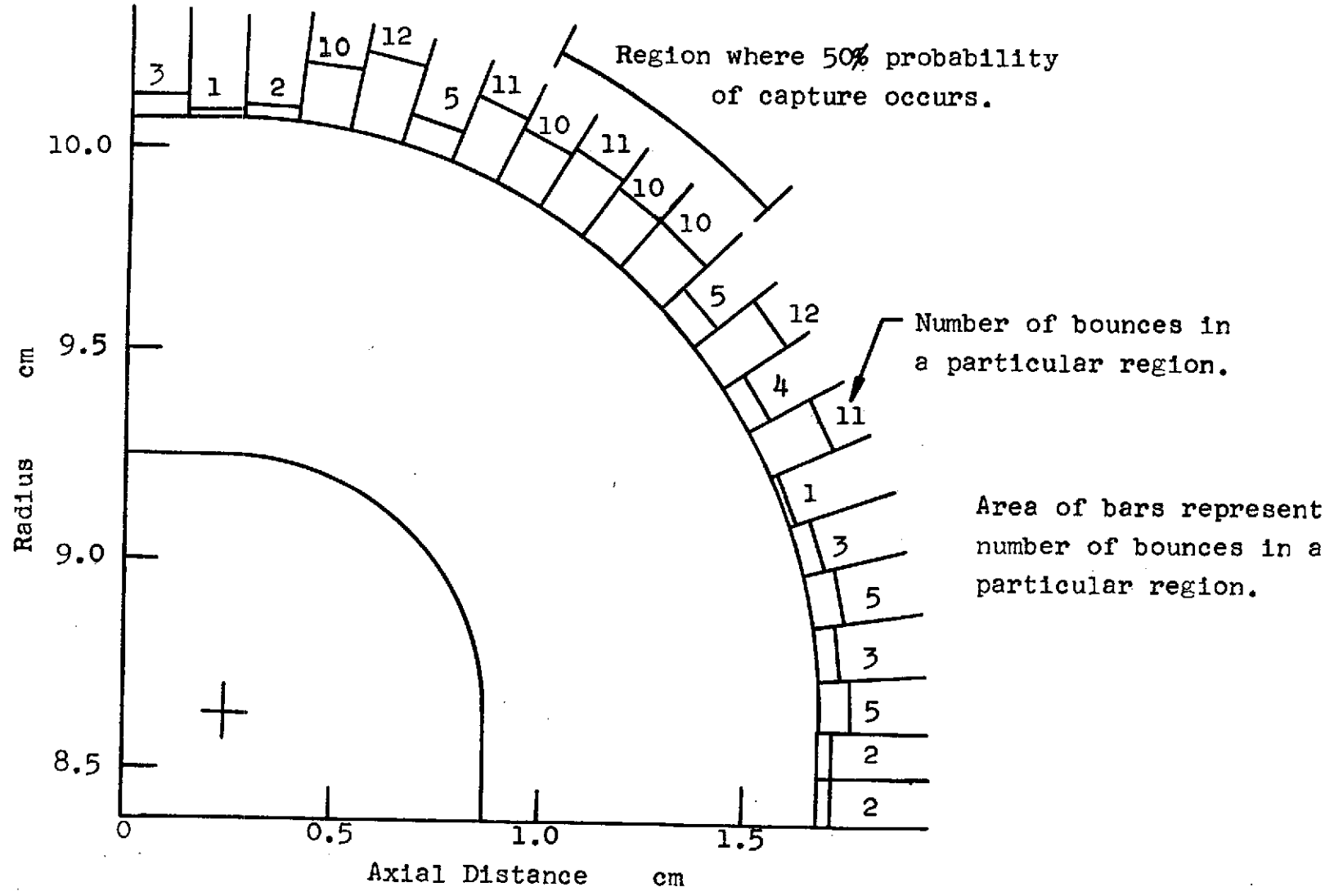

FIGURE 32. SUMMARY OF DATA ON PARTICLE BOUNCES.

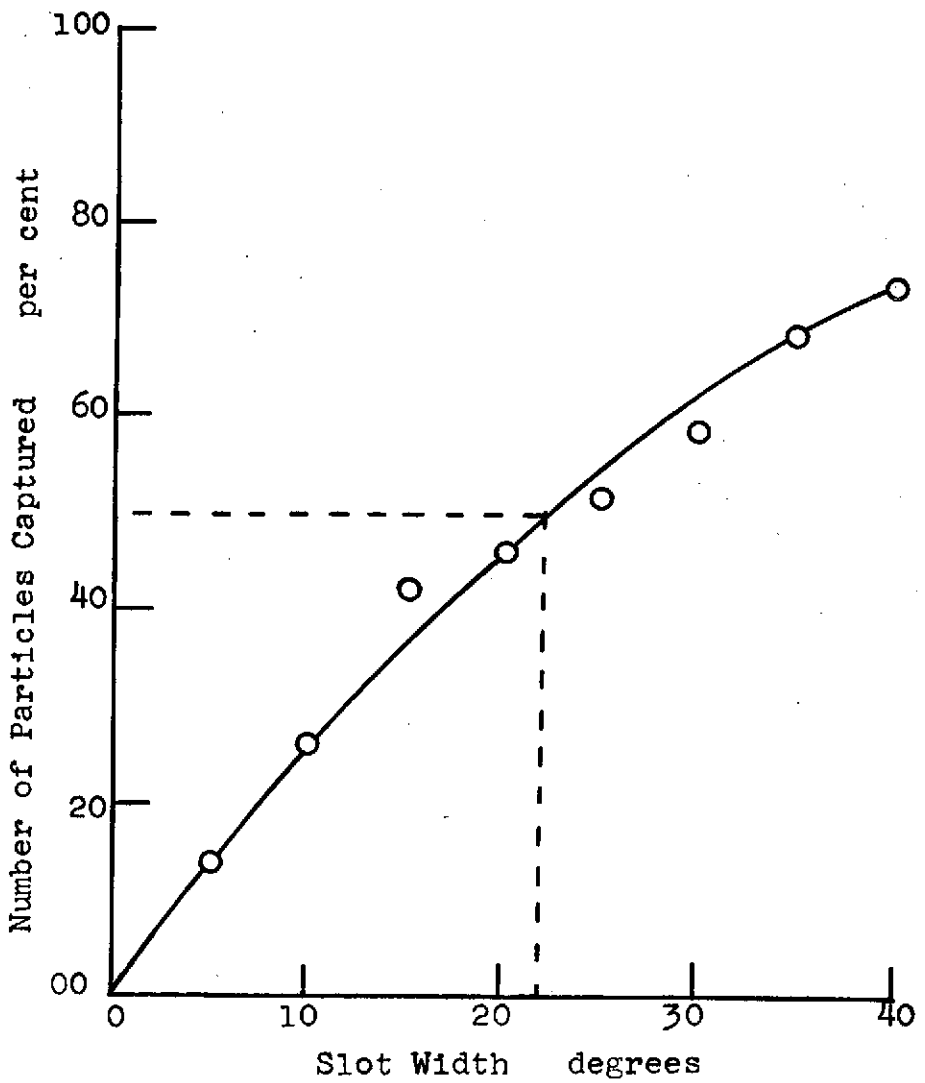

FIGURE 33. PARTICLE TRAP EFFECTIVENESS VERSUS SIZE FOR SLOT CENTERED AT 35°.

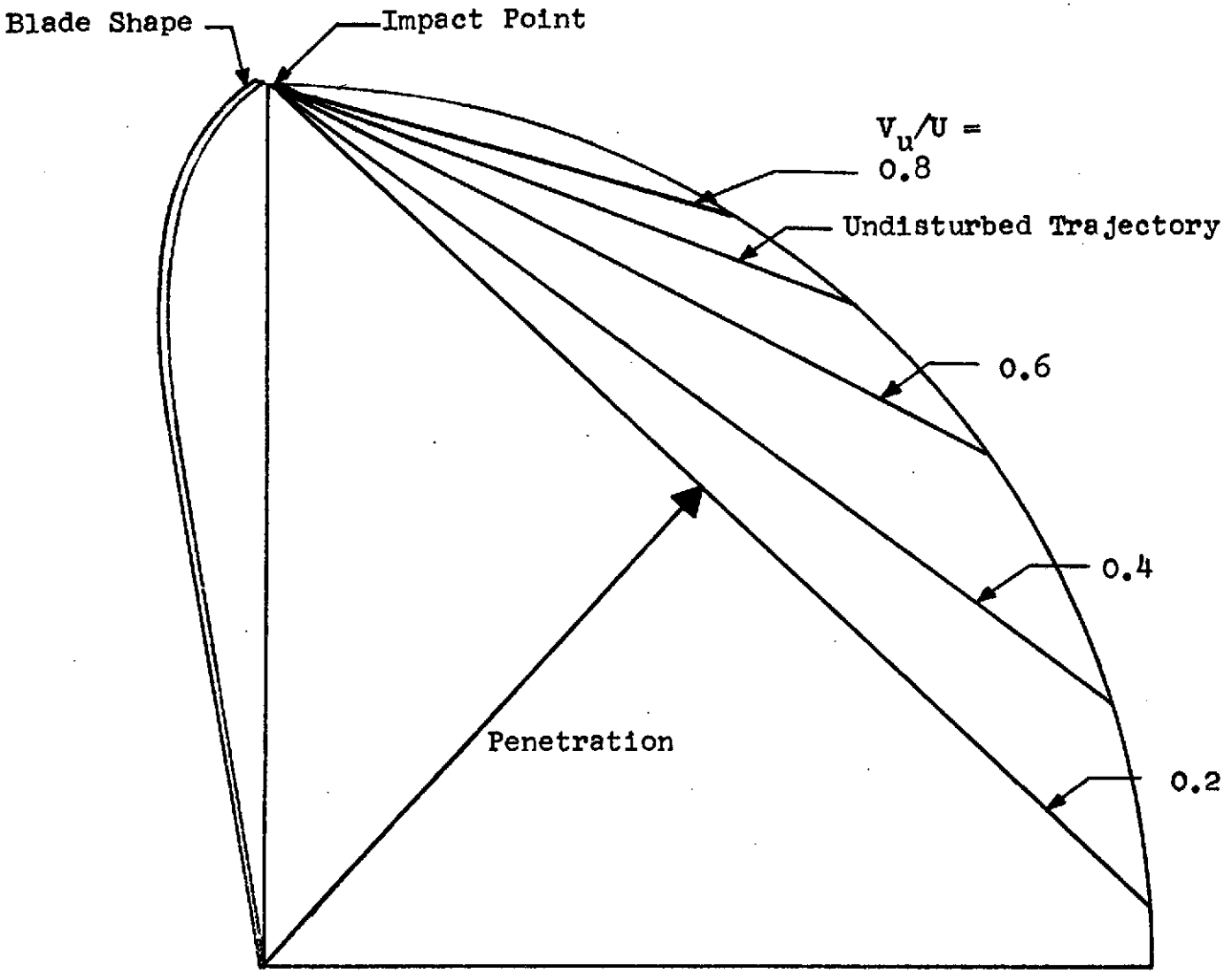

FIGURE 34. EFFECT OF INLET VELOCITY ON PENETRATION.

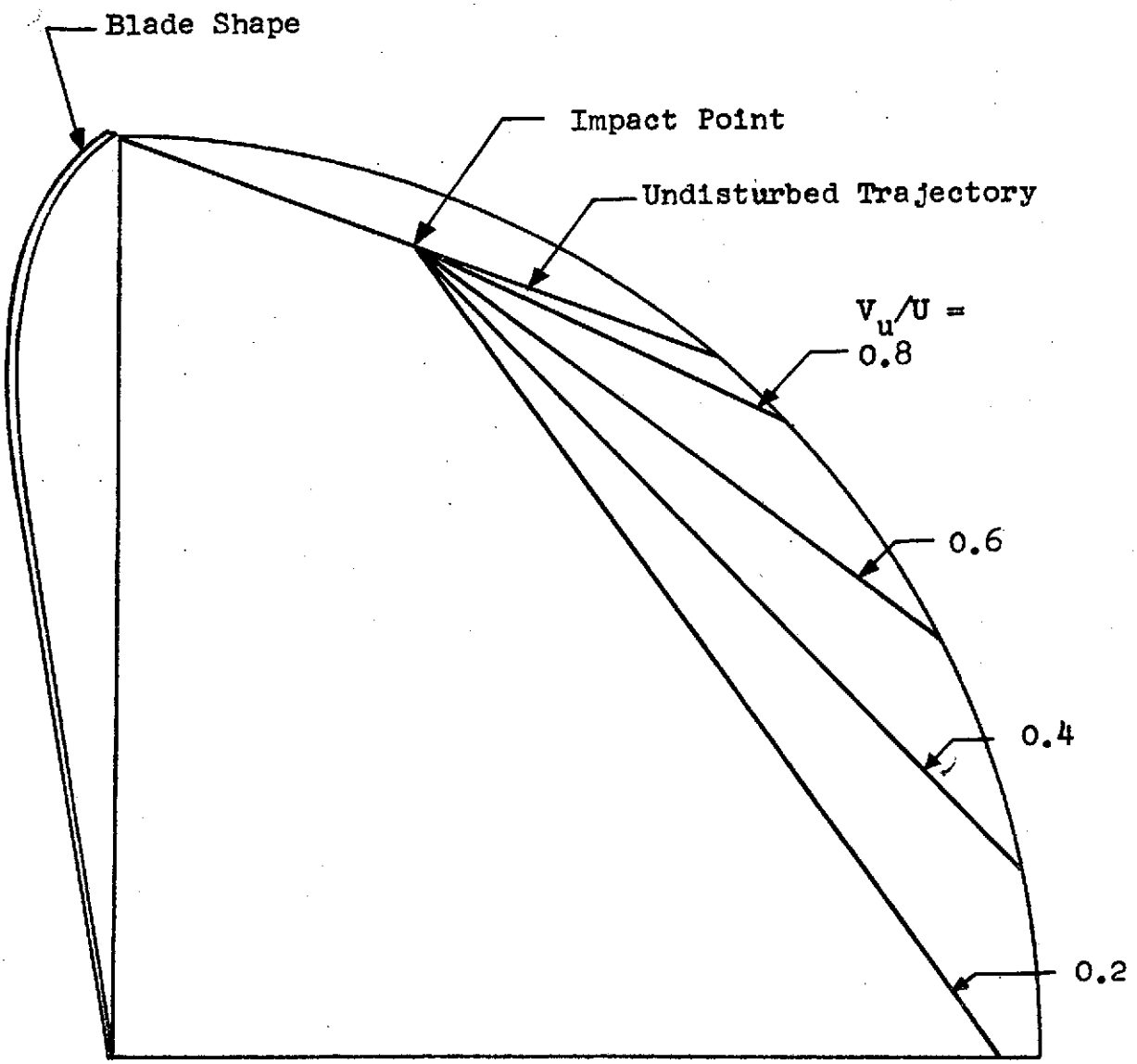

FIGURE 35. EFFECT OF INLET VELOCITY ON PENETRATION.

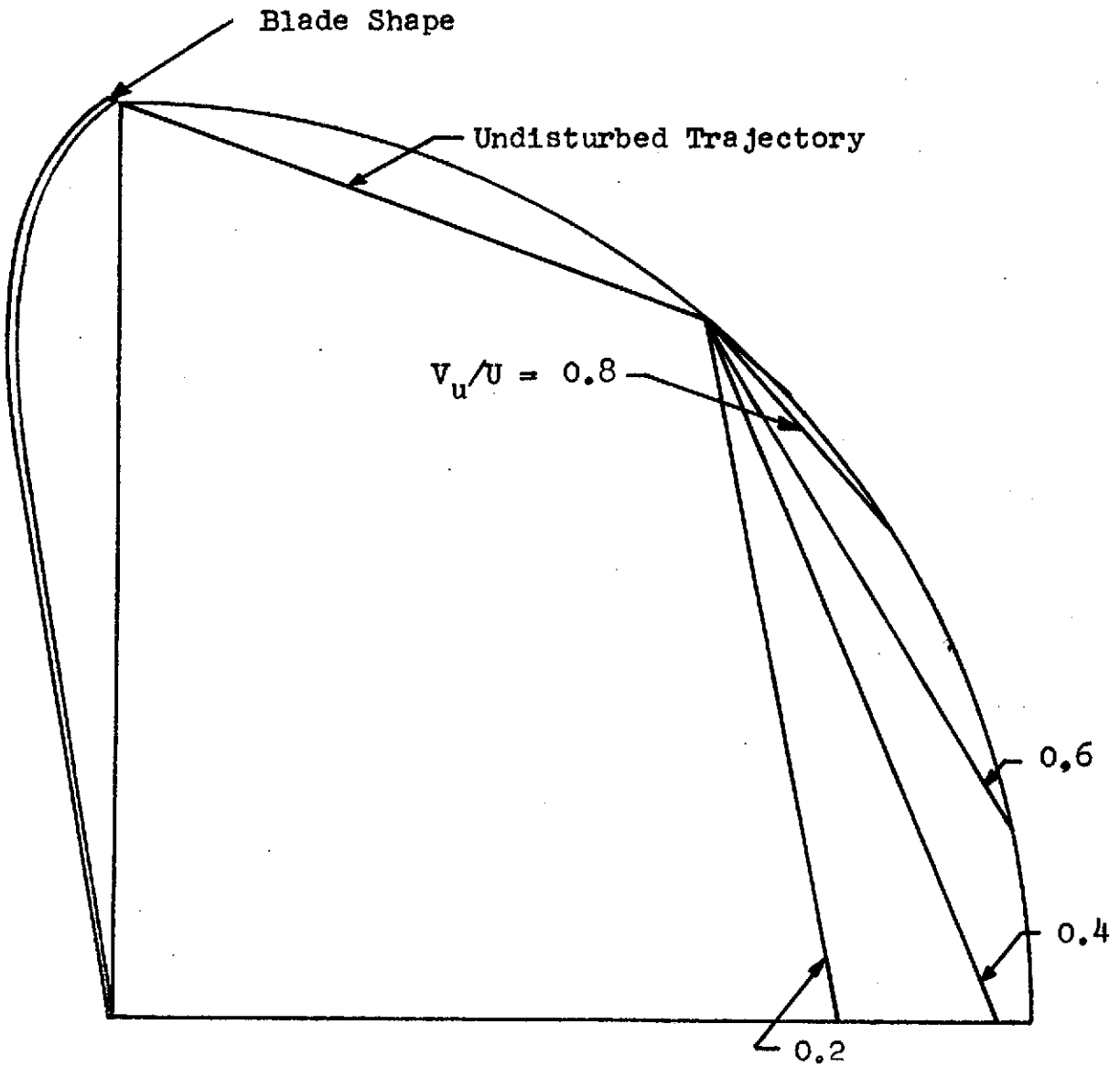

FIGURE 36. EFFECT OF INLET VELOCITY ON PENETRATION.

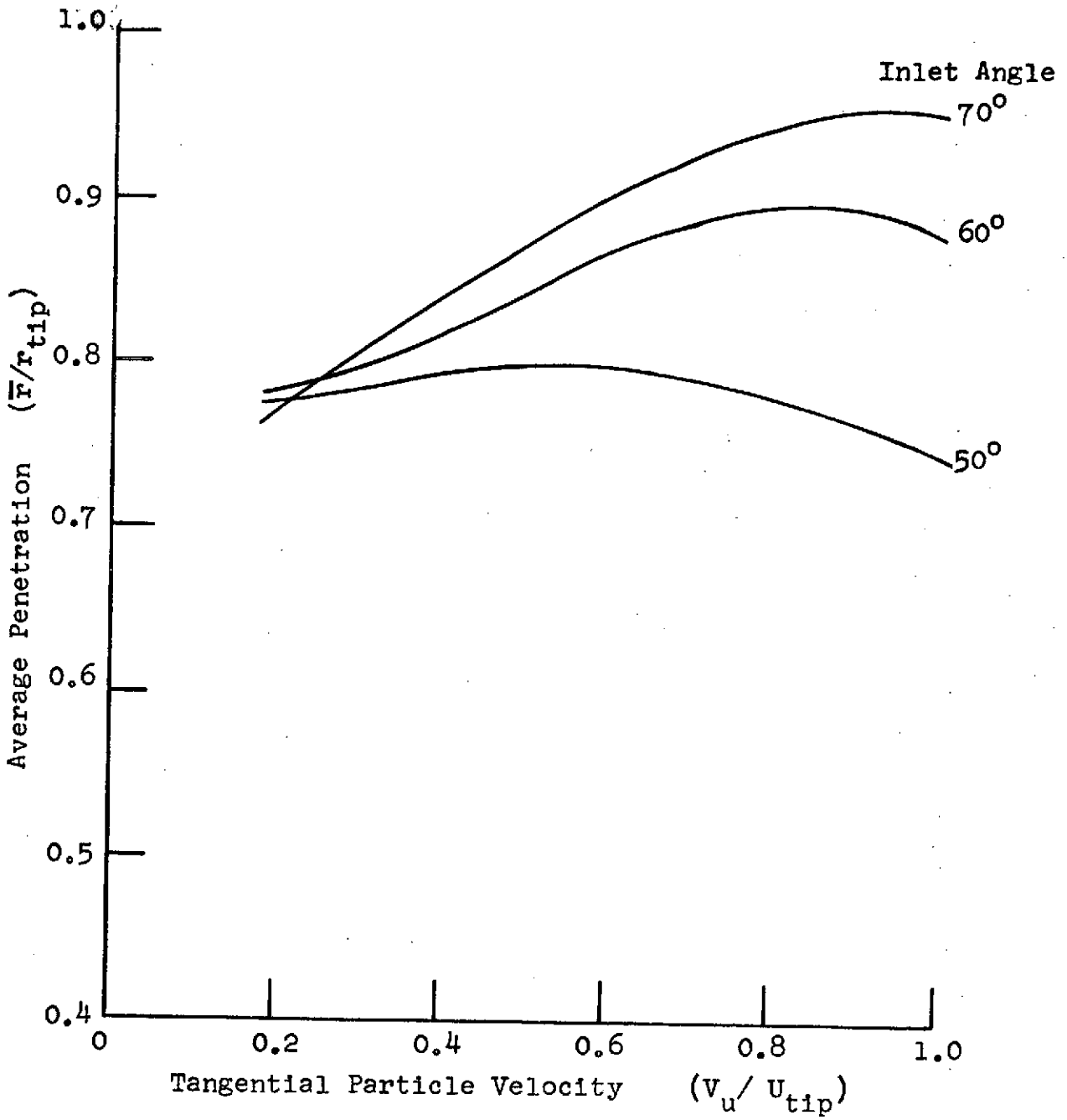

FIGURE 37. EFFECT OF INLET ANGLE ON PENETRATION.

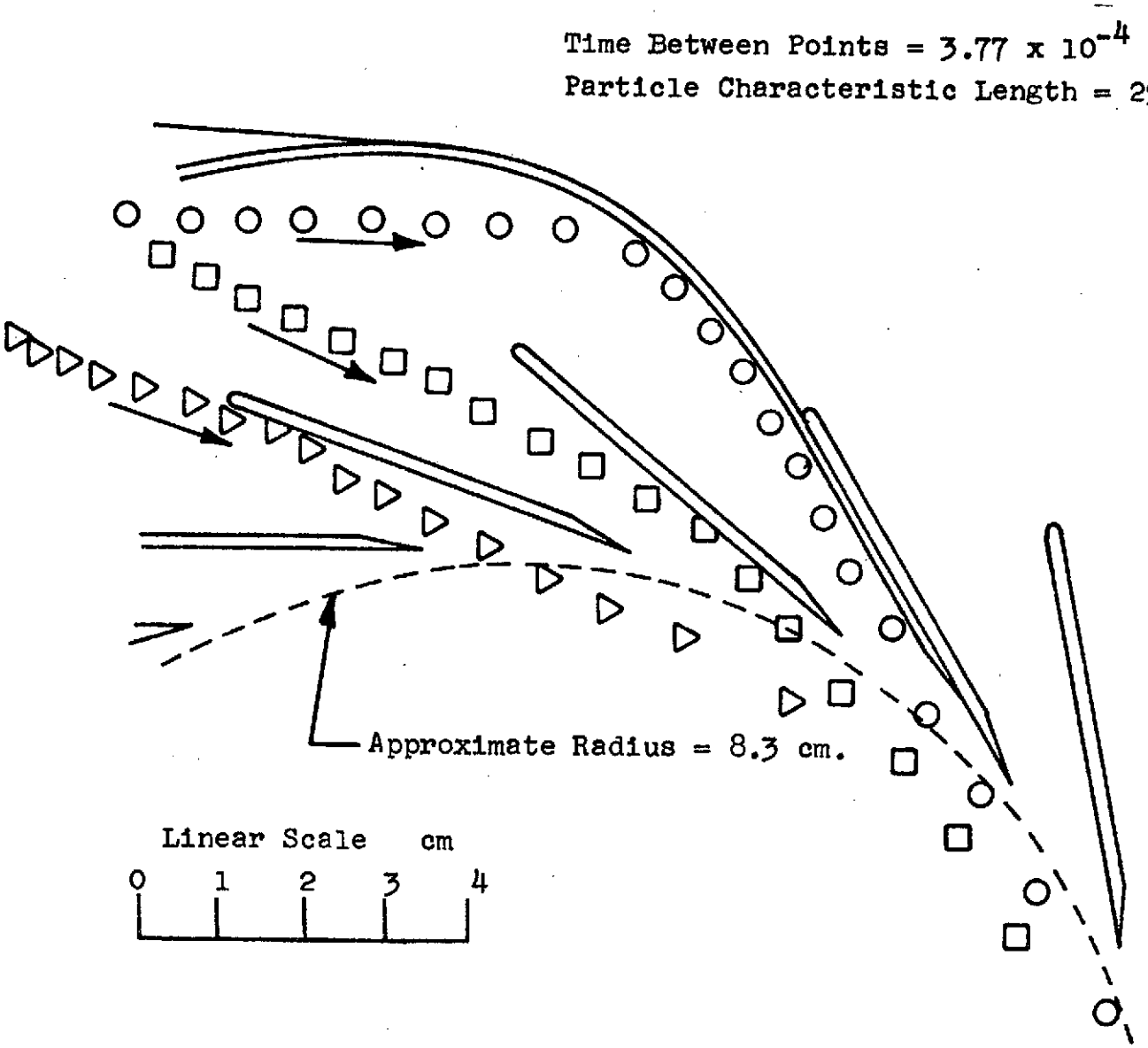

FIGURE 38a. EXPERIMENTAL TRAJECTORIES IN THE NOZZLES
TYPICAL TRAJECTORIES OF PARTICLES THAT BOUNCE ONCE.

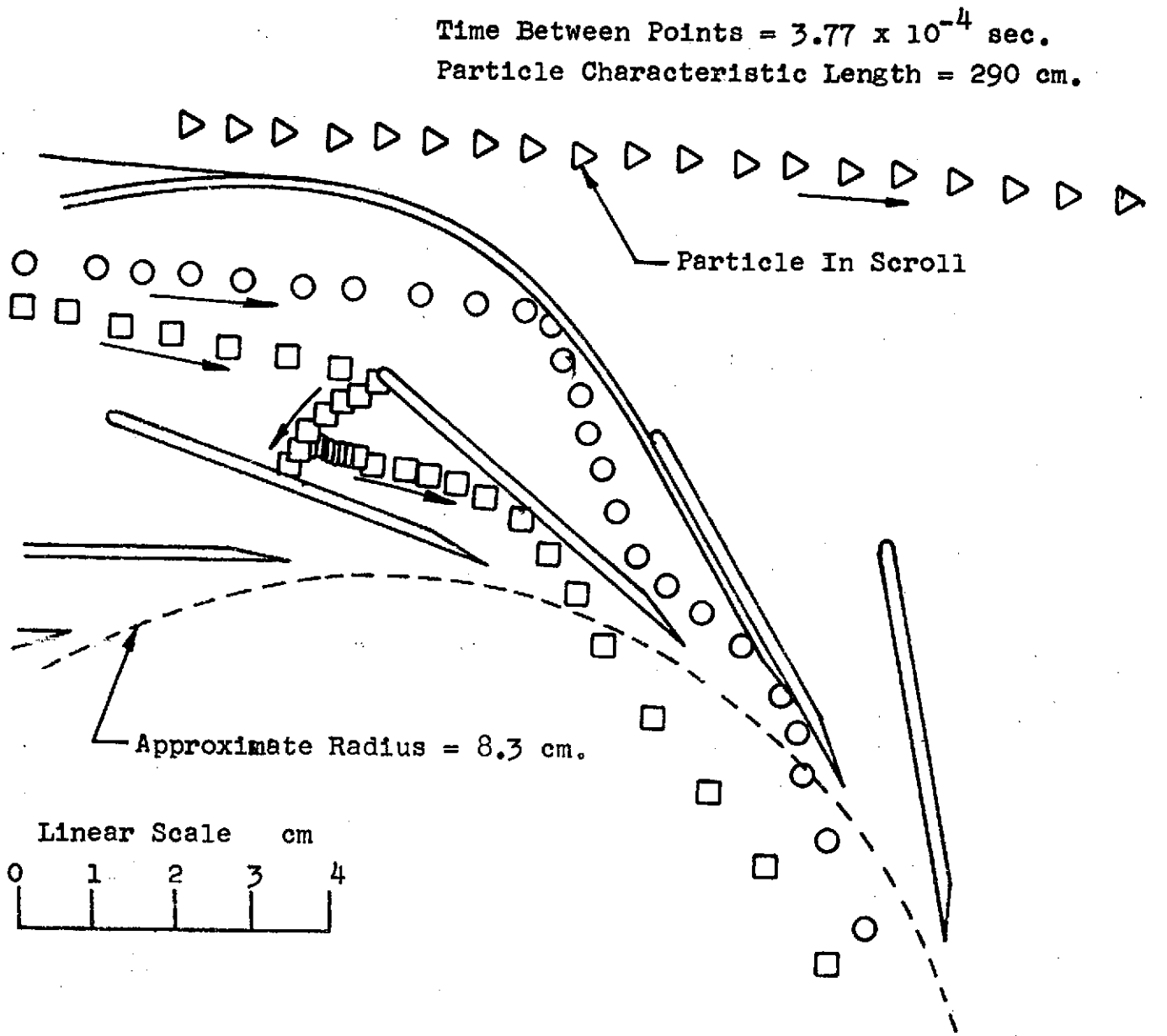

FIGURE 38b. EXPERIMENTAL TRAJECTORIES IN THE NOZZLES
TRAJECTORIES OF PARTICLES THAT BOUNCE SEVERAL TIMES.

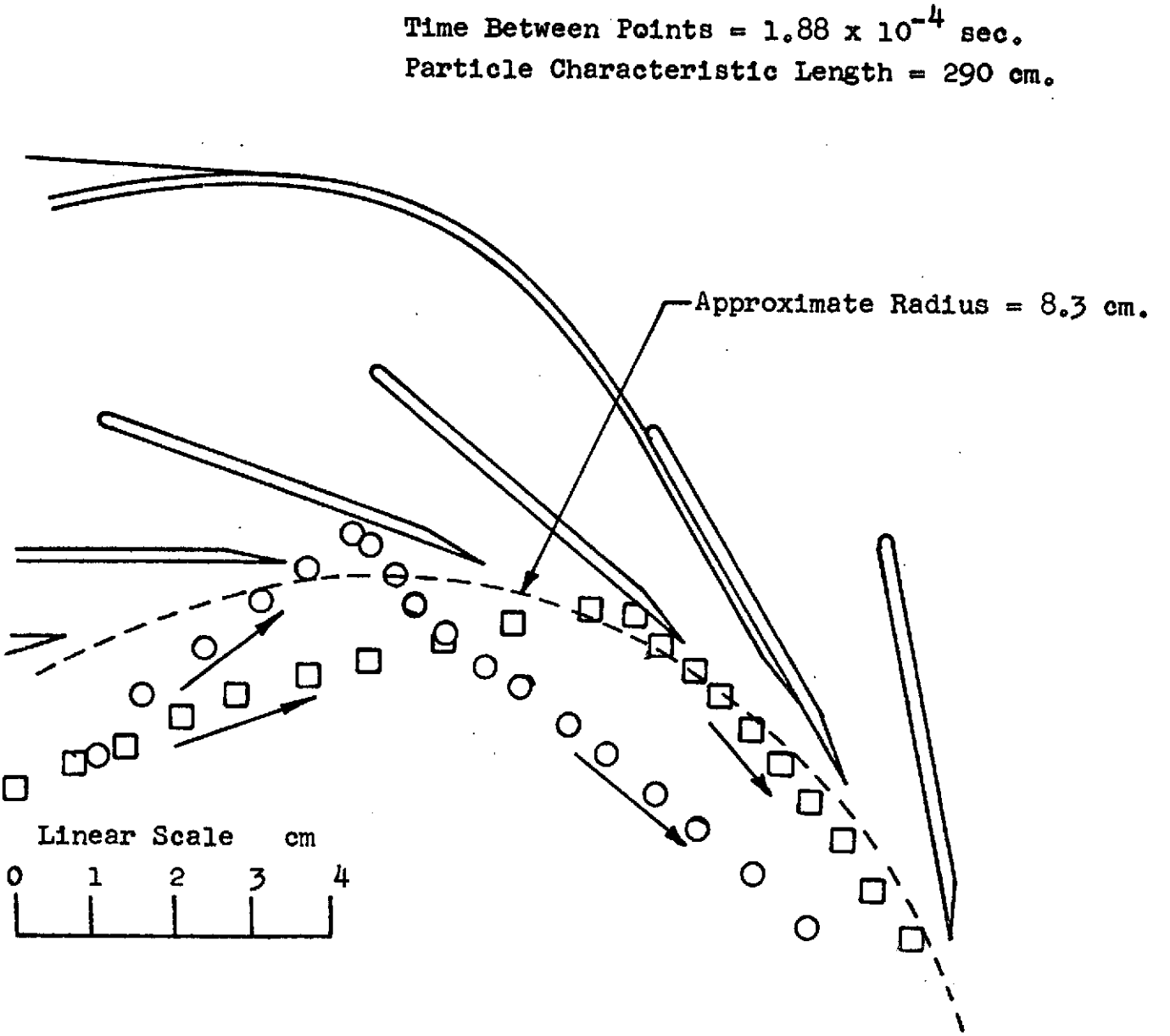

FIGURE 38c. EXPERIMENTAL TRAJECTORIES IN THE VORTEX.

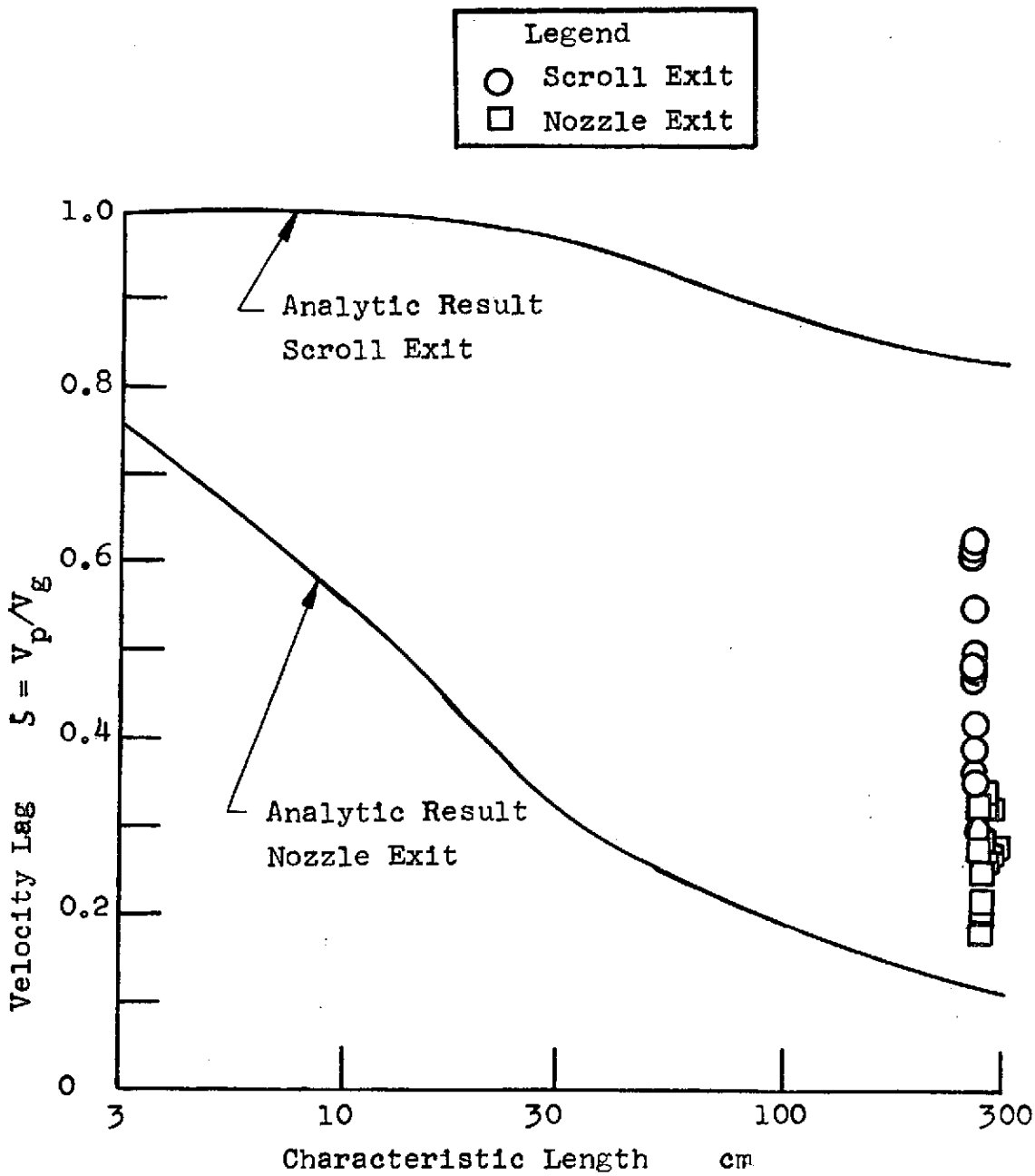

FIGURE 39. EXPERIMENTALLY DETERMINED VELOCITY LAG.

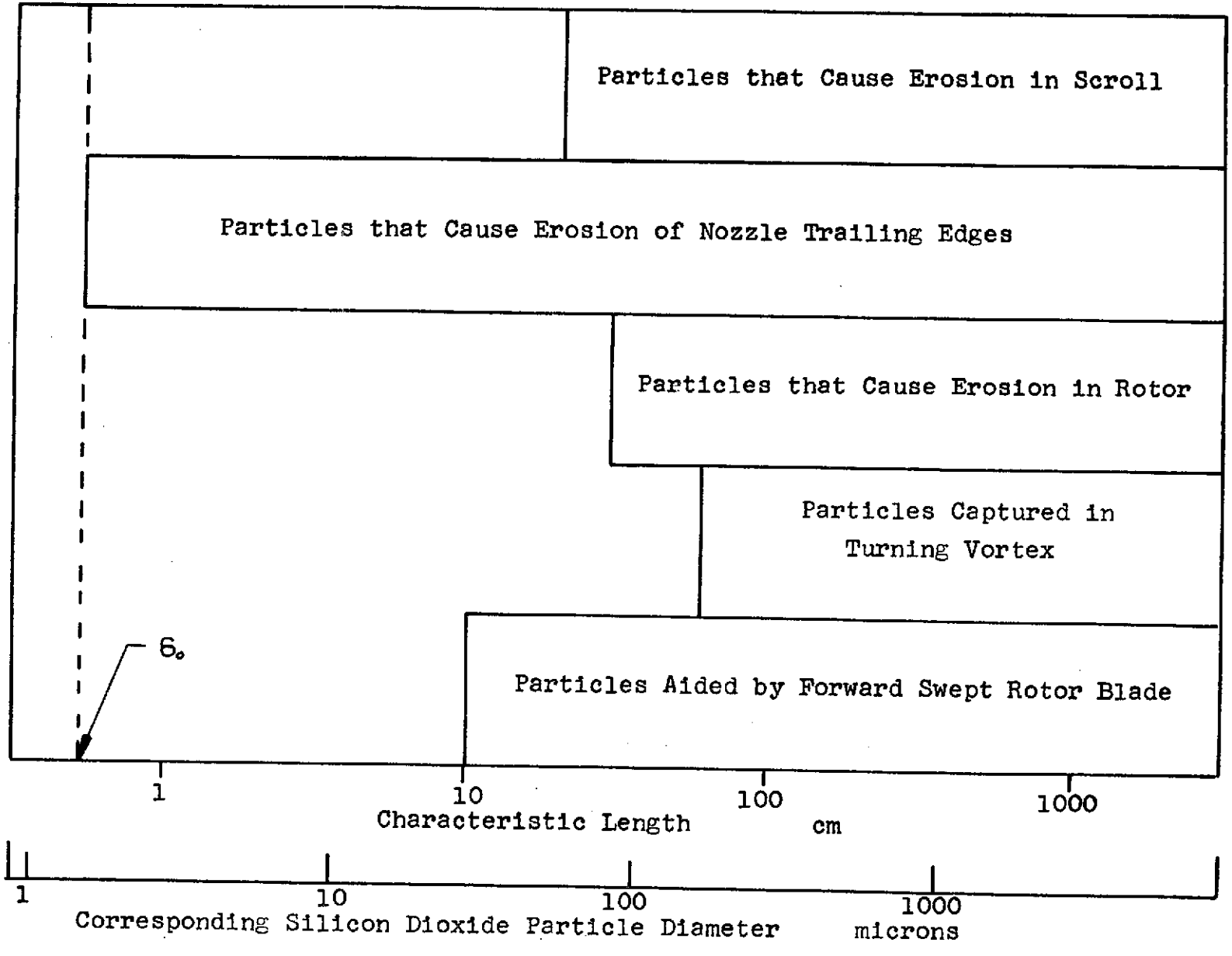

FIGURE 40. SUMMARY OF RESULTS.